VERTICAL GROUND MOTION INFLUENCE ON SEISMICALLY ISOLATED & UNISOLATED BRIDGES

A THESIS SUBMITTED TO
THE GRADUATE SCHOOL OF NATURAL AND APPLIED SCIENCES
OF
MIDDLE EAST TECHNICAL UNIVERSITY

BY

NAİM ESER REYHANOĞULLARI

IN PARTIAL FULFILLMENT OF THE REQUIREMENTS
FOR
THE DEGREE OF MASTER OF SCIENCE
IN
CIVIL ENGINEERING

APRIL 2010

Approval of the thesis:

VERTICAL GROUND MOTION INFLUENCE ON SEISMICALLY ISOLATED & UNISOLATED BRIDGES

Submitted by **NAİM ESER REYHANOĞULLARI** in partial fulfillment of the requirements for the degree of **Master of Science in Civil Engineering Department, Middle East Technical University** by,

Prof. Dr. Canan Özgen ________________
Dean, **Graduate School of Natural and Applied Sciences**

Prof. Dr. Güney Özcebe
Head of Department, **Civil Engineering Dept., METU** ________________

Assoc. Prof. Dr. Uğurhan Akyüz
Supervisor, **Civil Engineering Dept., METU** ________________

Examining Committee Members:

Prof. Dr. Murat Dicleli ________________________
Engineering Science Dept., METU

Assoc. Prof. Dr. Uğurhan Akyüz ________________________
Civil Engineering Dept., METU

Assoc. Prof. Dr. Ahmet Türer ________________________
Civil Engineering Dept., METU

Assist. Prof. Dr. Alp Caner ________________________
Civil Engineering Dept., METU

Assist. Prof. Dr. Özgür Kurç ________________________
Civil Engineering Dept., METU

Date: 19.04.2010

I hereby declare that all information in this document has been obtained and presented in accordance with academic rules and ethical conduct. I also declare that, as required by these rules and conduct, I have fully cited and referenced all material and results that are not original to this work.

Name, Last name : **Naim Eser REYHANOĞULLARI**

Signature :

ABSTRACT

VERTICAL GROUND MOTION INFLUENCE ON SEISMICALLY ISOLATED & UNISOLATED BRIDGES

Reyhanoğulları, Naim Eser
M.Sc., Department of Civil Engineering
Supervisor : Assoc. Prof. Dr. Uğurhan Akyüz

April 2010, 127 pages

In this study influences of vertical ground motion on seismically isolated bridges were investigated for seven different earthquake data. One assessment of bearing effect involves the calculation of vertical earthquake load on the seismically isolated bridges. This paper investigates the influence of vertical earthquake excitation on the response of briefly steel girder composite bridges (SCB) with and without seismic isolation through specifically selected earthquakes. In detail, the bridge is composed of 30m long three spans, concrete double piers at each axis supported by mat foundations with pile systems. At both end of the spans there exists concrete abutments to support superstructure of the bridge. SCBs which were seismically isolated with nine commonly preferred different lead-rubber bearings (LRB) under each steel girder were analyzed. Then, the comparisons were made with a SCB without seismic isolation. Initially, a preliminary design was made and reasonable sections for the bridge have been obtained. As a result of this, the steel girder bridge sections were checked with AASHTO provisions and analytical model was updated accordingly. Earthquake records were thought as the main loading sources. Hence both cases were exposed to tri-axial earthquake loads in order to understand the effects under such circumstances. Seven near fault earthquake data were selected by considering possession of directivity. Several runs using the chosen earthquakes were performed in order to be able to derive satisfactory comparisons between different types of isolators. Analytical calculations were conducted using well known structural analysis software (SAS) SAP2000. Nonlinear time history analysis was performed using the analytical model of the bridge with and without seismic isolation. Response data collected from SAS was used to determine the vertical load on the piers and middle span midspan moment on the steel girders due to the vertical and horizontal component of excitation. Comparisons dealing with the effects of horizontal only and horizontal plus vertical earthquake loads were introduced.

Keywords: Seismically Isolation, Bridges, Vertical Ground Motion, Nonlinear Time History, Lead Rubber Bearing.

ÖZ

DEPREMİN DÜŞEY BİLEŞENİNİN, SİSMİK OLARAK İZOLE EDİLMİŞ VE EDİLMEMİŞ KÖPRÜLERE OLAN ETKİLERİ

Reyhanoğulları, Naim Eser
Yüksek Lisans, İnşaat Mühendisliği Bölümü
Tez Yöneticisi : Doç. Dr. Uğurhan Akyüz

Nisan 2010, 127 sayfa

Bu tezde yedi farklı depremin düşey bileşenlerinin sismik olarak izole edilmiş köprülere olan etkileri incelendi.İlgili değerlendirmelerden biri depremin düşey bileşen kuvvetinin sismik olarak izole edilmiş köprüye olan etkisinin hesaplanmasıdır. Bu tez, özet olarak, depremin düşey bileşeninin sismik olarak izole edilmiş ve edilmemiş kompozit çelik köprünün (KÇK) davranışları üzerine olan etkileri özel olarak seçilmiş depremler vasıtasıyla incelemektedir. İncelenen köprü 30m uzunluğunda üç açıklıktan, her aksta kazık destekli radye temel ile bütünleşik iki adet beton ayaktan oluşmaktadır. Köprünün her iki ucunda üstyapıyı desteklemek amacıyla beton kıyı ayakları bulunmaktadır. Pratikte de genel olarak kullanılan ve çelik kirişlerin altına yerleştirilmiş, dokuz farklı kurşun çekirdekli kauçuk izolatör (KÇKI) ile izole edilmiş KÇK'lerin analizleri yapıldı. Analizler sonrası, izole edilmiş KÇK ile izole edilmemiş olan arasında da karşılaştırılmalar yapıldı. Köprünün son haline gelmesinde önce, bir ön tasarım yapıldı ve bu tarz bir köprüde kullanılabilecek kesitler belirlendi. Bunu takiben, belirlenen kesitler AASHTO kriterlerine gore kontrol edildi ve matematik modelde gerekli düzeltmeler yapıldı. Deprem kayıtları, köprü için asıl yük kaynakları olarak planlandı. Bu nedenle, her iki durumdaki köprü, depremin üç bileşeni ile yüklenme durumu karşısında nasıl tepki verdiklerini anlayabilmek amacıyla bu şekilde yüklendi. Direktivite özelliği bulunan yedi farklı deprem seçildi. Seçilen depremleri kullanarak, değişik türdeki izolatörler arasında tatmin edici bir karşılaştırma yapmayı sağlayabilecek sayıda birçok analiz yapıldı. Analizler iyi bilinen yapısal analiz program (YAP) SAP2000 kullanılarak yapıldı. Sismik olarak izole edilmiş ve edilmemiş analitik modeller, doğrusal elastik olmayan zaman tanım alanı hesap yöntemiyle analiz edildi. YAP'tan düşey ve yatay deprem bileşenlerinin etkileri sonucu elde edilen analiz çıktıları kullanılarak, ayaklarda ve izolatörlerde bulunan düşey kuvveti ve orta açıklıkta bulunan kirişin açıklık ortası eğilme momenti belirlendi. Son olarak, depremin sadece yatay bileşenlerinden ve hem yatay hem de düşey bileşenlerinden oluşan yüklemelerle alınan sonuçların karşılaştırılması sunuldu.

Anahtar kelimeler: Sismik İzolasyon, Köprüler, Depremin Düşey Bileşeni, Doğrusal Elastik Olmayan Zaman Tanım Alanı, Kuşun Çekirdekli Kauçuk İzolatör.

ACKNOWLEDGEMENTS

I would like to express my deepest gratitude to my supervisor Assoc. Prof. Dr. Uğurhan Akyüz for his guidance and advice throughout the research. Without his guidance and persistent help this dissertation would not have been possible.

I also owe my parents and brother a debt of gratitude for their effort on me in my entire life.

To My Family

who supported me in every endeavor

TABLE OF CONTENTS

LIST OF TABLES

TABLES

LIST OF FIGURES

FIGURES

CHAPTER 1

INTRODUCTION

1.1 Seismic Isolation Philosophy

A structure should remain elastic during seismic excitation to avoid damage and should also retain the ability to undergo large deformations to facilitate energy dissipation. These demands seem paradoxical with the application of regular structural elements. Therefore, special structural elements should be considered to accomplish these crucial two extremes. The seismic isolation systems can be accounted for the special structural elements which provide structural elements stress levels in elastic range and energy dissipation by large deformation capability.

There are two types of special structural elements which help improving seismic performance of a structure, first type is isolation devices and the second type is dissipation devices. The first type of elements (Isolation devices) have the main objective to increase the period of vibration of the structure towards a lower amplification range of the response spectrum for the design ground motion, thus reducing the input energy (i.e. force demand) into the structure; The second type of elements (Dissipation devices) provide mainly the supplemental damping thus reducing the displacement demand on structural or non-structural elements. Commonly, the combination of these kinds of devices will define a seismic isolation or base isolation system. As mentioned above, seismic isolation gives the opportunity of decoupling of the isolated portion of the structure from horizontal earthquake motion. This is executed by the base isolation bearings' lateral stiffness' being small comparing with the structures’ lateral stiffness. As a result of decoupling, there is a significant change of fundamental period of the isolated structure. In this case, the shifted period corresponds in the out of range of the predominant period of seismic excitation. Eventually, magnitudes of seismic loads are expected to be reduced remarkably.

Deformed shape of a structure exposed to earthquake tells the advantages of seismically isolation clearly.

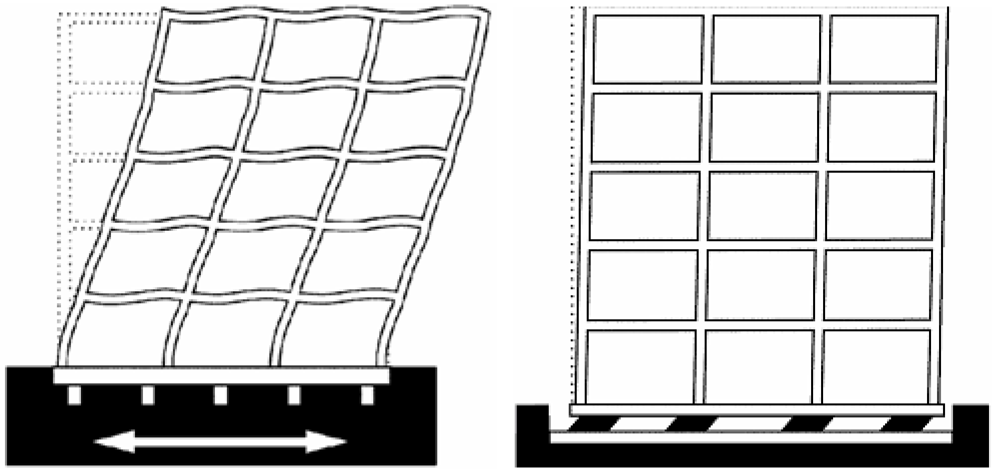

(a) (b)

Figure 1.1.1 Deformed Shape of (a) A Fixed Base Structure (b) A Seismically Isolated Structure. [1]

Figure 1.1.1 (a) and (b) illustrates deformed shapes of a fixed base structure and seismically isolated structure. It can be seen from deformed shape (a) that the structure makes rigid frame motion. As a result, earthquake effects are withstood by frames so stresses are generated in structural members. Especially, beam-column connections are the most vulnerable locations. In other words, all structural members tend to keep their position in case of lateral loads. This tendency leads to the stress concentration at beam-column connections. On the other hand, deformed shape (b) shows a rigid body motion which means structural members make very little deformation comparing to isolation system members. This leads to damping of earthquake effects in isolation system members without affecting structural members.

1.2. Aim

In this study one type of bridge with seismic isolation and without seismic isolation is considered. The investigated bridge type can be classified as lightweight structure. Hence, use of seismic isolation leads to an importance against vertical ground motions regarding weight of the structure.

From this point of view, the study intends to investigate the influence of vertical earthquake excitation on the response of briefly two alternatives of the same type of bridge through seven earthquakes. First alternative is seismically isolated steel girder composite bridge. Second is a regular steel girder composite bridge. Lead rubber bearings are used for seismic isolation. The intention of studying same type of bridge with seismic isolation and without seismic isolation is to be able to reach a comparison regarding influence of vertical component of earthquakes. Additionally, in order to reach more realistic and satisfactory comparisons between isolators on same bridge, a set composed of nine isolators which have different characteristic properties is used. Time history analyses are conducted using the structural analysis software SAP2000 [14]. For each earthquake two separate analysis cases are defined. Horizontal only and horizontal plus vertical ground motions are involved in time history analysis in order to compare the effects of vertical ground motion against horizontal ground motion. As a result response data collected from the analyses is used to determine the vertical load on the piers and isolators and middle span moment on the steel girders due to the earthquake excitations. A comparison between all configurations is introduced and discussed.

In the following chapter isolator properties and types are presented. Then Chapter 3 describes seismic isolation on bridges specifically. Moreover, Chapter 4 mentions the analysis cases used for the study and gives the internal force outputs deeply. Then, Chapter 5 introduces comparisons and discussions on response spectrums, member forces and bridges with and without seismic isolation. Finally, Chapter 6 presents conclusion of the study with the overall outcome attained as a result of the investigations.

1.3. Literature Survey

Vertical earthquake effect on bridges is a serious issue since it has considerable contribution to design stresses of structural members. This is why several studies regarding the vertical earthquake loads on bridges have been performed so far. Most of the studies focused on vertical ground motion influence on bridges without seismic base isolation.

A study by K. Kunnath, et al. [2] indicate that, studies in the past have clearly identified several potential issues that deserve additional attention. The study is undertaken with the objective of assessing the current provisions in The Caltrans Seismic Design Criteria (SDC) 2006 [3] for incorporating vertical effects of ground motions in seismic evaluation and design of ordinary highway bridges. In the code, it is required to take into account the vertical ground motion for ordinary highway bridges where the site peak rock acceleration is 0.6g or greater. In order to consider the vertical ground motion an equivalent static vertical load required to be applied to the superstructure to estimate the effects of vertical acceleration. The loading procedure aims to perform a separate analysis to check nominal capacity of superstructure against loading stated in SDC 006. As a result of the study, two major conclusions were found. First, vertical ground motions have significant effects on the axial force demand in columns. Second, vertical ground motions have significant effects on moment demands at the middle of the span. Particularly, for the case of the shear demand and shear capacity fluctuations. It should also be noted that axial forces vary at much higher frequencies than lateral forces. Hence, the sudden shifts in shear capacity as the column goes from compression to tension may require further investigation. On the other hand, the study concludes the amplification of negative moments in the midspan section as the primary issue that needs to be involved in the SDC-2006. In particular, the current requirement that vertical ground motions be considered only for sites where the expected peak rock acceleration is at least 0.6 g is considered not to be an adequate basis to assess the significance of vertical effects. According to K. Kunnath et al. a more detailed SDC criteria shall be created about the design specification for the consideration of vertical effects by means of a static load equivalent to 25% of the dead load applied in the upward direction.

P. Warn and S. Whittaker [4] work vertical earthquake loads on seismic isolation systems in bridges. The study summarizes and presents sample results from earthquake simulation testing performed on a bridge model isolated with low damping rubber bearing and lead rubber bearings. Results from the testing program were used to investigate the influence of vertical excitation on the vertical load carried by the isolation system and the axial load of individual bearings. As a result of simulations, significant amplifications in the vertical response for both the low damping rubber bearing and lead rubber bearing bridge configurations were experimentally observed. However from a comparison of amplification factors for both the isolated and fixed-base configurations estimated using spectral analysis suggests the isolation system itself results in only a marginal increase in amplification over the fixed-base bridge for the model and systems considered in the study. Hence, those results suggest that the vertical flexibility of the bridge-isolation system should not be ignored for design. Use of the peak ground acceleration of the vertical component would underestimate the vertical earthquake load on the isolation system. They concluded that, the spectral analysis procedure considering the full vertical stiffness of the isolator lead to more reasonable and accurate estimates of the vertical earthquake load on the isolation system for the bridge model and isolation systems.

One of the studies on seismically isolated bridges is done by M. Dicleli and S. Buddaram [5]. The study covers effect of isolator and ground motion characteristics on seismically isolated bridges. They show that, the maximum isolator displacement decreases as the A_p/V_p ratio of the ground motion increases or the V^2_p/A_p ratio of the ground motion decreases. A_p and V_p are peak ground acceleration and peak ground velocity, respectively. The dependency of the maximum isolator displacement on the A_p/V_p (or V^2_p/A_p) ratio of the ground motion indicates that the choice of the seismic ground motion according to the characteristics of the bridge site is crucial for a correct design of the seismically isolated bridge. In [5], it is also indicated that the maximum isolator displacement increases as the A_pW/Q_d ratio increases. W and Q_d are tributary weight of bridge superstructure and isolator characteristic strength, respectively. The isolator design displacement capacity is considered to be generally governed by AASHTO's [6] minimum isolator displacement requirement for ground motions with A_p/V_p ratios larger than 9. For ground motions with low A_p/V_p ratio the characteristic strength of the isolator is found to have less significant effect on the maximum isolator force than maximum isolator displacement. In [5] it is revealed that for the same A_pW/Q_d ratio, the isolator displacement is linearly proportional to the magnitude of the peak ground acceleration. Thus, if the ground motion is scaled by a factor, the characteristic strength needs to be increased by a factor much larger than that to keep the magnitude of the isolator displacement within a prescribed limit.

Furthermore, the post-elastic stiffness of the isolator is observed to have a significant impact on the magnitude of the maximum isolator force. Generally, it increases with increasing post-elastic stiffness of the isolator. The variation of the maximum isolator force as a function of the post-elastic stiffness becomes important for ground motions with low A_p/V_p ratio.

N. Makris and J. Black [7] investigates the ‘’goodness’’ of peak ground velocity as a dependable intensity measure for the earthquake shaking of civil structures. The first of observations were stated in the early 1970s by Bolt [8]. Bolt identified coherent ground velocity pulses radiating from the rapidly slipping fault which results in an energetic wave pattern that was called “fling.” In the late 1970s, Bertero et al [9] described that what makes near-source ground motions particularly destructive to a variety of structures is primarily the area under the relatively long acceleration pulses (~1–1.5s long). Bertero’s explanation is briefly includes the area under the acceleration pulse was to be the ‘’incremental’’ ground velocity in an effort to distinguish between the net increment of the ground velocity along a monotonic segment of its time history and the peak ground velocity that might be the result of a succession of high-frequency one-sided acceleration spikes. In [7] it is revealed that, what is more significant to most civil structures are local, shorter duration acceleration pulses that override the long period pulses which generated unusually large, ground displacements while the motions recorded during the 1999 Chi Chi earthquake exhibit ground displacements on the order of 8 m and ground velocities reaching 3m/s. Additionally, these local acceleration pulses, having a duration of 0.5-1.5s, are merely the destructive acceleration pulses initially identified by Bertero.

G.A. McRae and H. Tagawa [10] undertook a dynamic inelastic time-history analyses of single-degree-of-freedom (SDOF) bilinear oscillators in order to determine the ability of the Coefficient Method (FEMA273/FEMA356) [11] and the Capacity Spectrum Method (ATC-40) [12] to predict the total displacement demands of simple structures. Both the Coefficient Method (CM) and the Capacity Spectrum Method (CSM) were calibrated to obtain the exact inelastic response displacements for near-fault (NF) and far-fault (FF) shaking. As a result of dynamic inelastic analyses of single degree of freedom bilinear oscillators G.A. McRae and H. Tagawa [10] indicates that, oscillators with demands estimated by the CM, and with fundamental periods less than about 0.8s, were not affected significantly by near-fault shaking effects. For longer fundamental period oscillators, oscillator strengths may need to be increased by more than 60% to account for inelastic shaking effects from NF sites in the region of positive directivity compared to that for shaking from Far Fault (FF) or NF near-epicenter sites for the same target displacement ductility. NF shaking did not cause significant trends in the displacement demands of oscillators evaluated by the CSM method.

The severe effects due to near fault (NF) records with directivity leads the selection of ground motions, it is decided to use near fault (NF) records with directivity effects. In this point of view, directivity is an important issue for earthquake selection and needs to be investigated. According to U.S. Geological Survey (USGS) [13] earthquake directivity is the focusing of wave energy along the fault in the direction of rupture. This means that, exclusive of local site conditions such as soft soil, if the earthquake is large enough, ground motions will be distributed in an elongated pattern centered along the axis of the fault. Eventually, there is stronger ground motions and damage. In other words, distance to the fault is not the only consideration for ground motion amplitude: direction is also important. When a fault ruptures unilaterally with the epicenter at or near one end of the fault break, the radiated waves are stronger in one direction along the fault.

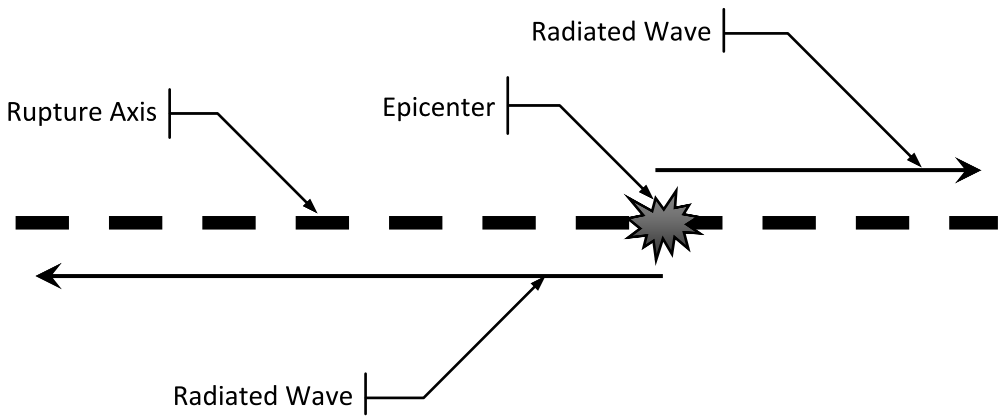

Figure 1.2.1 Map View of a Right-Lateral Strike Slip Fault

Directivity is caused by the constructive interference (piling up) of the S-waves, due to the rupture propagation. Figure 1.2.1 shows a map view of a right-lateral strike slip fault. The dashed line represents the surface projection of the rupture. The star is the epicenter and the arrows which start from the star show the direction of horizontal slip. A real fault is a plane, not a line that may extend deep in the ground. To make the description simple, depth is ignored and only the horizontal component of rupture is discussed. However, usually there is some vertical component to the rupture: some small earthquakes rupture directly up dip.

To understand directivity, the earthquake should be illustrated as a series of small earthquakes, moving outward from the epicenter as shown on Figure 1.2.2.

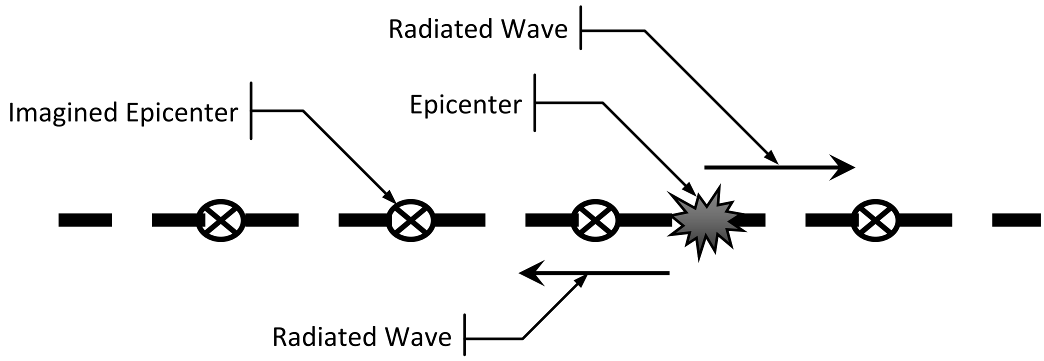

Figure 1.2.2 Map View of a Right-Lateral Strike Slip Fault with imaginary small sub events

In Figure 1.2.2 the asterisks represent the epicenters of the small sub-events or rupture pieces. The arrows move along the fault, from imagined epicenter to imagined epicenter, representing rupture along the fault. As the S-waves from each epicenter travel along the fault, they are reinforced by waves generated by the newly ruptured segments. The closer the rupture velocity to the S-wave velocity, the more the waves reinforce each other and the stronger the directivity. As a rule of thumb, rupture velocities in moderate earthquakes are commonly estimated to be between 50 and 85 percent of S-wave velocity.

CHAPTER 2

SEISMIC ISOLATORS

2.1. Isolator Properties and Types

2.1.1. Theoretical Basis

A brief description is stated herein regarding the theory of seismic isolation. In general, a two mass structural model is assumed to be the

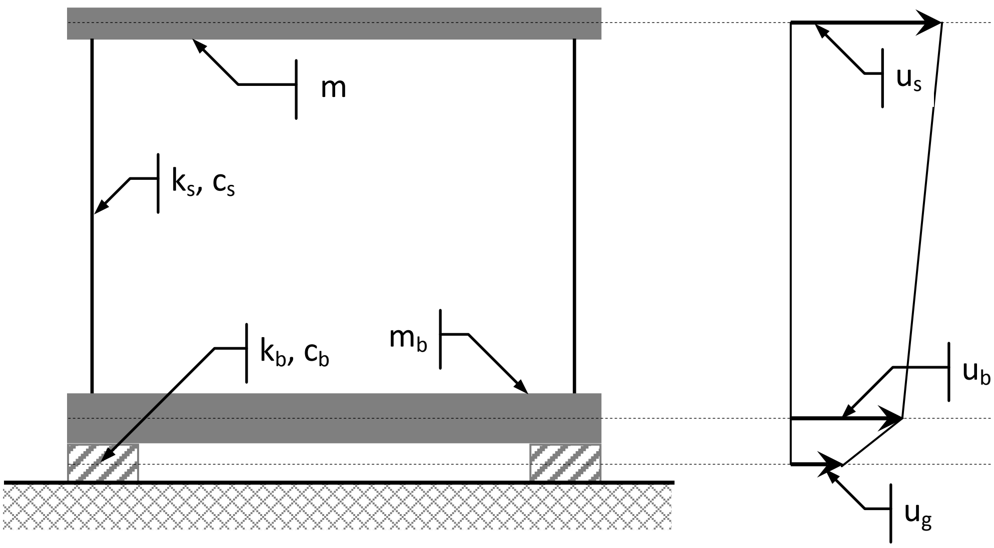

Figure 2.1-1 Two Degree-of-Freedom (DOF) Isolated System

base point of seismic isolation theory. Figure 2.1-1 illustrates the two mass structural model. In the figure, m_s represents the superstructure, m_b represents the mass of base floor above isolation, k_s and c_s are structure stiffness and damping relatively, k_b and c_b are stiffness and damping of isolator relatively and u_s, u_b and u_g are absolute displacements of superstructure, base floor and ground, relatively. Relative displacements can be defined as, *Isolation System Displacement* $: v_b = u_b - u_g$ (Eqn. 2.1-1)

The Interstory Drift $: v_s = u_s - u_b$ (Eqn. 2.1-2)

The equations of motion of two DOF model are,

$$(m + m_b)\ddot{v}_b + m\ddot{v}_s + c_b\dot{v}_b + k_b v_b = -(m + m_b)\ddot{u}_g \quad \text{(Eqn. 2.1-3)}$$

$$m\ddot{v}_b + m\ddot{v}_s + c_s\dot{v}_s + k_s v_s = -m\ddot{u}_g \quad \text{(Eqn. 2.1-4)}$$

In matrix notation,

$$\begin{bmatrix} M & m \\ m & m \end{bmatrix}\begin{pmatrix} \ddot{v}_b \\ \ddot{v}_s \end{pmatrix} + \begin{bmatrix} c_b & 0 \\ 0 & c_s \end{bmatrix}\begin{pmatrix} \dot{v}_b \\ \dot{v}_s \end{pmatrix} + \begin{bmatrix} k_b & 0 \\ 0 & k_s \end{bmatrix}\begin{pmatrix} v_b \\ v_s \end{pmatrix} = -\begin{bmatrix} M & m \\ m & m \end{bmatrix}\begin{pmatrix} 1 \\ 0 \end{pmatrix}\ddot{u}_g$$

(Eqn. 2.1-5)

where $M = m + m_b$

Mass ratio can be defined as

$$\gamma = {}^{m}/_{M} \quad \text{(Eqn. 2.1-6)}$$

And nominal frequencies ω_b and ω_s are

$$\omega_b{}^2 = {}^{k_b}\Big/_{(m + m_b)} \quad \text{(Eqn. 2.1-7)}$$

$$\omega_s{}^2 = {}^{k_s}/_{m} \quad \text{(Eqn. 2.1-8)}$$

Let $\varepsilon = {}^{\omega_b{}^2}\Big/_{\omega_s{}^2}$ and assume $\varepsilon = 0(10^2)$

The damping factors β_b and β_s are

$$2\omega_b\beta_b = {}^{c_b}/_{m + m_b} \quad \text{(Eqn. 2.1-9)}$$

$$2\omega_s\beta_s = {}^{c_s}/_{m} \quad \text{(Eqn. 2.1-10)}$$

In terms of these quantities, the basic equations of motion become

$$\gamma\ddot{v}_s + \ddot{v}_b + 2\omega_b\beta_b\dot{v}_b + {\omega_b}^2 v_b = -\ddot{u}_g \qquad \text{(Eqn. 2.1-11)}$$

$$\ddot{v}_s + \ddot{v}_b + 2\omega_s\beta_s\dot{v}_s + {\omega_b}^2 v_s = -\ddot{u}_g \qquad \text{(Eqn. 2.1-12)}$$

The modes of the isolated system are $\underline{\emptyset}^1$ and $\underline{\emptyset}^2$ where

$$\underline{\emptyset}^{i^T} = \left({\emptyset_b}^i, {\emptyset_s}^i\right) \qquad i = 1, 2$$

With frequencies ω_1 and ω_2. The characteristic equation for the frequencies is

$$(1-\gamma)\omega^4 - ({\omega_s}^2 + {\omega_b}^2)\omega^2 + {\omega_s}^2{\omega_b}^2 = 0 \qquad \text{(Eqn. 2.1-13)}$$

And the solutions to the first order in ε are

$${\omega_1}^2 = {\omega_b}^2(1-\gamma\varepsilon) \qquad \text{(Eqn. 2.1-14)}$$

$${\omega_2}^2 = {{\omega_s}^2}\Big/{1-\gamma}\,(1+\gamma\varepsilon) \qquad \text{(Eqn. 2.1-15)}$$

Also mode shapes with ${\emptyset_b}^i = 1 \quad i = 1, 2$

$$\underline{\emptyset}^{1^T} = (1, \varepsilon) \qquad \underline{\emptyset}^{2^T} = \left\{1, -\frac{1}{\gamma}(1-(1-\gamma)\varepsilon)\right\} \qquad \text{(Eqn. 2.1-16)}$$

Original displacements in modal coordinates,

$$v_b = q_1{\emptyset_b}^1 + q_2{\emptyset_b}^2 \qquad \text{(Eqn. 2.1-17)}$$

$$v_s = q_1{\emptyset_s}^1 + q_2{\emptyset_s}^2 \qquad \text{(Eqn. 2.1-18)}$$

where q_1 and q_2 are time dependent modal coefficients.

We note that modal quantities M_i, L_i are given by

$$M_i = \underline{\emptyset}^{i^T} M \underline{\emptyset}^i \qquad \text{(Eqn. 2.1-19)}$$

$$M_i L_i = \underline{\emptyset}^{i^T} \mathbf{Mr} \qquad \text{(Eqn. 2.1-20)}$$

To first order in ε, modal quantities become,

$$M_1 = M(1 + 2\gamma\varepsilon) \qquad \text{(Eqn. 2.1-21)}$$

$$M_2 = M \; {(1-\gamma)[1 - 2(1-\gamma)\varepsilon]}/{\gamma} \qquad \text{(Eqn. 2.1-22)}$$

$$L_1 = 1 - \gamma\varepsilon \qquad L_2 = \gamma\varepsilon \qquad \text{(Eqn. 2.1-23)}$$

When $v_{b,}$ v_s are expressed in terms of $\underline{\emptyset}^1$ and $\underline{\emptyset}^2$, the modal coefficients q_1, q_2 of the form

$$\ddot{q}_1 + 2\omega_1\beta_1\dot{q}_1 + \lambda_1\dot{q}_2 + {\omega_1}^2 q_1 = -L_1\ddot{u}_g \qquad \text{(Eqn. 2.1-24)}$$

$$\ddot{q}_2 + 2\omega_2\beta_2\dot{q}_2 + \lambda_2\dot{q}_1 + {\omega_2}^2 q_2 = -L_2\ddot{u}_g \qquad \text{(Eqn. 2.1-25)}$$

The terms $2\omega_1\beta_1$and $2\omega_2\beta_2$ are computed from

$$M_i 2\omega_i\beta_i = \underline{\emptyset}^{i^T} \begin{bmatrix} c_b & 0 \\ 0 & c_s \end{bmatrix} \underline{\emptyset}^i \qquad \text{(Eqn. 2.1-26)}$$

From which we obtain

$$2\omega_1\beta_1 = 2\omega_b\beta_b(1 - 2\gamma\varepsilon) \qquad \text{(Eqn. 2.1-27)}$$

$$2\omega_2\beta_2 = {1}/{1-\gamma}\,(2\omega_s\beta_s + 2\gamma\omega_b\beta_b) \qquad \text{(Eqn. 2.1-28)}$$

Results as

$$\beta_1 = \beta_b \left(1 - {}^{3}\!/_{2}\,\gamma\varepsilon\right) \qquad \text{(Eqn. 2.1-29)}$$

$$\beta_2 = {\beta_s + \gamma\beta_b\varepsilon^{0.5}}\Big/{(1-\gamma)^{0.5}\left(1 - \frac{\gamma\varepsilon}{2}\right)} \qquad \text{(Eqn. 2.1-14)}$$

The coupling coefficient λ_1 and λ_2 are computed from

$$\lambda_1 M_1 = \underline{\emptyset}^{1^T} \begin{bmatrix} c_b & 0 \\ 0 & c_s \end{bmatrix} \underline{\emptyset}^2 \qquad \text{(Eqn. 2.1-32)}$$

$$\lambda_2 M_2 = \underline{\emptyset}^{2^T} \begin{bmatrix} c_b & 0 \\ 0 & c_s \end{bmatrix} \underline{\emptyset}^1 = \lambda_1 M_1 \qquad \text{(Eqn. 2.1-33)}$$

Therefore,

$$\lambda_1 M_1 = (1, \varepsilon) \begin{bmatrix} c_b & 0 \\ 0 & c_s \end{bmatrix} \binom{1}{-a} = c_b - \varepsilon a c_s \qquad \text{(Eqn. 2.1-34)}$$

where,

$$a = {}^{1}\!/_{\gamma}\,[1 - (1-\gamma)\varepsilon] \qquad \text{(Eqn. 2.1-35)}$$

Substituting M_1, M_2 into the Eqn. 2.1-32 and Eqn.2.1-33,

$$\lambda_1 = \frac{2\omega_b\beta_b M - \varepsilon\left\{\frac{1}{\gamma}[1-(1-\gamma)\varepsilon]\right\} 2\omega_s\beta_s m_s}{M(1+2\gamma\varepsilon)}$$

$$= 2\omega_b[\beta_b(1-2\gamma\varepsilon) - \varepsilon^{0.5}\beta_b] \qquad \text{(Eqn. 2.1-36)}$$

$$\lambda_2 = \frac{2\omega_b\beta_b M - \varepsilon\left\{\frac{1}{\gamma}[1-(1-\gamma)\varepsilon]\right\} 2\omega_s\beta_s m_s}{\frac{M(1-\gamma)}{\gamma}[1-2(1-\gamma)\varepsilon]}$$

$$= 2\omega_b\{\beta_b[1 + 2(1-\gamma)\varepsilon] - \varepsilon^{0.5}\beta_s\}^{\gamma}/_{1-\gamma} \qquad \text{(Eqn. 2.1-37)}$$

In most of the structural applications it is assumed that the damping is small enough that the effect of the off-diagonal components (here λ_1, λ_2) are negligible and that the required solution can be obtained from the uncoupled modal equations of motions.

$$\ddot{q}_1 + 2\omega_1\beta_1\dot{q}_1 + {\omega_1}^2 q_1 = -L_1\ddot{u}_g \qquad \text{(Eqn. 2.1-38)}$$

$$\ddot{q}_2 + 2\omega_2\beta_2\dot{q}_2 + {\omega_2}^2 q_2 = -L_2\ddot{u}_g \qquad \text{(Eqn. 2.1-39)}$$

If the time history of the ground motion $\ddot{u}_g(t)$ is known, then modal components $q_1(t), q_2(t)$ are computed from

$$q_1 = -\frac{L_1}{\omega_1}\int_0^t \ddot{u}_g\,(t-\tau)e^{-\omega_1\beta_1\tau}\sin\omega_1\tau\,d\tau \qquad \text{(Eqn. 2.1-40)}$$

$$q_2 = -\frac{L_2}{\omega_2}\int_0^t \ddot{u}_g\,(t-\tau)e^{-\omega_2\beta_2\tau}\sin\omega_2\tau\,d\tau \qquad \text{(Eqn. 2.1-41)}$$

Also maximum value estimates of $q_1,\ q_2$ can be given by

$$|q_1|_{max} = L_1 S_D(\omega_1, \beta_1) \qquad \text{(Eqn. 2.1-42)}$$

$$|q_2|_{max} = L_2 S_D(\omega_2, \beta_2) \qquad \text{(Eqn. 2.1-43)}$$

where $S_D(\omega, \beta)$ is the displacement response spectrum for the ground motion $\ddot{u}_g(t)$, at frequency ω and damping factor β.

In order to estimate the various response quantities from the peak spectral values, it is necessary to use the Square Root of Some of Squares (SRSS) method. The values of the maximum isolation system displacement and structural deformation are given by

$$|v_s|_{max} = \left[\left({\emptyset_2}^1 |q_1|_{max}\right)^2 + \left({\emptyset_2}^2 |q_2|_{max}\right)^2\right]^{0.5} \quad \text{(Eqn. 2.1-44)}$$

$$|v_b|_{max} = \left[\left({\emptyset_1}^1 |q_1|_{max}\right)^2 + \left({\emptyset_1}^2 |q_2|_{max}\right)^2\right]^{0.5} \quad \text{(Eqn. 2.1-45)}$$

Substituting Eqn. 2.1-42 and Eqn. 2.1-43 obtained from $\emptyset_1$, $\emptyset_2$, $|q_1|_{max}$, $|q_2|_{max}$ into Eqn. 2.1-44 and Eqn. 2.1-45, then,

$$|v_s|_{max} = \varepsilon\{(1-2\gamma\varepsilon)^2[S_D(\omega_1,\beta_1)]^2 + [1-2(1-\gamma)\varepsilon]^2[S_D(\omega_2,\beta_2)]^2\}^{0.5}$$

(Eqn. 2.1-46)

$$|v_b|_{max} = \{(1-\gamma\varepsilon)^2[S_D(\omega_1,\beta_1)]^2 + \gamma^2\varepsilon^2[S_D(\omega_2,\beta_2)]^2\}^{0.5}$$

(Eqn. 2.1-47)

The term $\varepsilon^2 S_D(\omega_2,\beta_2)$ can be neglected with earthquake spectra where the displacement at high frequencies $(i.e., \omega_2)$ is much smaller than at lower frequencies $(i.e., \omega_1)$. Then

$$|v_b|_{max} = (1-\gamma\varepsilon)S_D(\omega_1,\beta_1) \quad \text{(Eqn. 2.1-48)}$$

Also terms higher than ε^2 can be neglected. Then

$$|v_s|_{max} = \varepsilon[S_D(\omega_1,\beta_1)^2 + S_D(\omega_2,\beta_2)^2]^{0.5} \quad \text{(Eqn. 2.1-49)}$$

Additionally, the base shear coefficient, C_S is

$$C_S = \left| {}^{k_s v_s}/_{m} \right|_{max} = {\omega_s}^2 |v_s|_{\max} \quad \text{(Eqn. 2.1-50)}$$

Substituting Eqn. 2.1-49 into Eqn. 2.1-50, C_S becomes,

$$C_S = {\omega_s}^2 \varepsilon[S_D(\omega_1,\beta_1)^2 + S_D(\omega_2,\beta_2)^2]^{0.5}$$

$$= [S_A(\omega_1, \beta_1)^2 + \varepsilon^2 S_A(\omega_2, \beta_2)^2]^{0.5} \qquad \text{(Eqn. 2.1-51)}$$

Thus, considering only the first terms leads to

$$|v_s|_{max} = {}^{\varepsilon S_V}/_{\omega_b} = \varepsilon S_D(\omega_b, \beta_b) \qquad \text{(Eqn. 2.1-52)}$$

$$|v_b|_{max} = {}^{S_V}/_{\omega_b} = S_D(\omega_b, \beta_b) \qquad \text{(Eqn. 2.1-53)}$$

The design base shear coefficient C_S is

$$C_S = {}^{k_s v_s}/_{m} = \omega_s{}^2 v_s \qquad \text{(Eqn. 2.1-54)}$$

Becomes

$$C_S = \omega_b S_V \left[1 + \varepsilon^2 \frac{\omega_2{}^2}{\omega_1{}^2}\right]^{0.5} = S_A(\omega_b, \beta_b) \left(1 + \frac{\varepsilon}{1-\gamma}\right)^{0.5}$$

$$\cong S_A(\omega_b, \beta_b) \qquad \text{(Eqn. 2.1-55)}$$

indicating that for small and a typical design spectrum, the isolation system can be designed, at least in the initial phase, for a relative base displacement of $S_D(\omega_b, \beta_b)$ and the building for base shear coefficient $S_A(\omega_b, \beta_b)$. The reduction in base shear as compared with a fixed-base structure, where $C_S = S_A(\omega_b, \beta_b)$ is given by

$$\text{Reduction in Base Shear} = {}^{S_A(\omega_b, \beta_b)}\Big/_{S_A(\omega_s, \beta_s)} \qquad \text{(Eqn. 2.1-56)}$$

Which for a constant velocity spectrum is $\omega_b \ / \ \omega_s$ or roughly of order $\varepsilon^{0.5}$; this underestimates the reduction in base shear because, in general β_b will be larger than β_s.

2.1.2. General Features

Seismic isolation is used to increase the period of vibration of a rigid structure. Thus the isolator reduces the amount of the seismic input energy on the system by dissipation. The functions of an isolator can be summarized as follows,

I. Supporting gravity loads with high stiffness
II. Providing lateral flexibility (period shift)
III. Providing restoring force
IV. Energy dissipation by hysteresis
V. High lateral rigidity under service loads (wind loads)

Depending on the area of use and ability several types of anti-seismic devices exist. Common types of anti-seismic devices are:

- Elastomeric bearings: Natural Laminated, Lead Core Rubber Bearing (LRB) and High Damping Rubber Bearing (HDRB);
- Friction Dampers;
- Metallic Dampers: yielding steel systems, lead extrusion devices;
- Viscous and Viscoelastic Dampers: Taylor Devices;
- Self-centering Dampers: Shape Memory Alloys, Energy Dissipation Restraints, SHAPIA Devices;
- Lock-up Devices.

Among these types the most commonly used ones are the elastomeric devices and the friction dampers. However this study investigates deeply the response of structures with only elastomeric bearings. On the other hand, in order to understand the force-displacements relationships of all common types; friction, viscous and hysteretic behaviors are discussed.

2.1.2.1. Friction Behavior

Sliding devices shows friction behavior and are grouped in two types depending on the surface types. Sliding devices with spherical sliding surface of radius R_b (e.g. Friction Pendulum Bearings) and vertical force through the device N_{sd}, provide a restoring force proportional to the design displacement u_d (Figure 2.1-2);

$$F_{restoring} = {N_{sd}}/{R_b}\, u_d \qquad \text{(Eqn. 2.1-57)}$$

and force displacement relationship considering small displacement approximation given in Eqn. 2.1-58.

$$F_{max} = {N_{sd}}/{R_b}\, u_d + \mu_d N_{sd}\, \mathrm{sign}(u) \qquad \text{(Eqn. 2.1-58)}$$

where, μ_d is the coefficient of friction between sliding device surfaces.

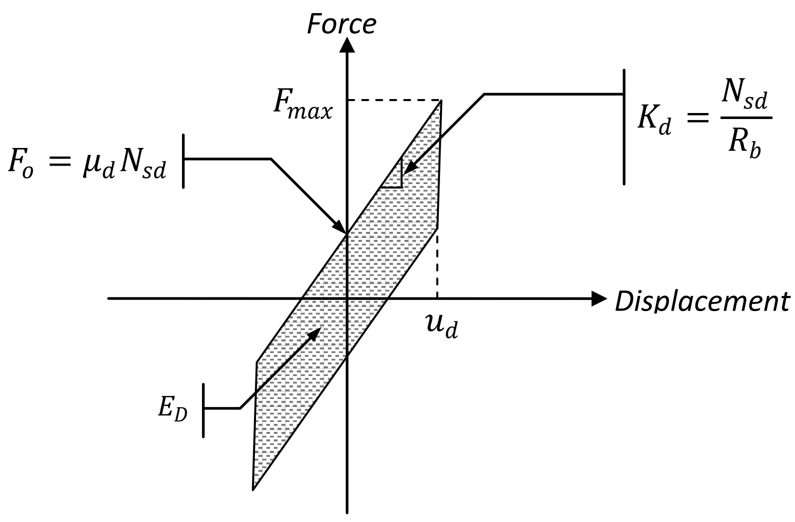

Figure 2.1-2 Sliding Friction Hysteretic Behavior for Curved Surfaces

Secondly, sliding devices, with flat sliding surface, limit the force transmitted to the superstructure to

$$F_{max} = \mu_d N_{sd} \, \mathrm{sign}(u) \quad \text{(Eqn. 2.1-59)}$$

Since these devices don't have the ability to restore back to its original position after a substantial offset displacement, they should be used in combination with the devices providing adequate restoring force. Force-displacement relationship of the flat surface sliding devices is illustrated on Figure 2.1-3.

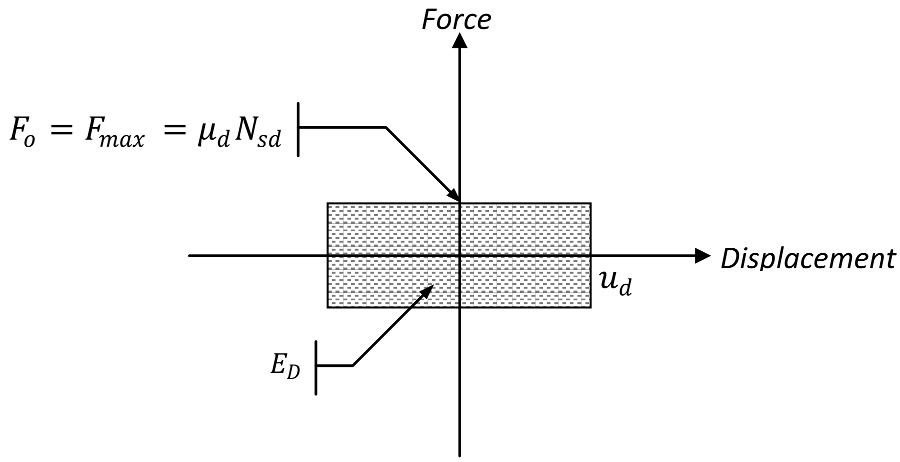

Figure 2.1-3 Sliding Friction Hysteretic Behavior for Flat Surfaces

2.1.2.2. Viscous Behavior

The force applied by viscous devices is proportional to v^{α}, where v is the velocity of motion and α is the exponent. Figure 2.1-4 shows the force-displacement relationship of general viscous behavior. The force is zero at the maximum displacement. Hence it does not contribute to the effective stiffness of the isolation system. The force displacement relationship of a viscous device is specific to the value of α.

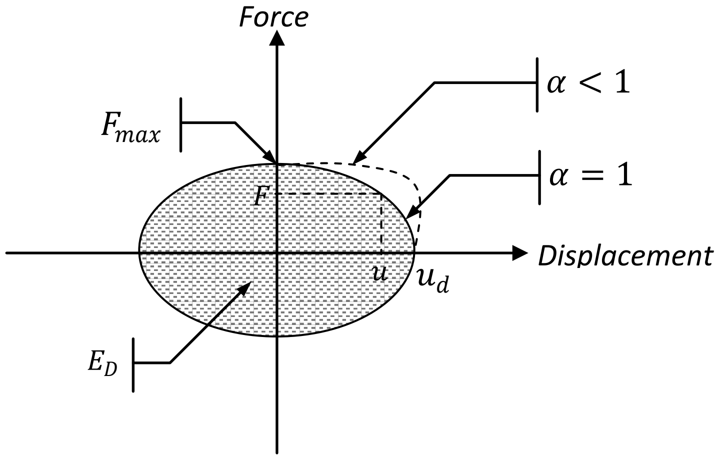

Figure 2.1-4 General Viscous Behavior

2.1.2.3. Hysteretic Behavior

The force-displacement relationship of isolator with hysteretic behavior is approximated by a bilinear relation showed on Figure 2.1-5. Following parameters are defined on the figure.

K_e	: Elastic Stiffness
K_d	: Post Elastic Stiffness
K_{eff}	: Effective Stiffness
F_y	: Yield Force
Q_d	: Characteristic Strength
E_D	: Energy dissipated per cycle at design displacement
u_d	: Design displacement
u_y	: Yield displacement

Hysteretic behavior depends on the effective stiffness. Effective stiffness is the ratio of max. displacement to max. force. Therefore, it is directly related with max. displacement. On the other hand, characteristic strength is related with post elastic and elastic stiffness not the displacement.

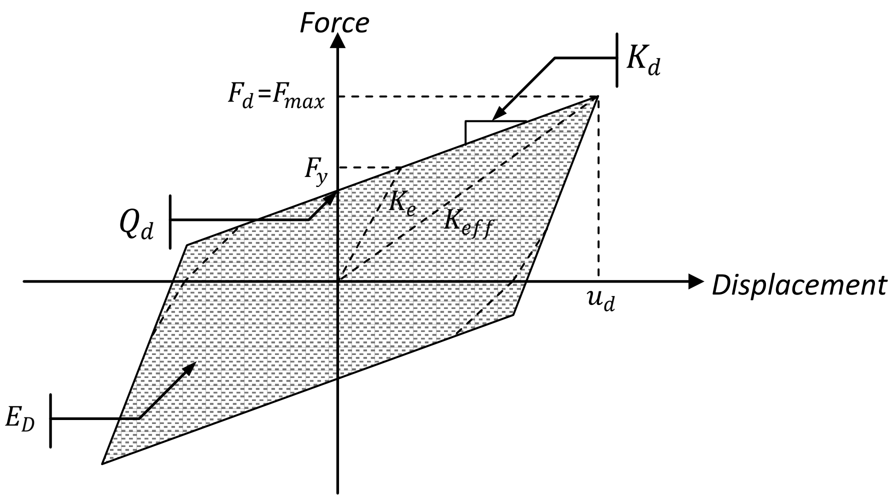

Figure 2.1-5 General Hysteretic Behavior

2.1.3. Isolator Types

There are many seismic isolators. The most commonly used two types are elastomeric bearings and friction pendulum type base isolators. This is why, only these two types are described in detail.

2.1.3.1. Elastomeric Bearings

An elastomeric isolation bearing consists of a number of rubber layers and steel shims, bonded in alternating layers, to produce a vertically stiff but horizontally flexible isolator. The alternating steel and rubber layers act to restrain the rubber layer from bulging laterally. This kind of bearings can provide flexibility and hysteretic/viscous damping forces.

They can be either low damping or high damping bearings. The insertion of a lead plug in an elastomeric isolator provides energy dissipation for seismic response and stiffness for static loads. Elastomeric bearings can be divided into three main groups;

- Natural Laminated Rubber Bearings
- Lead Core Rubber Bearings (LRB)
- High Damping Rubber Bearings (HDRB)

2.1.3.1.1. Natural-Laminated Rubber Bearings

Typical natural-laminated rubber bearings (Figure 2.1-6(a)) have the characteristic properties described in detail hereafter. Low damping elastomeric bearings have an equivalent viscous damping ratio $\xi \approx 0.05$ (±0.01).

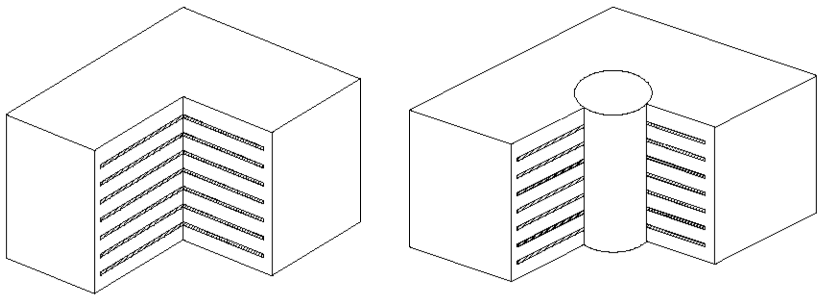

(a) (b)

Figure 2.1-6 Typical View of (a) Laminated and (b) Lead Core Rubber Bearing

❖ Vertical Stiffness

Vertical stiffness is required to determine vertical frequency of the isolator. In general, this parameter is provided by manufacturer but it can also be calculated by Eqn. 2.1-60,

$$K_v = {}^{E_c A}/_{t_r} \tag{Eqn. 2.1-60}$$

Where, E_c : Compression modulus of rubber steel composite under the specified vertical load. (Table 2.1-1)

t_r : Sum of rubber layers thickness.

A : Cross sectional area of steel plate.

Table 2.1-1 Shape Factor and E_c for Different Bearing Shapes

Bearing Shape	Shape Factor ($\mathbb{S}$)	E_c
Infinite Strip	b/t	$4G\mathbb{S}^2$
Circular Pad	$R/2t$	$6G\mathbb{S}^2$
Square Pad	$a/4t$	$6.73G\mathbb{S}^2$

Where, $\mathbb{S}$: Shape factor (Loaded Area/Force-Free Area)

t : Thickness of a single rubber layer.

b : Width of a single rubber layer.

R : Radius of circular pad.

G : Shear modulus.

Vertical stiffness is in the order of 1000-2000MN/m.

❖ Horizontal Stiffness

The actual value of the horizontal stiffness may be affected by the level of the vertical load. But this is neglected and lateral stiffness is calculated by the equation,

$$K_h = {}^{GA}/_{t_r} \tag{Eqn. 2.1-61}$$

and max shear strain,

$$\gamma = {}^{D}/_{t_r} \qquad \text{(Eqn. 2.1-62)}$$

Where, D : Maximum horizontal displacement.

❖ Critical Vertical Load

Since stability is an issue for the isolator similar to stability of column, critical vertical load of the isolator has to be taken into account. Critical vertical load is given by Eqn. 2.1-63,

$$P_{crit} = {}^{\sqrt{2}\pi G A \mathbb{S} r}/_{t_r} \qquad \text{(Eqn. 2.1-63)}$$

Where, r is radius of gyration.

2.1.3.1.2. *Lead Core Rubber Bearings (LRB)*

LRBs (Figure 2.1-6(b)) are same as the laminated bearings but apart from laminated bearings, a lead plug at the center core area of bearing takes place. Figure 2.1-7 shows typical plan view and section of LRB. The numbers given in the figure correspond to the LRB parts given below.

Table 2.1-2 Parts of Lead Core Rubber Bearings (LRB)

Pose Number	Part Description
1	Masonry Bottom Plate
2	Seismic Isolator
3	Steel Plate
4	Lead Plug
5	Vulcanized Top Plate
6	Masonry Top Plate
7	Assembling Bolts
8	Bottom Anchor Bar
9	Bottom Anchor Bolt
10	Top Anchor Bar
11	Top Anchor Bolt

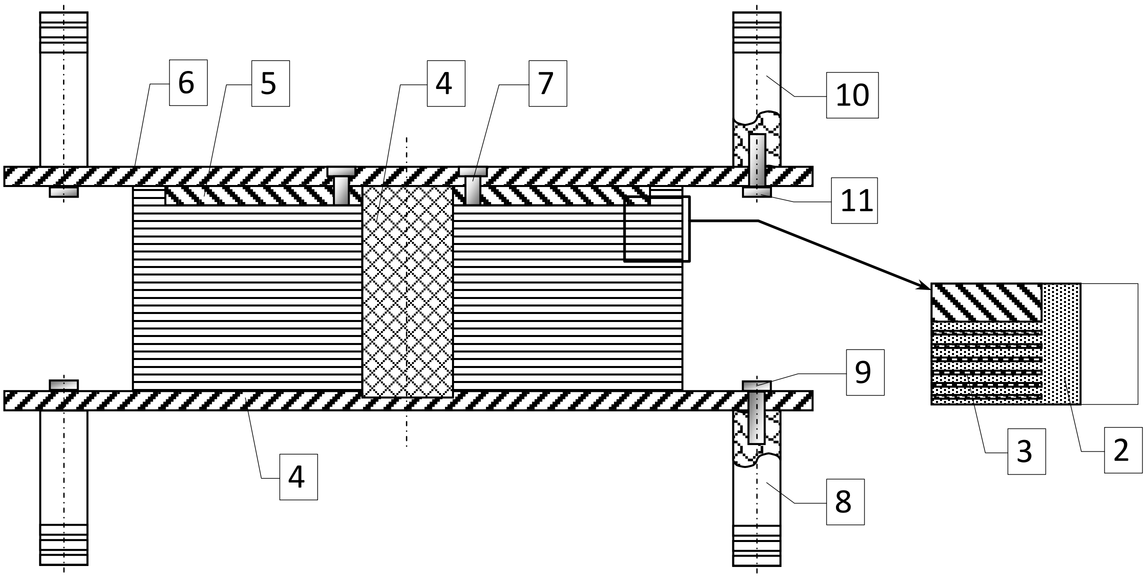

Section A-A

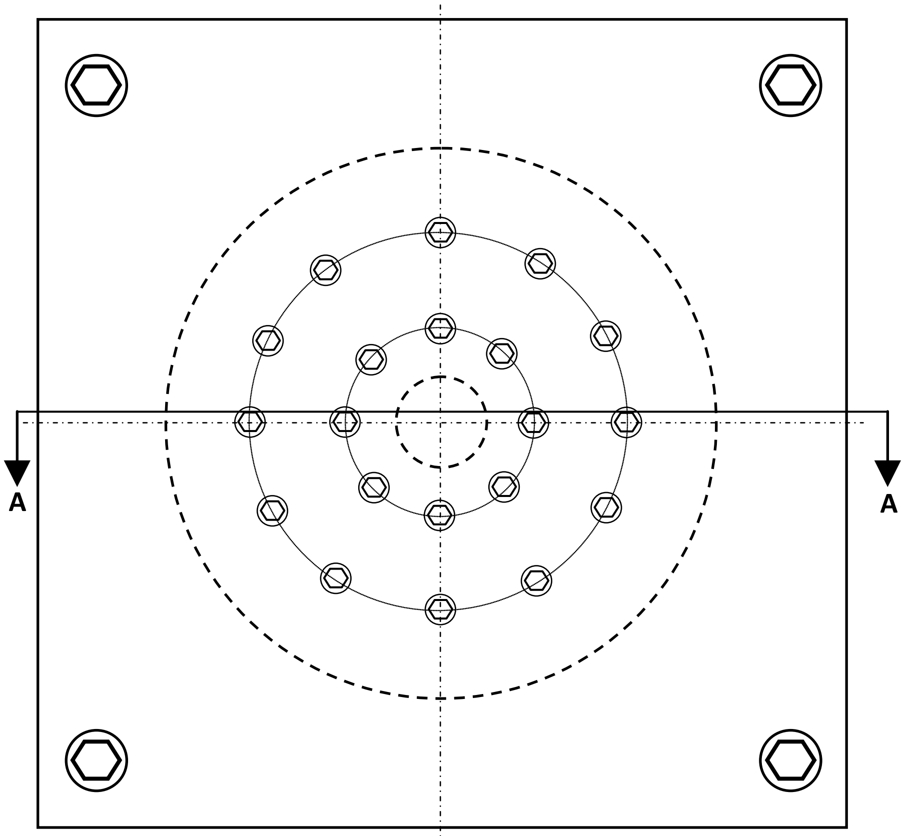

Plan View

Figure 2.1-7 Typical Plan View and Section of Lead Core Bearings

The insertion of lead plug in the bearing provides energy dissipation for lateral loads and vertical stiffness for static loads. LRB always considered to be modeled as bilinear elements. Bilinear element model is shown on Figure 2.1-8.

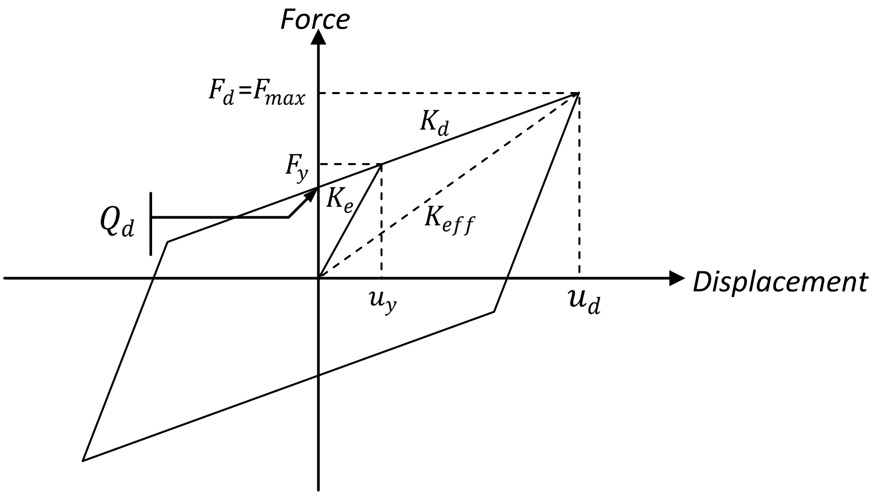

Figure 2.1-8 Bilinear Element Model for Lead Core Bearings

According to parameters provided in the figure mechanical characteristics of LRB are calculated using the equations stated hereafter. Generally, K_e is taken as $10K_d$.

$$K_{eff} = K_e + {}^{Q_d}/_{u_d} \qquad \text{(Eqn. 2.1-64)}$$

In this equation characteristic strength value is estimated from yield stress of lead (≈10.5MPa) and lead core area. Additionally, natural frequency is given by,

$$\omega = \sqrt{{}^{K_{eff}\, g}/_{W}} \qquad \text{(Eqn. 2.1-65)}$$

Where, W : total load on isolator.

Effective damping is given by,

$$\beta_{eff} = {}^{4Q\left(u_d - u_y\right)}\Big/_{2\pi K_{eff} D^2} \qquad \text{(Eqn. 2.1-66)}$$

2.1.3.1.3. High Damping Rubber Bearing(HDRB)

HDRB consist of alternate layers of rubber and steel plates of limited thickness bonded by vulcanization, being able to support vertical loads with limited deflection, due to very high vertical stiffness. As well, they are able to support operating horizontal loads (e.g. wind), with very low displacements.

HDRB can provide both period shift and energy dissipation: the rubber compound presents damping capability, at least corresponding to 10% of equivalent viscous damping, and normally dependent on the bearing displacement. The rubber compound is designed to withstand very large shear deformations, much larger than the standard elastomeric bearings. The rubber compound stiffness is much higher (up to 4 times) for small deformations and reduces for large deformations.

2.1.3.2. Friction Pendulum System

The Friction Pendulum System (FPS) is a sliding restoring device. The system is based on the principle of the sliding pendulum motion. It consists of two sliding plates, one of which with a spherical stainless steel surface, connected by a lentil-shaped articulated slider covered by a teflon-based high bearing capacity composite material. The slider is generally locked on a vertical stud with a special hollowed end which allows free rotation of the slider and a perfect contact with the sliding surface at all times like shown on Figure 2.1-9 .

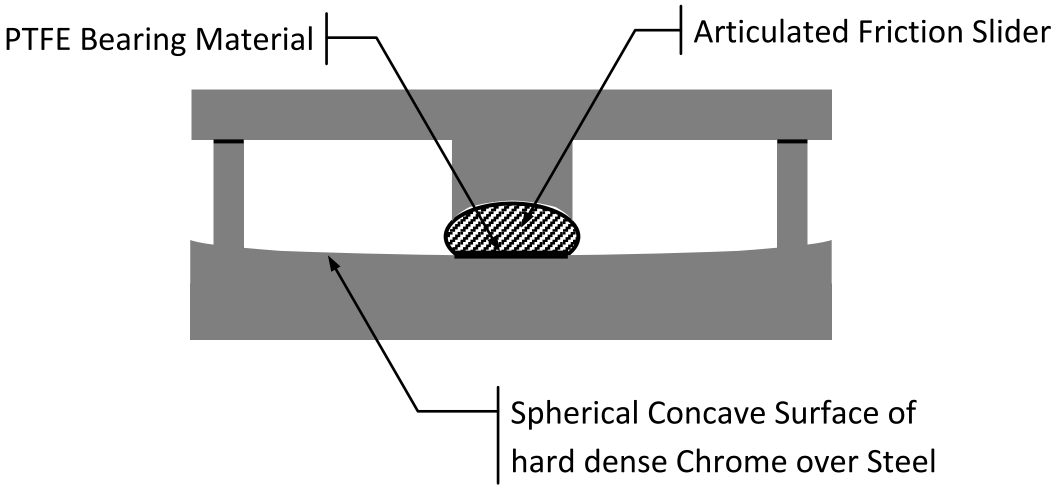

Figure 2.1-9 Typical Section of Friction Pendulum System

During the earthquake, the slider moves on the spherical surface lifting the structure and dissipating energy by friction between the spherical surface and the slider. This motion leads to a period (T) of with radius of curvature of ditch (R),

$$T = 2\pi \sqrt{R/g} \qquad \text{(Eqn. 2.1-67)}$$

and with a total weight on the device (W), the horizontal stiffness of FPS is,

$$K_v = W/R \qquad \text{(Eqn. 2.1-68)}$$

Frictional force which is generated in the device against any lateral motion depends on the materials used in the device. The common practice of friction coefficient (μ) between slider and spherical surface is 0.02-0.03 for very slow slip rates. For typical seismic velocities it ranges around 0.10-0.15 depending on lubrication in both cases. Additionally, effective stiffness (K_{eff}) , effective damping (β_{eff}) of FPS is given as follows,

$$K_{eff} = \left({}^{W}\!/_{R} \right) + \left({}^{\mu W}\!/_{D} \right) \qquad \text{(Eqn. 2.1-69)}$$

$$\beta_{eff} = \left({}^{2}\!/_{\pi} \right) \left({}^{\mu}\!\Big/_{{}^{D}\!/_{R} + \mu} \right) \qquad \text{(Eqn. 2.1-70)}$$

and the resisting force (F), is equal to summation of the restoring force due to the rise of the mass and the friction force between the slider and the concave surface.

$$F = \left({}^{W}\!/_{R} \right) D + \mu W \,(\operatorname{sign} \dot{D}) \qquad \text{(Eqn. 2.1-71)}$$

2.2. *Mathematical Modeling of Isolators*

Mathematical modeling of all types of isolators depends on the idealized models. Since this study investigates deeply, structures with a base isolation system composed of lead rubber bearings, mathematical modeling of other types is not discussed.

While modeling the isolators, characteristic properties provided by the manufacturers are used. The characteristic properties provided are obtained from the experiments made on real specimens by the manufacturers. After the test and interpretation of the results a detailed catalog cut-sheet is prepared and published.

It is well known that there are several commercial softwares available for the analysis of structures. In this study SAP2000 [14] is used for the analysis of the steel composite bridge models with seismic isolation and without seismic isolation.

Mathematical modeling of isolators depends on especially type of analysis. The input parameters vary with the linear or nonlinear analysis. For linear analysis, linear isolator model involving definition of linear elastic properties of isolators is used. On the other hand, for nonlinear analysis, bilinear isolator model involving effective properties of isolators is used.

In this study isolators are modeled as nonlinear link elements. Hence, effective stiffness, damping, yield strength and post yield stiffness ratio are defined. By definition, yield strength is the force at yield of isolator. Post yield stiffness ratio stands for ratio of plastic stiffness to elastic stiffness. This ratio is usually taken as 0.1 for design purposes. The basic characteristic properties are chosen from a manufacturers catalog cut-sheet. Furthermore, other mentioned properties for nonlinear analyses are calculated to be used on the analyses program. 9 different commercially available isolators are investigated in the study. All isolators are chosen from LRB in order to investigate the response with damping. The overall diameters, rubber thicknesses and layers, lead core diameters and all mounting plate properties differ from one isolator to other. Hence, a wide range of isolators are used in the study. Table 2.2-1 shows the characteristic properties and calculated additional properties of the isolators which are used for modeling. In the table, bold letters and numbers show the calculated properties and the rest are taken from the manufacturer's cut-sheet. Additionally, the labels of the commercially available isolators are shown as *ISO-XX* where *XX* is suffix starting from 01 to 09. Therefore the difference that comes out in results may be distinguished easily.

Moreover, Figure 2.2-1 shows a typical bilinear model with the characteristic properties of *ISO-01*. Figure 2.2-1 illustrates which property corresponds to where on a typical bilinear model of an isolator. On other hand, Figure 2.2-2 shows all of the isolators with their input parameters on the same graph. This figure may be identified as a comparative graph which is showing the variety between properties of used isolator.

Table 2.2-1 Characteristic Properties and Calculated Additional Properties of the Selected Isolators

Isolator ID	Isolator Diameter	Isolator Height	# Rubber Layers	Lead Diameter	Post Yield Stiffness	***Elastic Stiffness***	Compression Stiffness	***Effective Stiffness***	Characteristic Strength
	D_I	H	N	D_L	K_d	$\boldsymbol{K_e}$	K_v	$\boldsymbol{K_{eff}}$	Q_d
	mm	mm		mm	kN/mm	***kN/mm***	kN/mm	***kN/mm***	kN
ISO-01	355	150	5	0-100	0.20	***2.00***	100.00	***0.85***	65.00
ISO-02	455	175	6	0-125	0.30	***3.00***	100.00	***0.96***	110.00
ISO-03	570	205	8	0-180	0.50	***5.00***	500.00	***1.25***	180.00
ISO-04	800	230	8	0-230	0.70	***7.00***	1000.00	***1.48***	265.00
ISO-05	900	255	9	0-255	0.70	***7.00***	1400.00	***1.65***	355.00
ISO-06	1050	305	12	0-305	0.90	***9.00***	2100.00	***2.13***	580.00
ISO-07	1260	355	16	0-355	1.20	***12.00***	3700.00	***2.60***	755.00
ISO-08	1360	405	18	0-380	1.40	***14.00***	5100.00	***2.95***	890.00
ISO-09	1550	455	22	0-405	1.80	***18.00***	6500.00	***3.49***	1025.00

Table 2.2-1 Characteristic Properties and Calculated Additional Properties of the Selected Isolators (continued)

Isolator ID	Maximum Displacement	***Design Displacement***	***Yield Displacement***	Axial Load Capacity	***Effective Damping***	***Design (max) Strength***	***Post-Yield Stiffness ratio***	*Yield Strength*
	u_{max}	u_d	u_y	P_{max}	β_{eff}	F_d	K_d/K_e	F_y
	mm	***mm***	***mm***	kN		***kN***	***kN***	*kN*
ISO-01	150	***100***	***36***	700.00	***0.31***	***85.00***	***0.10***	*72.22*
ISO-02	250	***167***	***41***	1150.00	***0.33***	***160.00***	***0.10***	*122.22*
ISO-03	360	***240***	***40***	1800.00	***0.32***	***300.00***	***0.10***	*200.00*
ISO-04	510	***340***	***42***	4000.00	***0.29***	***503.00***	***0.10***	*294.44*
ISO-05	560	***373***	***56***	5800.00	***0.31***	***616.33***	***0.10***	*394.44*
ISO-06	710	***473***	***72***	8500.00	***0.31***	***1006.00***	***0.10***	*644.44*
ISO-07	810	***540***	***70***	20500.00	***0.30***	***1403.00***	***0.10***	*838.89*
ISO-08	860	***573***	***71***	27600.00	***0.29***	***1692.67***	***0.10***	*988.89*
ISO-09	910	***607***	***63***	40000.00	***0.28***	***2117.00***	***0.10***	*1138.89*

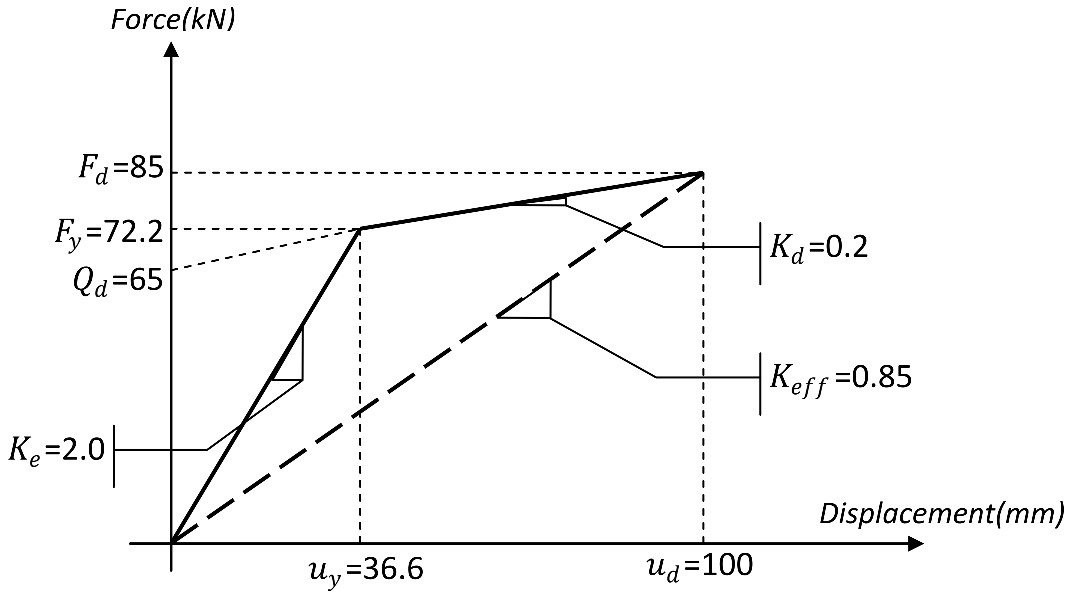

Figure 2.2-1 Typical Bilinear Isolator Model (*ISO-01*)

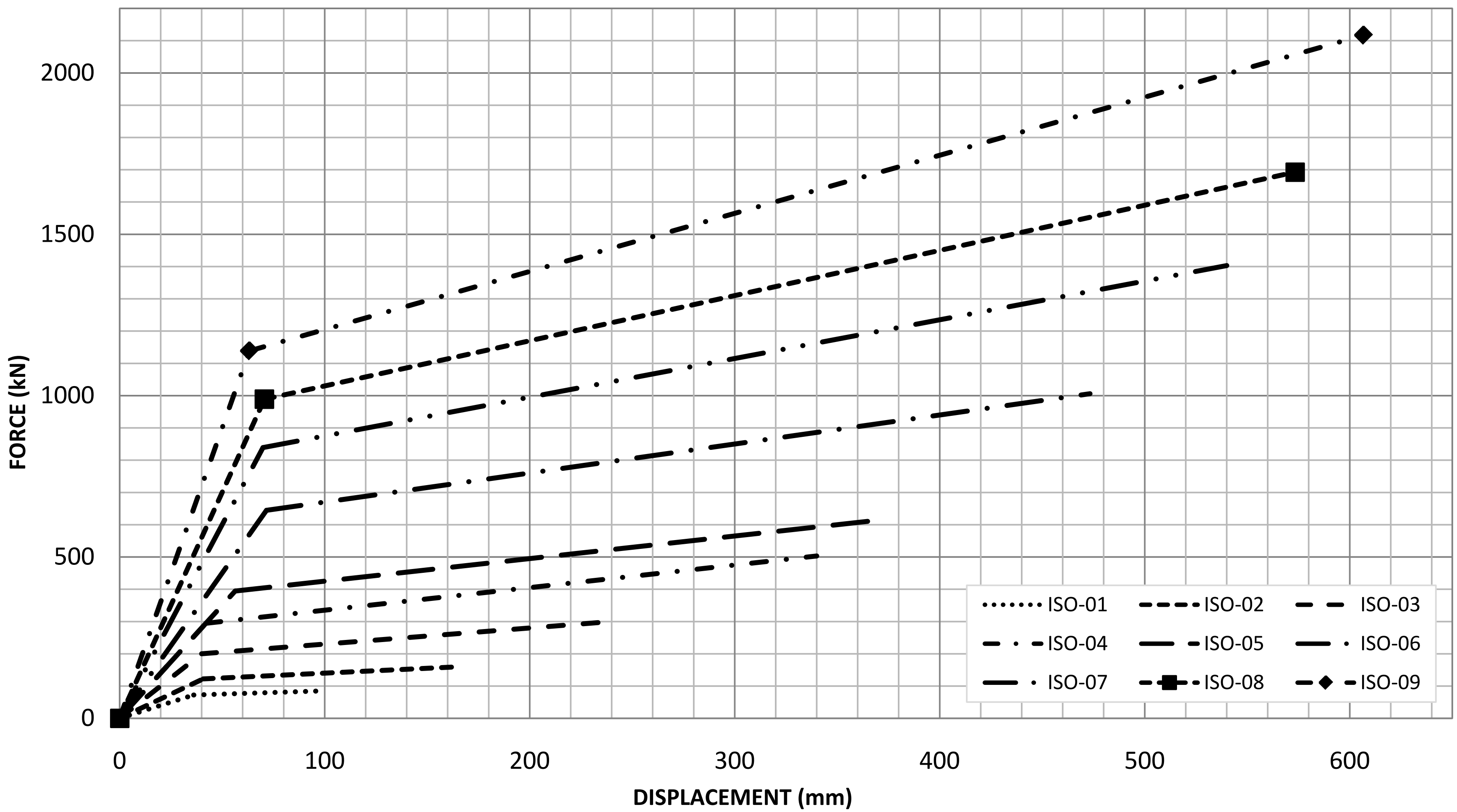

Figure 2.2-2 Comparative Graph of Bilinear Models for Chosen Isolators

CHAPTER 3

SEISMIC ISOLATION ON BRIDGES

3.1. Introduction to Seismic Isolation on Bridges

Seismic isolation devices like elastomeric bearings and friction pendulums are described in detail so far in order to provide foreground information related with the seismic isolation in general. In this respect, the following questions arise. Which isolation system is used at which conditions or on which structures? Eventually, each type of isolation system can be used on all types of structures unless the system is located at the correct location of the structure. The selection of the type of system depends on several issues like site conditions, engineer's judgment and economical needs of the structure. Therefore, the design directly governs the selection of system. It is important to discuss the location of seismic isolation systems on a structure. These systems aim to provide a separation of superstructure from substructure. Since, substructure is directly restrained by ground in most cases, it is stiffer than superstructure. This is the common idea behind the selection of location of seismic isolation system. For instance, on buildings, isolators are used beneath columns over foundation. Figure 3.1-1 shows an onsite application of seismic isolators on a building. Also, all devices are connected to each other by beams. Connecting the isolators to each other is a common practice for application of seismic isolation systems on buildings. Hence, all of the isolation system elements show same deformation when the structure is exposed to a lateral load.

In some cases, seismic isolation systems are preferred to distinguish two stiff structural systems from each other to prevent transformation of lateral load to each other. On bridges the aim of use of seismic isolation systems are more likely to the second case described.

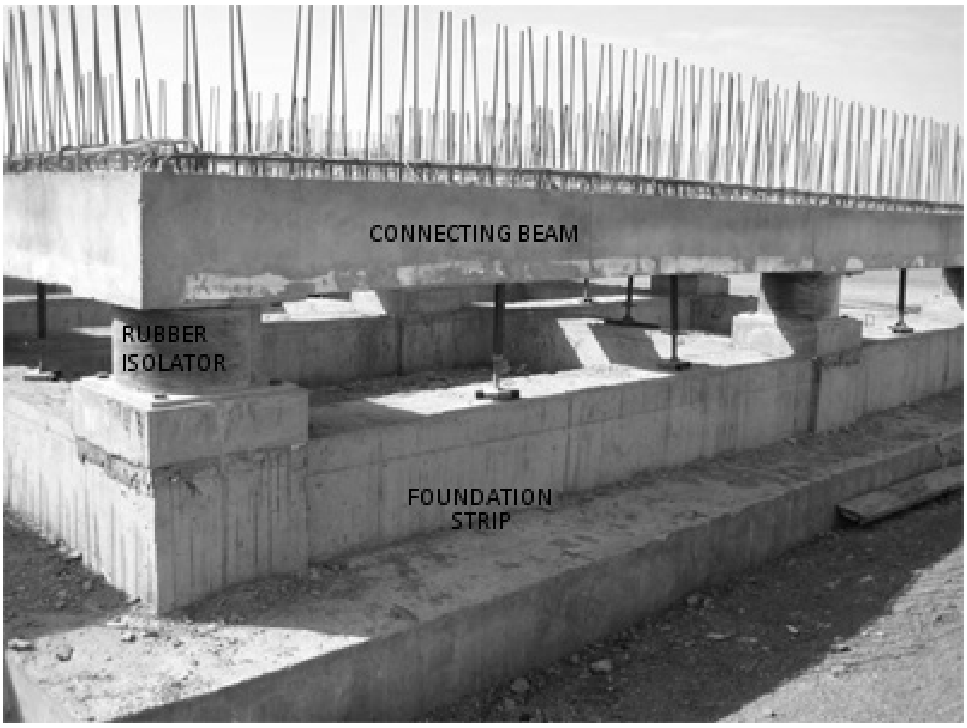

Figure 3.1-1 Seismic Isolator on a Building [15]

In general, bridges are composed of two structural systems: substructure and superstructure. Substructure is composed of abutments, piles piers and diaphragm beams. Steel and reinforced concrete (R/C.) structural beams and R/C deck form the superstructure. The interface between substructure and superstructure is the location of seismic isolation system on seismically isolated bridges. In detail, the seismic isolation elements like isolators are located beneath the structural beams and top of the piers. Figure 3.1-2 shows the location of isolators used on a bridge with post tensioned girder. It can be seen from figure that isolators are placed at the top of each column. As a result the seismic isolation system is formed to provide energy dissipation between substructure and superstructure by alleviating the effect of earthquake forces from substructure to the superstructure.

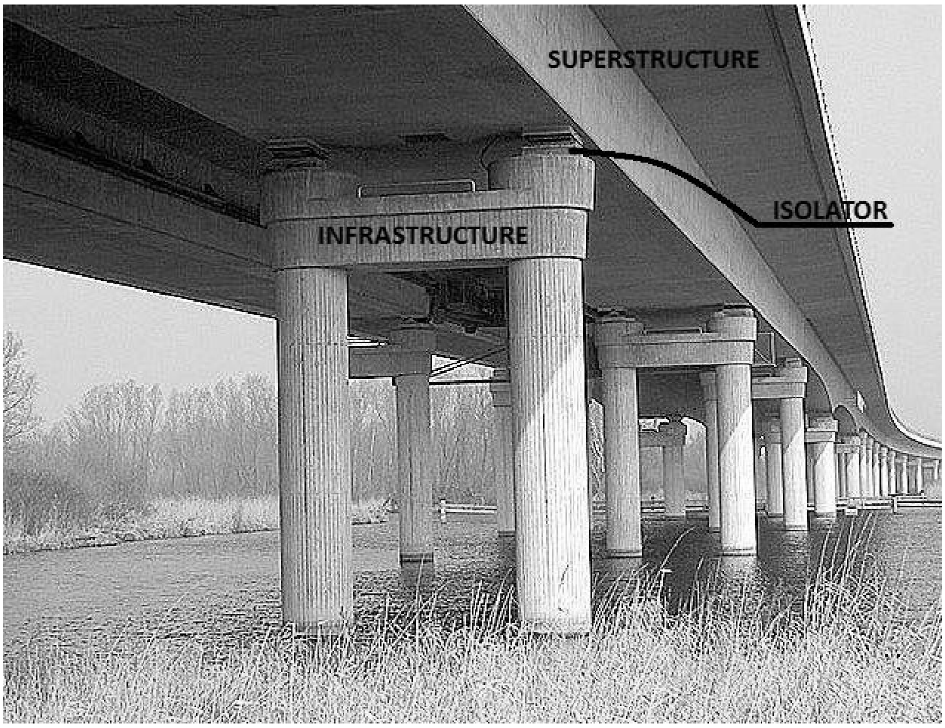

Figure 3.1-2 Seismic Isolator on a Bridge [16]

Today, several new structural elements are developed by means of investigations and technology such as pre-tensioning, post-tensioning suspension cables, seismic isolators, etc. Each technological development creates new chances to construct more special bridges. Particularly, seismic isolation systems enable to construct long span bridges than the ones constructed in the past. Because of the capability of separating substructure and superstructure, the superstructure of bridges don't prone to carry the loads transmitted from substructure due to earthquakes. Figure 3.1-3 shows an example of how long bridges can be constructed today by means of seismic isolation systems.

Figure 3.1-3 Seismically Isolated Bridge [17]

3.2. *Bridge Specifications and Properties*

Bridge selection is the most important step in this study regarding the ability to observe the excitation due to vertical ground motion.

Type of bridge clearly implies that what type of structural system will be preferred. Here, it is well worth telling some major structural systems classified by how the principle forces are distributed throughout the structure. It is known that most of the bridges employ all of the principle forces to some degree, however only some of them predominate. These principle forces are grouped as compression, tension, bending and shear. Figure, 3.2-1 shows the bridge taxonomic chart grouped by lineage and principle forces employed. In general, type of the bridge within a construction site act on efficiency of it. The efficiency of a bridge may be classified as structural and economic efficiency. In a few words, structural efficiency is the ratio of carried load to weight of the bridge. Additionally, economic efficiency (site and traffic dependent) is the ratio of savings by constructing the bridge instead of other alternatives to its lifetime cost (materials, labor, machinery, engineering, cost of money, insurance, maintenance, refurbishment, and ultimately demolition and associated disposal, recycling, and reuse). On the issue of both efficiencies, following examples indicate how site specific properties govern selection of the bridge type. Bridges employing only compression are thought to be structurally inefficient, but may be highly cost efficient where suitable materials are available near the site and the cost of labor is low. For medium spans, trusses or box beams are usually most economical, while in some cases, the appearance of the bridge may be more important than its cost efficiency. Also, the longest spans usually require suspension bridges due to their ease of construction and safety.

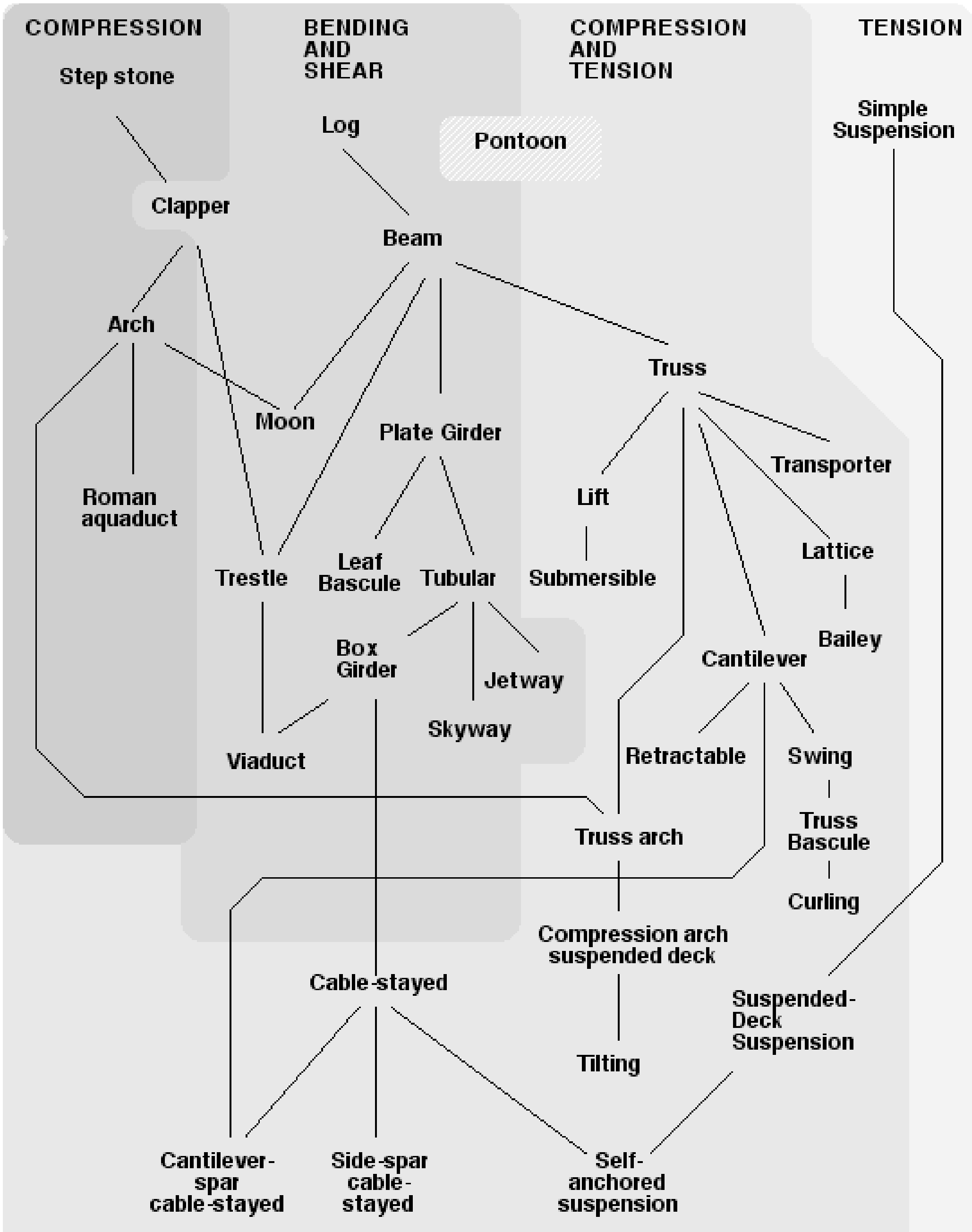

Figure 3.2-1 Bridge Taxonomic Chart by Principle Forces Employed [18]

In this study a steel girder composite bridge is considered because it is in the group of beam type bridges (see Figure 3.2-1). As a result, influences on bending of beam can be observed. Also, composite steel girder bridge may be classified as relatively more lightweight than other type bridges.

The made up steel girder composite bridge which was investigated in an earlier study done by M. Eröz, R. DesRoches [19],has been chosen (See Figure 3.2-2). This is a regular steel girder bridge with R/C piers and piles. The fundamental structural elements are derived from the previous study and developed through this study. After developing the bridge an initial design is performed in order to see whether the bridge is complying with the AASHTO [6] provisions or not. For this reason, main girder and R/C piers are checked against major loads applied to the bridge. For the sake of safety of initial design, AASHTO Strength I [20] load combination limit state is used. Strength I load combination involves dead load and live load with load factors 1.25 and 1.75, respectively. After adequate number of iterations on sections, the structural elements of the bridge are finalized.

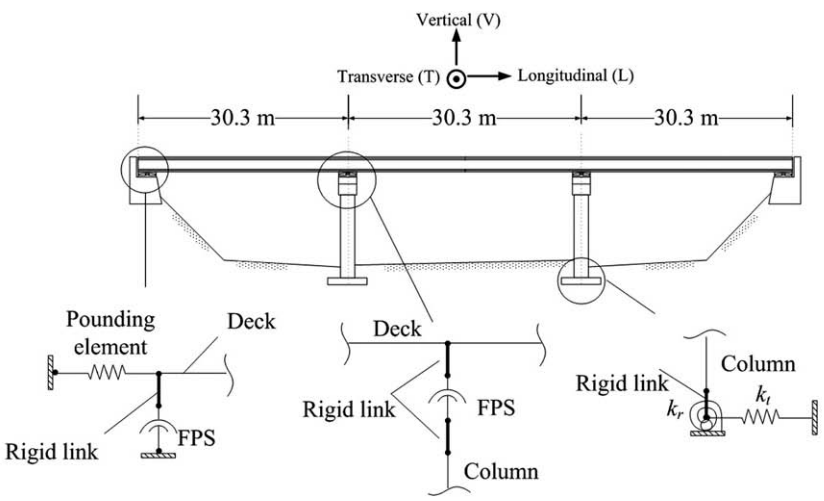

Figure 3.2-2 Original Bridge Configuration Used for Developing the Bridge [21]

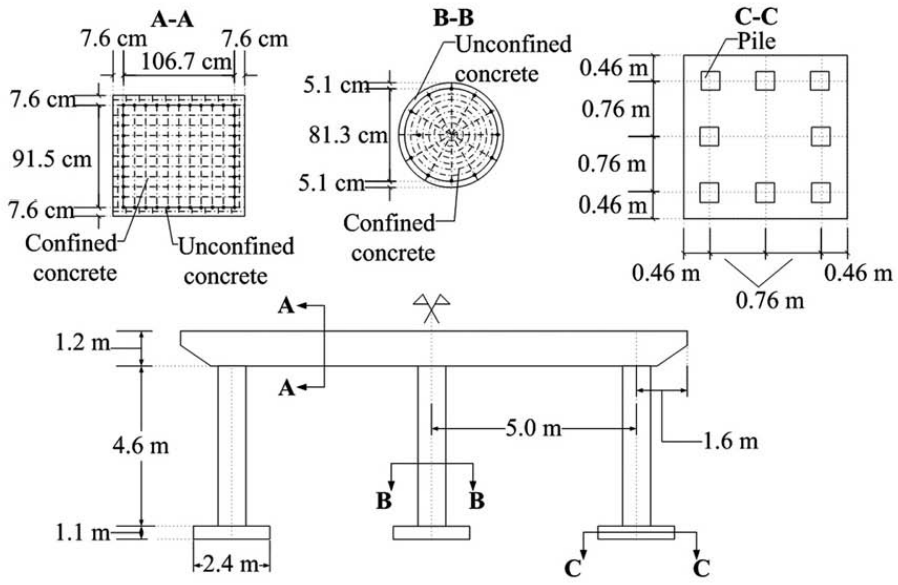

Figure 3.2-2 Original Bridge Configuration Used for Developing the Bridge [21] (continued)

Following sectional element properties with the given material properties are considered in this study. Concrete is thought to be C-35 per TS-500 [22] classification and for steel it is thought to be St-52 per TS-648 [23] classification. Basic characteristic properties for concrete and steel are shown on Table 3.2-1.

Table 3.2-1 Characteristic Material Properties for Concrete and Steel

Material Property	Concrete C-35	Steel St-52
Modulus of Elasticity *(E)* (GPa)	33	200
Poisson's Ratio	0.2	0.3
Coefficient of Thermal Expansion	9.90E-6	1.17E-5
Shear Modulus *(G)* (GPa)	13.7	77
Concrete Compressive Strength (f'_c) (MPa)	35	N/A
Steel Tensile (Ultimate) Stress (f_u) (MPa)	N/A	510
Steel Yield Stress (f_y) (MPa)	N/A	353

Overall bridge layout is derived from the bridge shown on Figure 3.2-2 so the number of span is 3 and the span length is 30.3m. Figure 3.2-3 and Figure 3.2-4 show elevation of the bridge on the long and on the short axis, respectively. From top to bottom structural members and sectional properties are as follows; R/C deck is 0.25m thick. One of the most important members of the bridge is certainly steel girders. An I shaped steel girder is used. The geometric properties of the steel girder is as follows; depth of the beam is 1.30m, width of top and bottom flanges is 0.40m, thickness of the top and bottom flanges is 0.03m and thickness of the web is 0.02m (Figure 3.2-5). Pier Cap beam is composed of a rectangular section with a width and a height of 1.2m. Circular R/C pier has a diameter of 0.9m and a height of 4.6m. R/C mat foundation has plan dimensions of 3.6m to 3.6m with a thickness of 1.1m. Finally, circular R/C pile has a diameter of 0.45m and a height of 4.5m. Foundation and pile details are illustrated in Figure 3.2-6. Moreover, soil underneath the foundation is considered to be a common soil type of clayey medium dense sand with a subgrade reaction modulus of 35GPa/m [24].

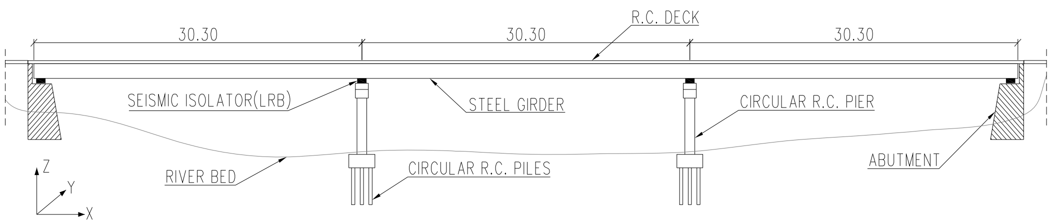

Figure 3.2-3 Bridge Elevation in the Long Axis

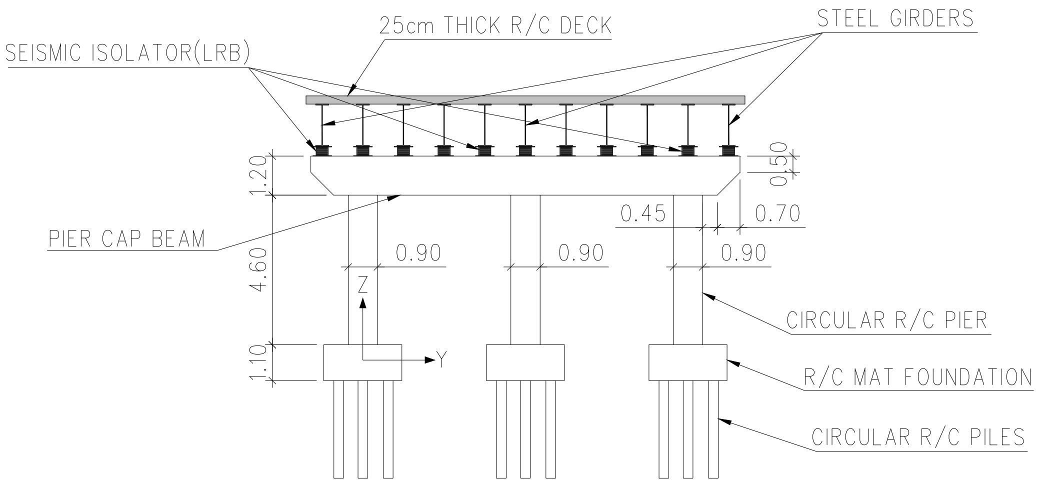

Figure 3.2-4 Bridge Elevation in the Short Axis

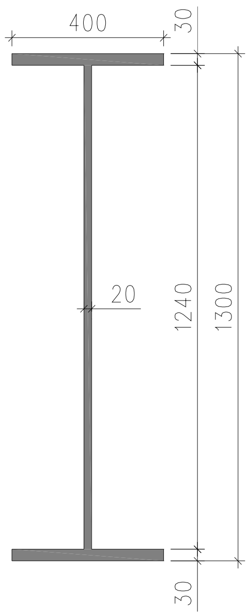

Figure 3.2-5 Geometric Properties of I Shaped Steel Girder

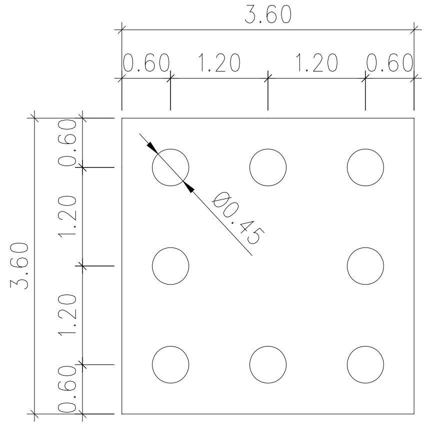

PLAN

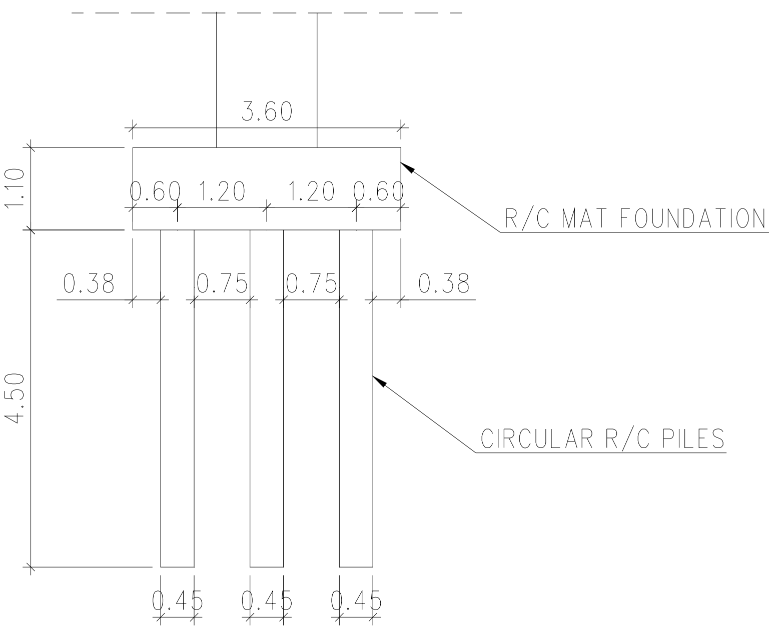

SECTION

Figure 3.2-6 R/C Mat Foundation and R/C Circular Pile Details

3.3. *Mathematical Modeling of Specified Bridge*

To investigate the triaxial ground motion on the studied bridge a 3D model is prepared. Bridge is modeled using the predefined sections and elements like area and frame sections and nonlinear link elements. Additionally, transfer of forces at rigid connection zones are controlled by custom defined rigid link elements. These are made up from frame sections by multiplying piers sectional properties with 100 and 10. Frame section properties are summarized in Table 3.3-1.

Table 3.3-1 Frame Section Properties

Property	Dia. Beam	Pier	Pile	Steel Girder	Cross Beam	Rigid Link
Area *(m^2)*	1.44	0.636	0.071	0.0488	0.009	64
Torsional Constant *(m^4)*	0.292	0.064	7.95E-4	1.0E-5	2.25E-7	0.64
Major Inertia *(m^4)*	0.173	0.032	3.98E-4	0.013	6.08E-4	3.2
Minor Inertia *(m^4)*	0.173	0.032	3.98E-4	3.21E-4	4.30E-5	3.2
Major Shear Area *(m^2)*	1.2	0.573	0.064	0.02	0.005	5.73
Minor Shear Area *(m^2)*	1.2	0.573	0.064	0.026	0.004	5.73
Major Section Modulus *(m^3)*	0.288	0.072	0.003	0.0198	0.002	-
Minor Section Modulus *(m^3)*	0.288	0.072	0.003	0.002	2.9E-4	-
Major Radius of Gyration *(m)*	0.346	0.225	0.075	0.513	0.253	-
Minor Radius of Gyration (*m)*	0.346	0.225	0.075	0.081	0.068	-

Figure 3.3-1 shows complete bridge mathematical model with frame and area sections. It needs to be noted that all elements located at the centerline axis of real elements. Additionally, exact view of the bridge rendered with extruded frame and area sections is given in Figure 3.3-2.

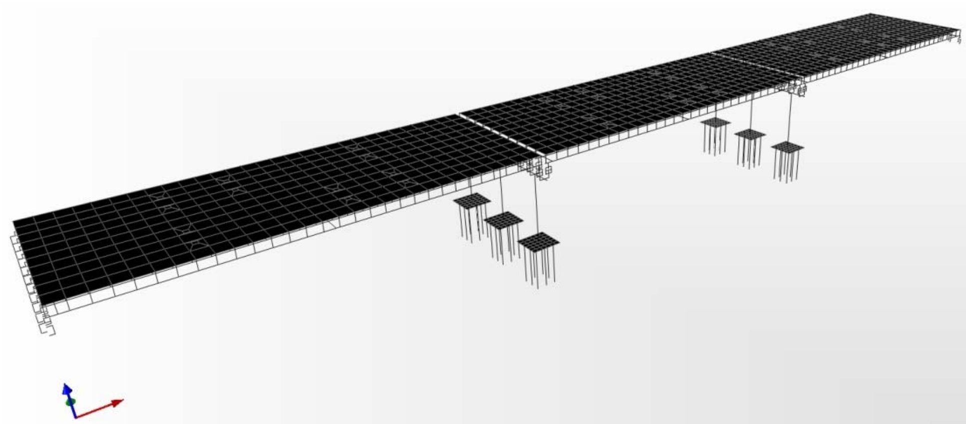

Figure 3.3-1 Complete Mathematical Model of the Bridge

Figure 3.3-2 Complete Mathematical Model of the Bridge-Extruded View

Cross beams between steel girders are modeled as shown in Figure 3.3-3. There are three spans with 11 steel girders and 3 cross beams at each span.

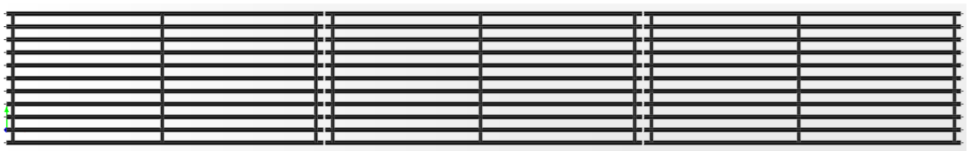

Figure 3.3-3 Steel Girders and Cross Beams-Extruded View

Connection rigid zones are expected to behave much stiffer than normal sections. Therefore, rigid links (RLs) are introduced in model. The main aim of RLs is to transfer forces from one member to another considering the stiff rigid connection zones. RLs are used widely in the model because there are several intersections between sections due to section centerline modeling. Figure 3.3-4 shows section centerline modeling for pier pile and foundation. On figure the foundation as a horizontal element intersects with pier and piles because of its thickness. This is why there are nodes defined on pier and piles at the point of intersection between foundation edge and pier and piles edges. Hence, the frames close to foundation are defined as RLs.

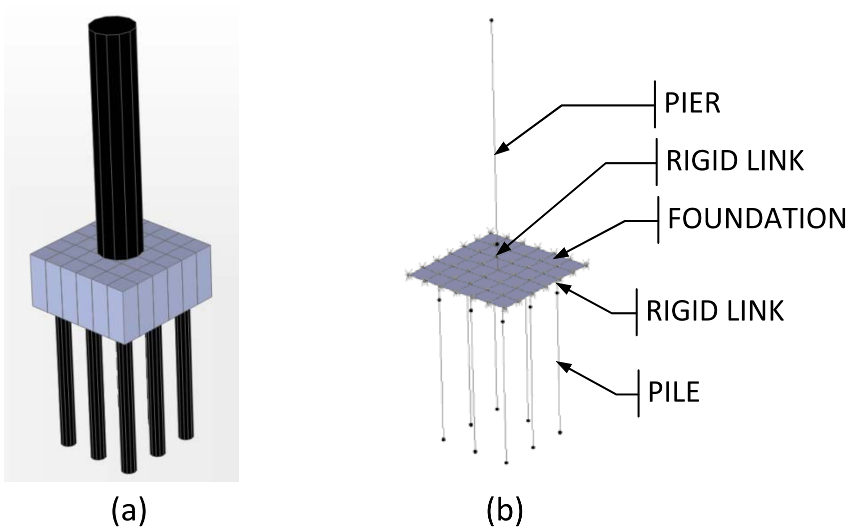

Figure 3.3-4 (a) Extruded Section Model (b) Section Centerline Model

LRBs are modeled just underneath the steel girders as shown on Figure 3.3-5.

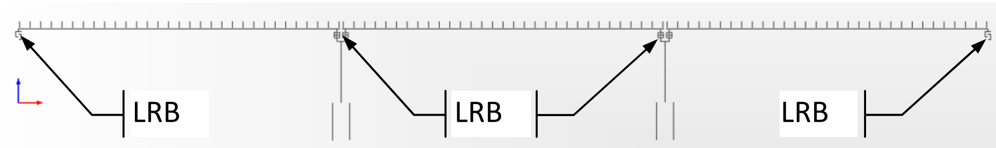

Figure 3.3-5 Locations of LRB on Model

In addition to modeling of structural element, soil-structure interaction is modeled, too. Since the modeling is done in 3D, soil-structure interaction is also defined in a 3D manner. As stated hereunto, soil condition is assumed as clayey medium dense sand and modulus of subgrade reaction equals to 35GPa/m [24]. Soil underneath the mat foundation is neglected due to compaction issues. Just the piles are assumed to provide vertical restraint. In lateral directions foundation is restrained to prevent any deflection in these directions because the lateral deflection is neglected in most of the practical applications. Moreover, since piles are assumed to behave as friction piles, surrounding soil is modeled as line spring in order to act both positive and negative friction forces on piles. Soil structure interaction defined using the spring elements described is a commonly preferred method as studied in [2].

3.4. Selected Ground Motion Properties

Earthquakes (EQ) are generally grouped in accordance with three properties; peak ground accelerations (PGA) and peak ground velocities (PGV), soil classifications and possession of directivity. In this study, soil classifications and possession of directivity are considered as constant parameters and PGA and PGV vary to investigate response of the bridge under different conditions.

Soil classification is described as an important parameter for an EQ since soil properties have direct influences on propagation waves generated by ground motions. Hence, it is decided to choose EQs whose site classes are same for a reasonable comparison. Soil classes are defined according to soil average shear wave velocities in different codes. Table 3.4-1 presents the soil average shear wave velocity ranges for soil classes in USGS, NEHRP [25] and IBC [26]. The table shows that, NEHRP and IBC classification are similar while USGS classification is totally different. In the study, the soil classification criteria of USGS is preferred since the EQs record source Peer Strong Motion Database [27] directly gives soil classification as per USGS and it is chosen as EQs record source. Moreover, a soil class of "C" as per USGS classification is selected for all chosen EQs and stations.

Table 3.4-1 Soil Classifications as per USGS, NEHRP [25] and IBC [26]

Soil Class Designation	Soil Profile	Soil Average Shear Wave Velocity - (m/s)		
		USGS	NEHRP	IBC
A	Hard Rock	≥ 750	≥ 1500	≥ 1520
B	Rock	360 – 750	760 – 1500	762 – 1520
C	Very Dense Soil and Soft Rock	180 – 360	360 – 760	366 – 762
D	Stiff Soil Profile	≤180	180 – 360	183 – 366
E	Soft Soil Profile	-	≤180	≤183

EQs used in this study are classified as being near fault ground motions involving directivity. It is worth to note that, classification of EQs according to criteria stated above is not a part of this study because this is completely a general topic which needs detailed investigation. Therefore, a dependable source is used to see the EQs classified as near fault ground motions involving directivity. The source is a previous study done by G.A MacRae and H. Tagawa [10] which investigates methods to estimate some specific structures using far-fault and near-fault directivity record sets. The near fault directivity record sets in [10] are considered to be a dependable list of near fault ground motions involving directivity.

PGAs and PGVs are very important for grouping EQs. Three components (two horizontal and one vertical) of the EQs are used in the study. The selected EQs' lateral components and vertical components are in the range of 0.268 g to 0.897 g, and 0.242 g to 0.586 g, respectively, regarding PGA. On the other hand, their horizontal components and vertical components are in the range of 46,9 cm/s to 109,3 cm/s and 18,4 cm/s to 38,5 cm/s, respectively, regarding PGV. Seven EQs are considered in this study in order to provide adequate range of ground acceleration and ground velocity. They are sorted by the ratio of SRSS of horizontal peak accelerations to vertical peak acceleration. As a result, a normalized EQs property ratio is formed to be used while constituting comparisons of results.

Table 3.4-2 shows the selected EQs with the specific properties given across. Abbreviations on the table are as follows,

- A_p : Peak ground acceleration,
- V_p : Peak ground velocity,
- $A_{p,HOR}$: SRSS of horizontal peak ground accelerations,
- $A_{p,VERT}$: Vertical peak ground accelerations,
- $A_{p,HOR,max}$: Maximum horizontal peak ground accelerations.

Additionally, Figures 3.4-1 to 3.4-7 shows two horizontal components and one vertical components' acceleration versus time graph for each EQ. For all graphs, X axis shows time in terms of seconds and Y axis shows the acceleration in terms of "g". The EQs time domains for analyses are considered as 15 seconds for all because the peak acceleration and velocity values for the selected EQs are always within the first 15 seconds of the records.

Table 3.4-2 Selected Earthquakes

No	Earthquake	Location	Station	Distance to Fault (km)	USGS Soil Class	Direction	A_p (g)	V_p (cm/sec)	A_p / V_p (1/sec)	$A_{p,HOR}$ (g)	$A_{p,HOR,max}$ / $A_{p,VERT}$	$A_{p,HOR}$ / $A_{p,VERT}$
1	Imperial (15/10/79)	California/ USA	El Centro Array #7	0.6	C	140 (UX)	0.338	47.617	*6.963*	*0.57*	*0.851*	***1.054***
						230 (UY)	0.463	109.261	*4.157*			
						Up (UZ)	0.544	26.310	*20.284*			
2	Imperial (15/10/79)	California/ USA	El Centro Array #5	1.0	C	140 (UX)	0.519	46.857	*10.866*	*0.64*	*0.966*	***1.197***
						230 (UY)	0.379	90.549	*4.106*			
						Up (UZ)	0.537	38.522	*13.675*			
3	Northridge (17/01/94)	California/ USA	Newhall	7.1	C	90 (UX)	0.583	74.878	7.638	0.83	1.077	**1.514**
						360 (UY)	0.590	96.879	5.974			
						Up (UZ)	0.548	31.532	*17.049*			
4	Düzce (12/11/99)	Turkey	Düzce	8.2	C	180 (UX)	0.348	59.990	*5.691*	*0.64*	*1.499*	***1.788***
						270 (UY)	0.535	83.506	*6.285*			
						Up (UZ)	0.357	22.605	*15.493*			

Table 3.4-2 Selected Earthquakes (continued)

No	Earthquake	Location	Station	Distance to Fault (km)	USGS Soil Class	Direction	A_p (g)	V_p (cm/sec)	A_p / V_p (1/sec)	$A_{p,HOR}$ (g)	$A_{p,HOR,max}$ / $A_{p,VERT}$	$A_{p,HOR}$ / $A_{p,VERT}$
						60 (UX)	0.268	65.740	*3.999*			
5	Kocaeli (17/08/99)	Turkey	Yarımca	2.6	C	330 (UY)	0.349	62.177	*5.506*	*0.44*	*1.442*	***1.818***
						Up (UZ)	0.242	30.814	*7.704*			
						52 (UX)	0.612	117.432	*5.113*			
6	Northridge (17/01/94)	California/ USA	Sylmar	6.4	C	142 (UY)	0.897	102.208	*8.609*	*1.09*	*1.531*	***1.853***
						Up (UZ)	0.586	34.587	*16.621*			
						EW (UX)	0.496	64.282	*7.569*			
7	Erzincan (13/03/92)	Turkey	Erzincan	2.0	C	NS (UY)	0.515	83.959	*6.017*	*0.72*	*2.077*	***2.883***
						Up (UZ)	0.248	18.373	*13.242*			

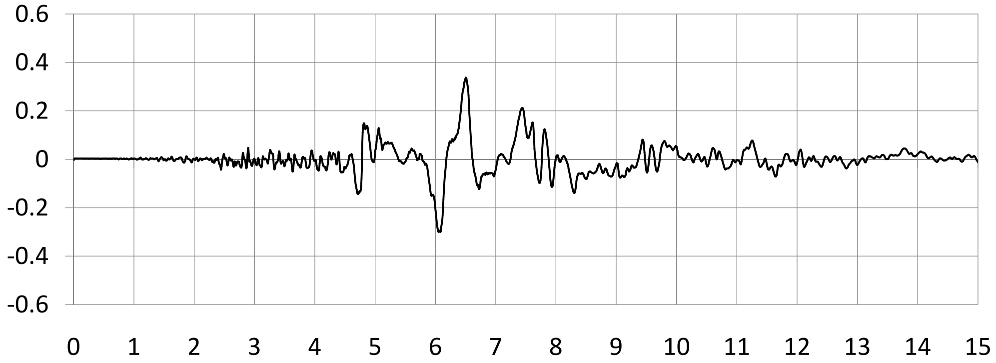

(a)

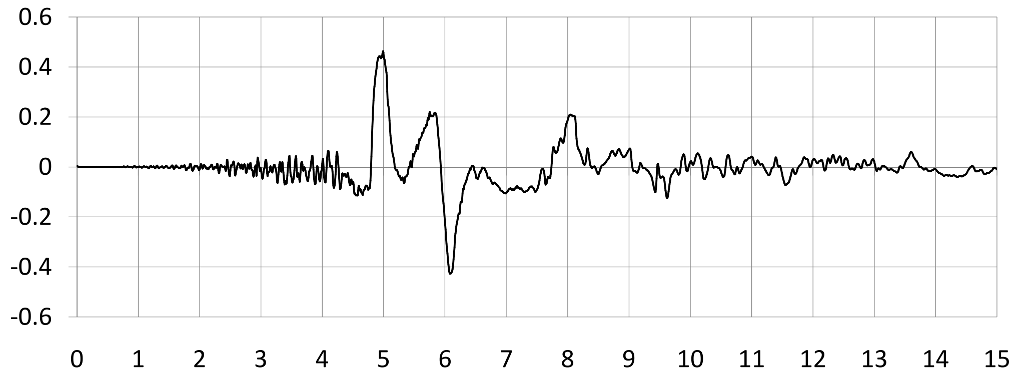

(b)

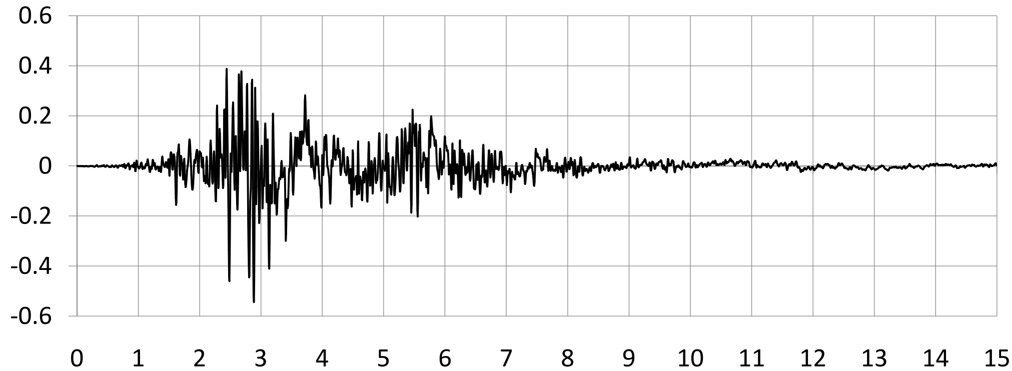

(c)

Figure 3.4-1 Ground Acceleration (g) & Time (s) Graph for Imperial Vlly EQ
Station: El Centro Array #7
Component: (a) 140° (b) 230° (c) Up

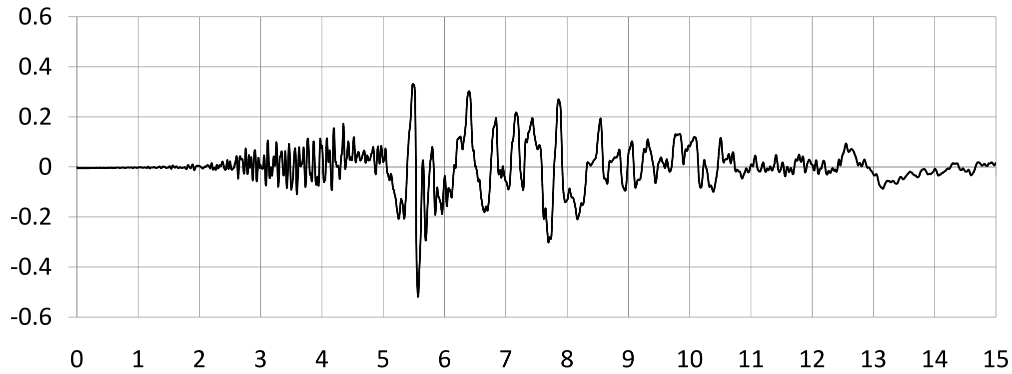

(a)

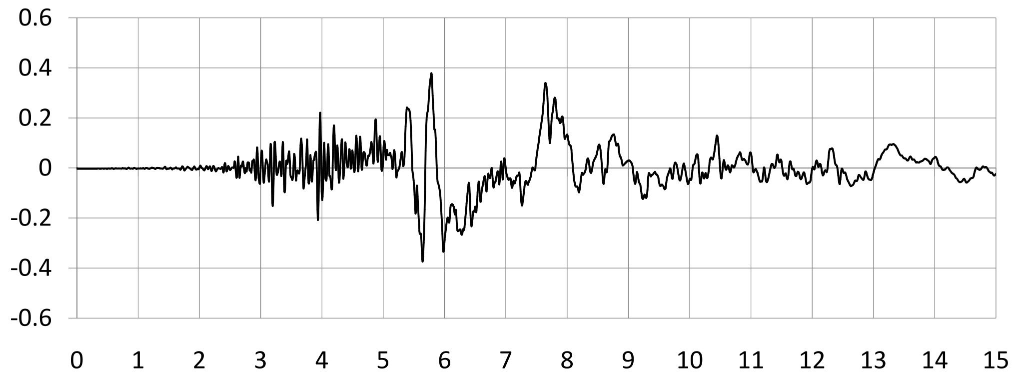

(b)

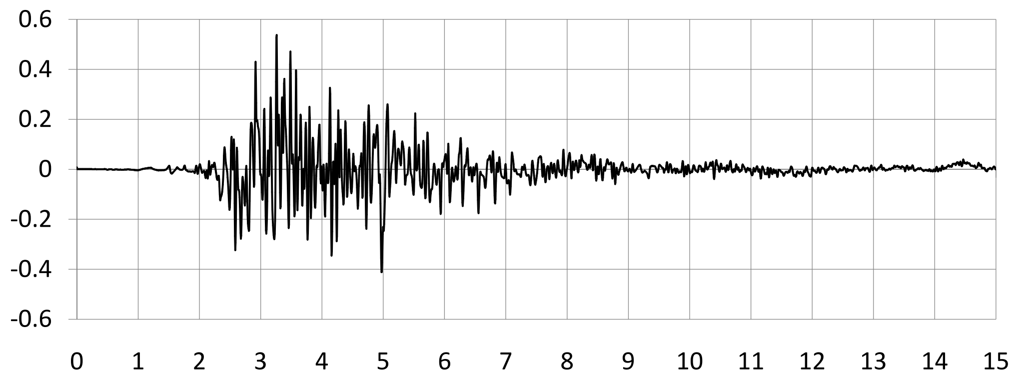

(c)

Figure 3.4-2 Ground Acceleration (g) & Time (s) Graph for Imperial Vlly EQ
Station: El Centro Array #5
Component: (a) 140° (b) 230° (c) Up

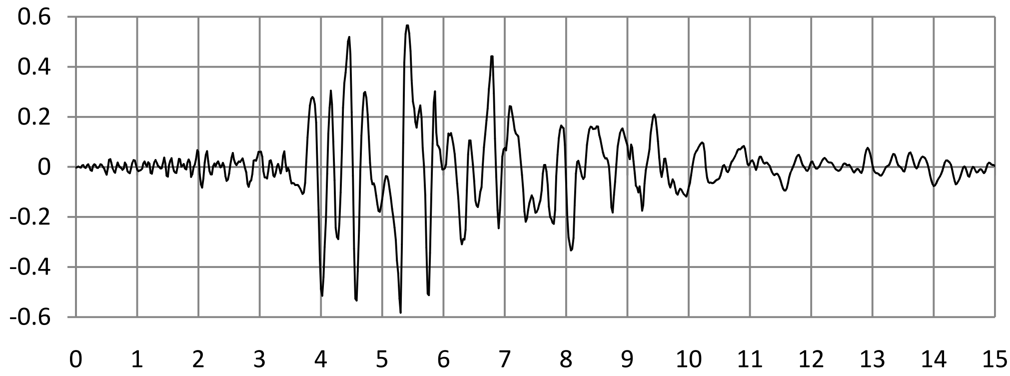

(a)

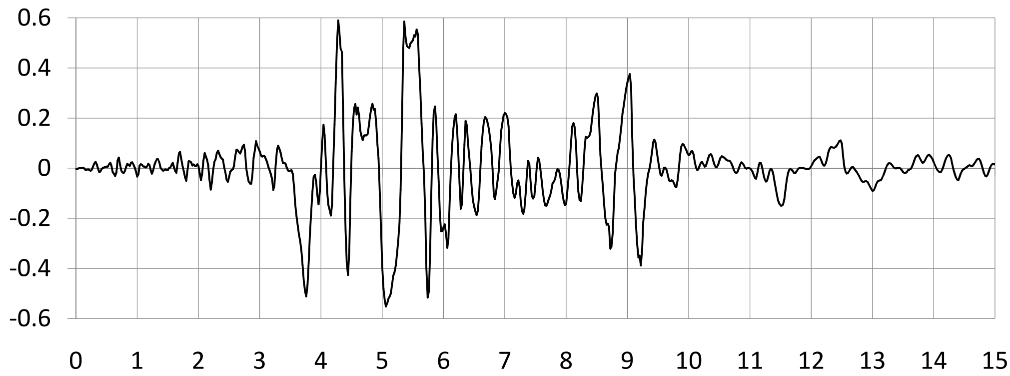

(b)

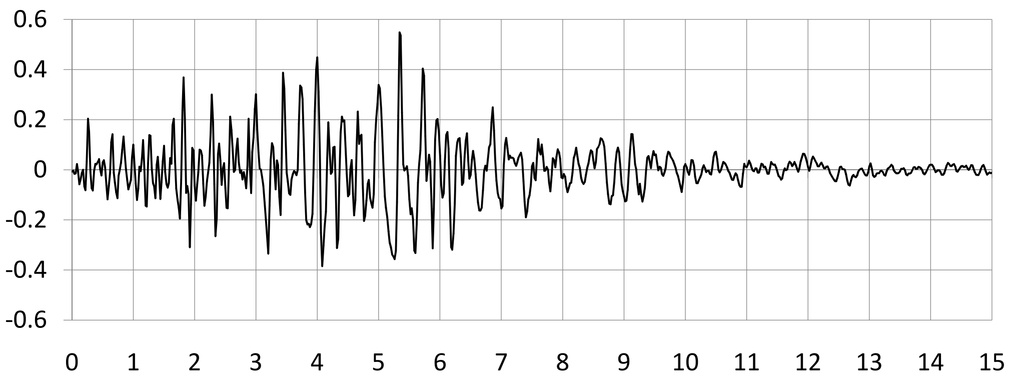

(c)

Figure 3.4-3 Ground Acceleration (g) & Time (s) Graph for Northridge EQ
Station: Newhall
Component: (a) 90° (b) 360° (c) Up

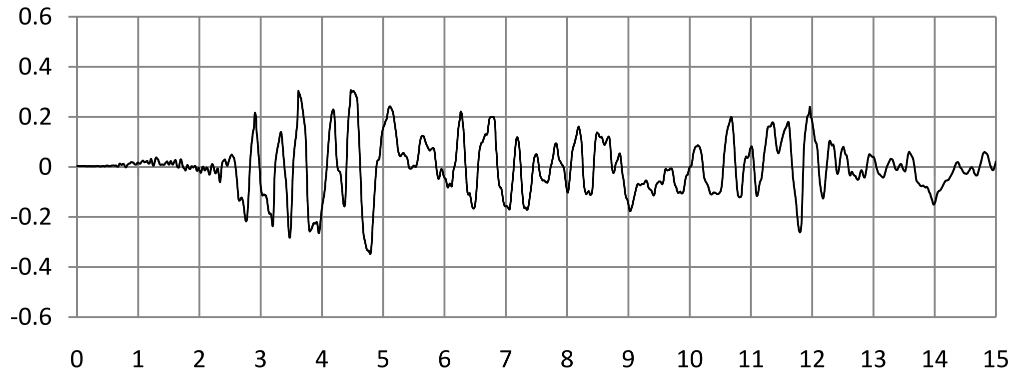

(a)

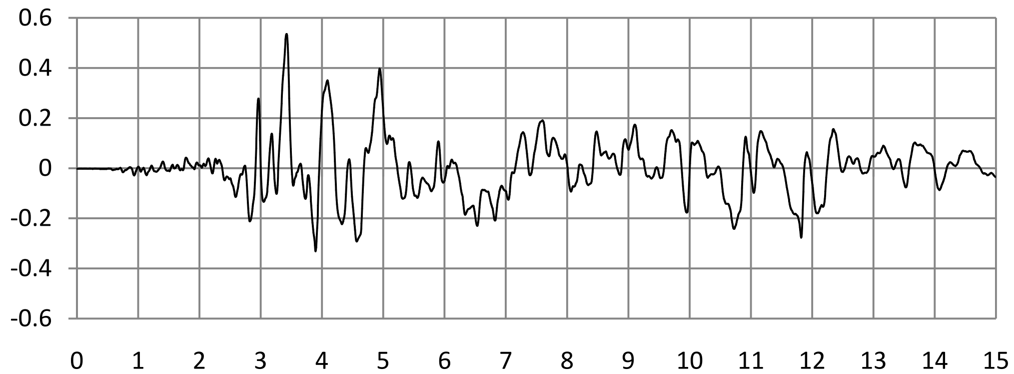

(b)

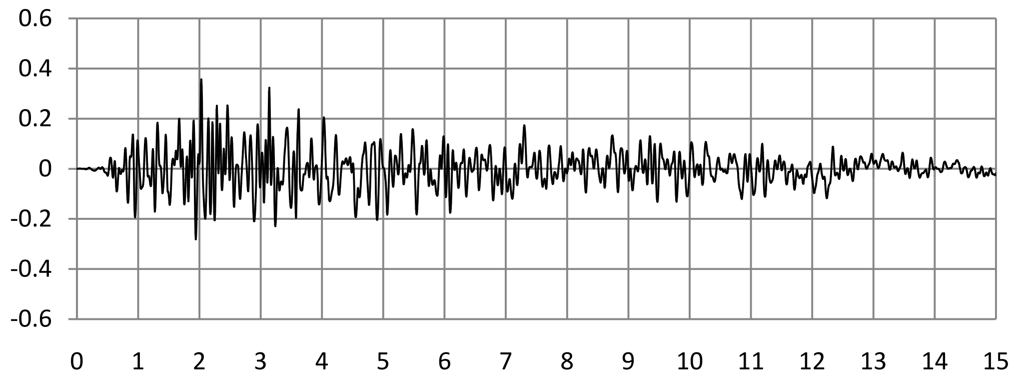

(c)

Figure 3.4-4 Ground Acceleration (g) & Time (s) Graph for Düzce EQ
Station: Düzce
Component: (a) 180° (b) 270° (c) Up

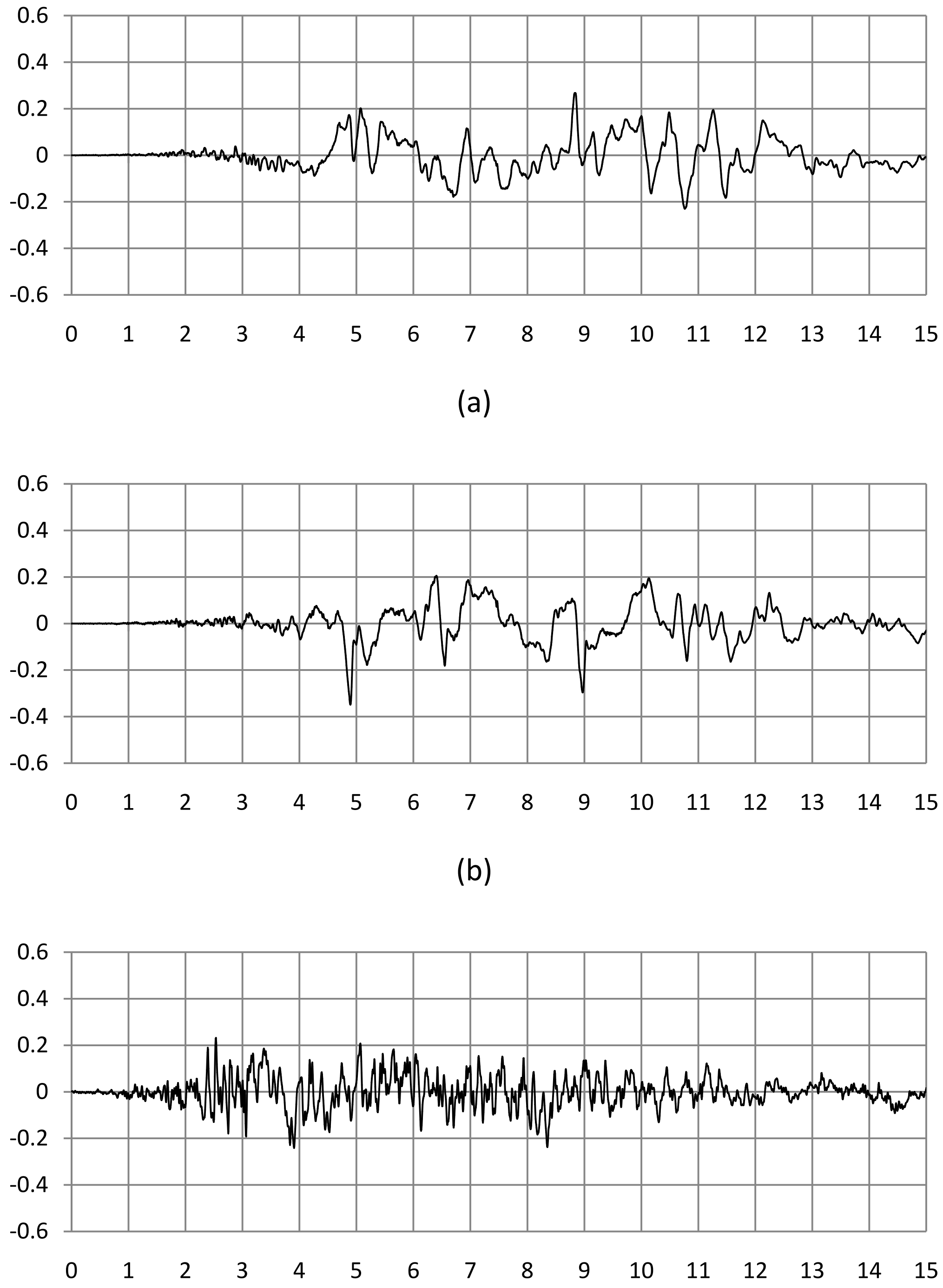

Figure 3.4-5 Ground Acceleration (g) & Time (s) Graph for Kocaeli EQ
Station: Yarımca
Component: (a) 60° (b) 330° (c) Up

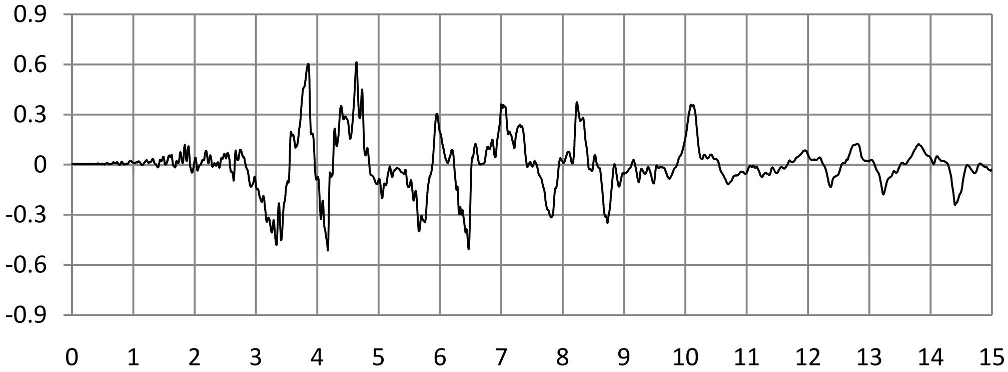

(a)

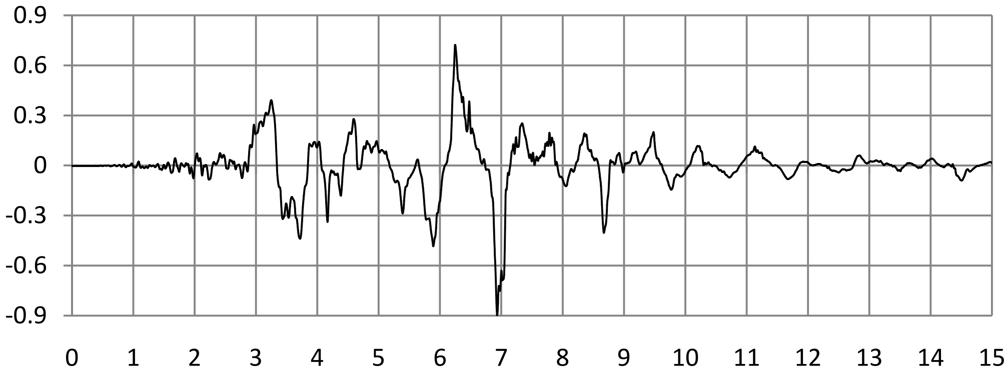

(b)

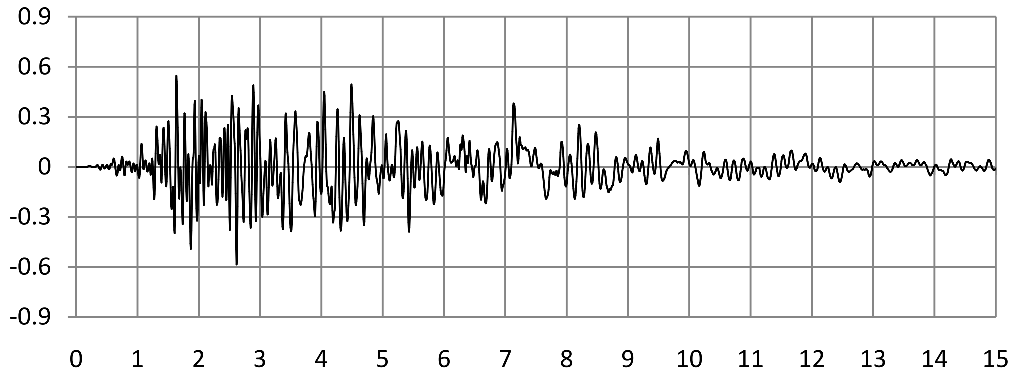

(c)

Figure 3.4-6 Ground Acceleration (g) & Time (s) Graph for Northridge EQ
Station: Sylmar
Component: (a) 52° (b) 142° (c) Up

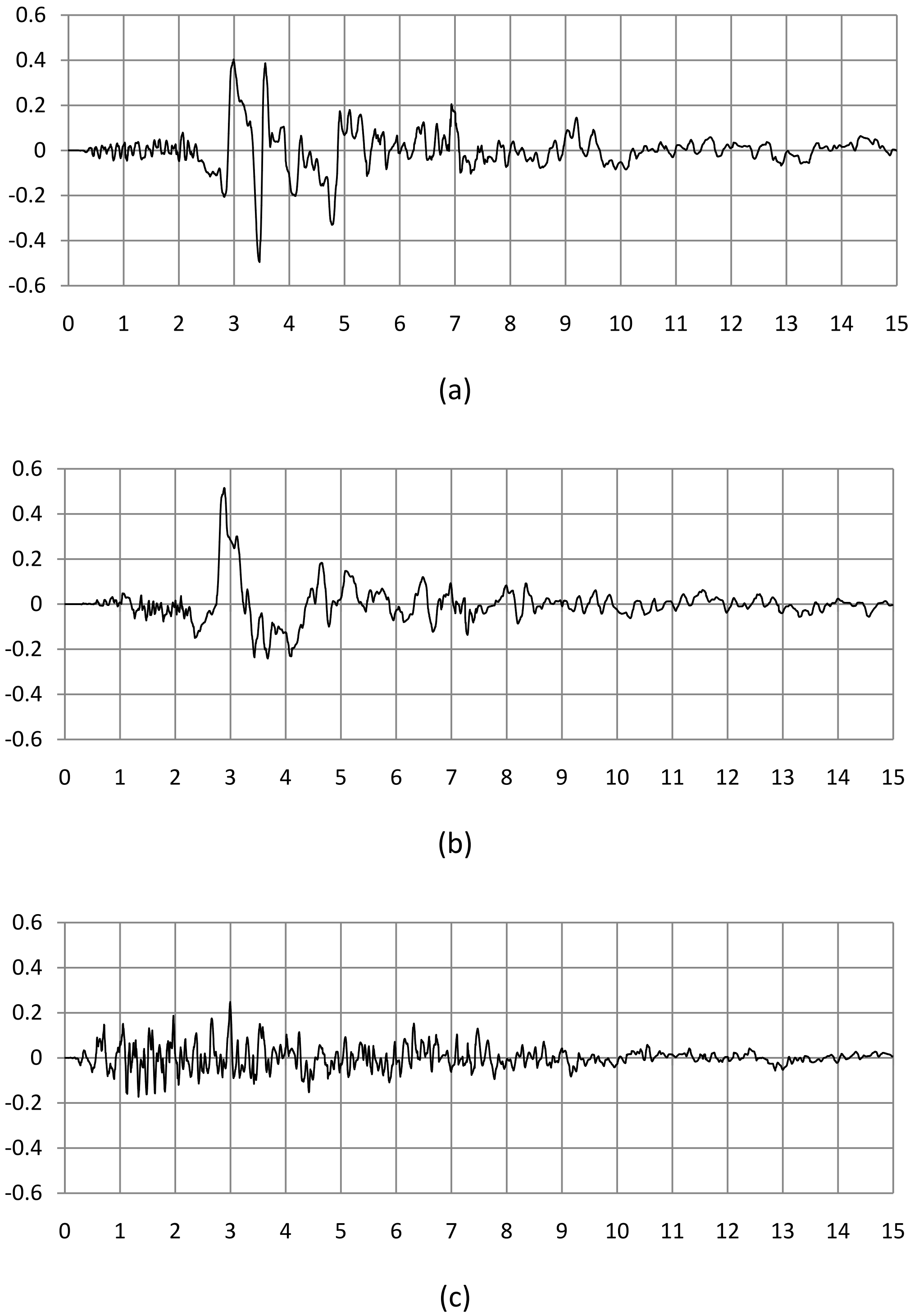

Figure 3.4-7 Ground Acceleration (g) & Time (s) Graph for Erzincan EQ
Station: Erzincan
Component: (a) EW (b) NW (c) Up

CHAPTER 4

ANALYSIS CASES & RESULTS

4.1. Ritz-Vector & Time History Analysis (THA)

Modal analysis is used to determine the vibration modes of a structure. Generally speaking, these modes are used to understand the behavior of a structure. There are two types of modal analysis such as Eigenvector and Ritz-vector analysis. Eigenvector analysis determines the undamped free vibration mode shapes and frequencies of the structural system. On the other hand, Ritz-vector analysis aims to find the mode shapes and frequencies that are excited by a particular loading. It is believed that Ritz-vectors may lead to a better basis than do eigenvectors regarding modal superposition with response-spectrum or time history analysis [28].

A previous study by Yuan and Dickens et al. [32] about mode superposition analysis (MSA) reveals that the natural free vibration mode shapes are not the best behavioral inputs for structures subjected to dynamic loads. Dynamic analysis based on a special set of load dependent Ritz-vectors yield more accurate results than use of same number of natural mode shapes. Ritz-vectors yield dependable results since they are created by taking into account the spatial distribution of the dynamic loading, however use of the natural mode shapes directly, means neglecting this important case. As a result, Ritz-vector analysis requires starting load vectors to initiate the procedure. In this study, acceleration type loading is applied in all three orthogonal directions (UX, UY and UZ) in order to excite all mode shapes with enough mass participation ratios in UX, UY and UZ directions.

In this study, nonlinear time history analysis (THA) is chosen as the type of analysis. THA is a step by step analysis of the dynamical response of a structure to an assigned variable loading within a time domain. It provides dynamic response of a structure using the solution of Eqn. 4.1-1.

$$\boldsymbol{K}\boldsymbol{u}(t) + \boldsymbol{C}\dot{\boldsymbol{u}}(t) + \boldsymbol{M}\ddot{\boldsymbol{u}}(t) = -\boldsymbol{M}\,\boldsymbol{r}\,\ddot{\boldsymbol{u}}_{\boldsymbol{g}} \qquad \text{(Eqn. 4.1-1)}$$

where $\boldsymbol{K}$ is the stiffness matrix, $\boldsymbol{C}$ is the damping matrix, $\boldsymbol{M}$ is the diagonal mass matrix, $\boldsymbol{u}$, $\dot{\boldsymbol{u}}$ and $\ddot{\boldsymbol{u}}$ are the displacements, velocities and accelerations of the structure, respectively. $\ddot{\boldsymbol{u}}_{\boldsymbol{g}}$ is the ground acceleration and $\boldsymbol{r}$ is the influence vector which represents the displacements of masses resulting from static application unit ground displacement.

THA can be linear or nonlinear, modal or direct-integration and transient or periodic. The nonlinearity is considered due to nonlinear Link/Support elements used for investigation. Use of these has the analysis type to be nonlinear modal THA. Additionally, transient analysis is indicated as a better type for EQ load since it is a one-time event with a beginning and an end.

Nonlinear modal time history analysis is performed in SAP2000 [14]. The method the software uses is an extension of the Fast Nonlinear Analysis (FNA) developed by Wilson et al. [29]. This method is to be used for linear elastic structural systems which have a limited number of predefined nonlinear elements. Eqn. 4.1-2 gives the dynamic equilibrium equations of linear elastic structure with predefined nonlinear link element.

$$\boldsymbol{K_L u}(t) + \boldsymbol{C\dot{u}}(t) + \boldsymbol{M\ddot{u}}(t) + \boldsymbol{r_N}(t) = -\boldsymbol{M\,r\,\ddot{u}_g} \qquad \text{(Eqn. 4.1-2)}$$

where $\boldsymbol{K_L}$ is the stiffness matrix for the linear elastic elements and $\boldsymbol{r_N}$ is the vector of forces from nonlinear degrees of freedom in the link elements. For the purpose of analysis, Eqn. 4.1-3 is defined as general stiffness matrix,

$$\boldsymbol{K} = \boldsymbol{K_L} + \boldsymbol{K_N} \qquad \text{(Eqn. 4.1-3)}$$

where, $\boldsymbol{K_L}$ is the stiffness of all the linear elements and the linear degrees of freedom of the link elements and $\boldsymbol{K_N}$ is the linear effective stiffness matrix of all of the nonlinear degrees of freedom. Then Eqn. 4.1-3 is substituted in Eqn. 4.1-2 and the dynamic equilibrium equation is obtained as,

$$\boldsymbol{Ku}(t) + \boldsymbol{C\dot{u}}(t) + \boldsymbol{M\ddot{u}}(t) = -\boldsymbol{M\,r\,\ddot{u}_g} - [\boldsymbol{r_N}(t) - \boldsymbol{K_N u}(t)] \qquad \text{(Eqn. 4.1-4)}$$

The FNA involves modal analysis which makes use of mode superposition crucial. For this reason, the dynamic equilibrium equation may be written in the form of Eqn. 4.1-5,

$$\Omega^2 \boldsymbol{a}(t) + \Lambda\boldsymbol{\dot{a}}(t) + \boldsymbol{I\ddot{a}}(t) = [\boldsymbol{q}(t) - \boldsymbol{q_N}(t)] \qquad \text{(Eqn. 4.1-5)}$$

where, Ω^2 is diagonal matrix of squared structural frequencies given by,

$$\Omega^2 = \Phi^{\mathrm{T}}\mathbf{K}\Phi \qquad \text{(Eqn. 4.1-6)}$$

Λ is the modal damping matrix which is assumed to be diagonal,

$$\Lambda = \Phi^{\mathrm{T}}\mathbf{C}\Phi \qquad \text{(Eqn. 4.1-7)}$$

$\mathbf{I}$ is the identity matrix,

$$\mathbf{I} = \Phi^{\mathrm{T}}\mathbf{M}\Phi \qquad \text{(Eqn. 4.1-8)}$$

$\mathbf{q}(\mathrm{t})$ is the vector of modal applied loads,

$$\mathbf{q}(\mathrm{t}) = \Phi^{\mathrm{T}}\mathbf{r}(\mathrm{t}) \quad \text{(Eqn. 4.1-9)}$$

$\mathbf{q_N}(\mathrm{t})$ is the vector of modal forces from the nonlinear elements,

$$\mathbf{q_N}(\mathrm{t}) = \Phi^{\mathrm{T}}[\mathbf{r}_{\mathrm{N}}(\mathrm{t}) - \mathbf{K}_{\mathrm{N}}\mathbf{u}(\mathrm{t})] \quad \text{(Eqn. 4.1-10)}$$

$\mathbf{a}(\mathrm{t})$ is the vector of modal displacement amplitudes,

$$\mathbf{u}(\mathrm{t}) = \Phi\mathbf{a}(\mathrm{t}) \quad \text{(Eqn. 4.1-11)}$$

and Φ is the matrix of mode shapes. Modal equations given above are coupled equations.

Using the default and rewritten equilibrium equations stated so far, an iterative solution within the following computation details is conducted by the program in order to reach a result. The iterative solution is carried out in each time step for the nonlinear modal equations. The right hand sides of all of the equations are assumed to vary linearly during a time step and the program uses exact, closed form integration to solve them in all iterations. The iterations are continued until the solution converges. In case of a divergence, the program divides the time steps into smaller sub steps and tries again.

4.2. Analysis Cases & Combinations

Three types of analysis cases are defined in the program. These are linear static, linear modal and nonlinear modal history (FNA) cases. Linear static type is used to define dead load and live load cases. Linear modal type is used to define Ritz-vector mode shape analysis case. Finally, the FNA type is used to define EQ loads. Table 4.2-1 shows the defined analysis cases with initial conditions. All cases started with a zero condition to discard effect of each analysis case to each other.

Table 4.2-1 Analysis Case Definitions

Analysis Case	Analysis Type	Initial Condition	Modal Case	Description
DL	Linear Static	Zero		Dead Load
LL	Linear Static	Zero	RitzVect	Live Load
RitzVect	Linear Modal	Zero	RitzVect	Mode Shape Case
EQ_.....+H	Nonlinear Modal History (FNA)	Zero	RitzVect	Horizontal components of the related EQ
EQ_.....+HV	Nonlinear Modal History (FNA)	Zero	RitzVect	Horizontal and Vertical components of the related EQ

For Ritz-vector case a tri-axial acceleration load is defined, since it is strictly required to define particular loads for this type of analysis. In addition to load definition, maximum number of modes is set as 17 to make sure 90%

mass participation in each orthogonal direction. Table 4.2-1 shows two different FNA cases for each EQ. One of them is created to observe the influence of only two orthogonal horizontal components of EQs and named with suffix “…+H”. Additionally, other one is created to observe the influence of both horizontal and vertical components of EQs and named with suffix “…+HV”.

For combined isolated bridge system, modal damping is chosen as 5% constant damping for all of the FNA cases. Also, number of output time steps and output step sizes are chosen considering the EQ data time step and length. Table 4.2-2 shows the details about the damping properties, the step size, numbers and types. It can be clearly seen from the table that the total history time is specified as 15 seconds.

Table 4.2-2 Modal History Definitions

Analysis Case	History Type	Number of Output Steps	Output Step Size	Damping Type/Ratio
EQ_IMV7+H	Transient	3000	0.005	Constant / 0.05
EQ_IMV7+HV	Transient	3000	0.005	Constant / 0.05
EQ_IMV5+H	Transient	3000	0.005	Constant / 0.05
EQ_IMV5+HV	Transient	3000	0.005	Constant / 0.05
EQ_NHWL+H	Transient	750	0.02	Constant / 0.05
EQ_NHWL+HV	Transient	750	0.02	Constant / 0.05
EQ_DZC+H	Transient	3000	0.005	Constant / 0.05
EQ_DZC+HV	Transient	3000	0.005	Constant / 0.05
EQ_KCL+H	Transient	3000	0.005	Constant / 0.05
EQ_KCL+HV	Transient	3000	0.005	Constant / 0.05
EQ_NSYL+H	Transient	3000	0.005	Constant / 0.05

Table 4.2-2 Modal History Definitions (continued)

Analysis Case	History Type	Number of Output Steps	Output Step Size	Damping Type/Ratio
EQ_NSYL+HV	Transient	3000	0.005	Constant / 0.05
EQ_ERZ+H	Transient	3000	0.005	Constant / 0.05
EQ_ERZ+HV	Transient	3000	0.005	Constant / 0.05

In the analysis, combinations are defined in accordance with strength criteria stated in AASHTO Section 3 [20]. Each analysis case involves only effects due to its defined load or EQ. This is why combinations are defined. They are aimed to be used for combining effects due to different case. The combinations are grouped into two: Strength-I and Extreme Event-I. Strength-I has one sub-item including dead load (DL) and live load (LL). On the other hand, Extreme Event-I has 15 sub-items. 14 of them are generated from DL, LL and EQs and one is from DL and LL. Extreme Event-I is abbreviated to read Comb1 to Comb 7. Also, type of combination for all of them is selected as linear add (see Table 4.2-3).

Table 4.2-3 Combination Definitions

Comb. Name	Comb Type	Analysis Case Type	Analysis Case Name	Scale Factor
STRENGTH-I	Linear Add	Linear Static	DL	1.25
		Linear Static	LL	1.75
Comb 1-H	Linear Add	Linear Static	DL	1.25
		Linear Static	LL	0.50
		FNA	EQ_IMV7+H	1.00
Comb 1-HV	Linear Add	Linear Static	DL	1.25
		Linear Static	LL	0.50
		FNA	EQ_IMV7+HV	1.00

Table 4.2-3 Combination Definitions (continued)

Comb. Name	Comb Type	Analysis Case Type	Analysis Case Name	Scale Factor
Comb 2-H	Linear Add	Linear Static	DL	1.25
		Linear Static	LL	0.50
		FNA	EQ_IMV5+H	1.00
Comb 2-HV	Linear Add	Linear Static	DL	1.25
		Linear Static	LL	0.50
		FNA	EQ_IMV5+HV	1.00
Comb 3-H	Linear Add	Linear Static	DL	1.25
		Linear Static	LL	0.50
		FNA	EQ_NHWL+H	1.00
Comb 3-HV	Linear Add	Linear Static	DL	1.25
		Linear Static	LL	0.50
		FNA	EQ_NHWL+HV	1.00
Comb 4-H	Linear	Linear Static	DL	1.25
		Linear Static	LL	0.50
		FNA	EQ_DZC+H	1.00
Comb 4-HV	Linear	Linear Static	DL	1.25
		Linear Static	LL	0.50
		FNA	EQ_DZC+HV	1.00
Comb 5-H	Linear Add	Linear Static	DL	1.25
		Linear Static	LL	0.50
		FNA	EQ_KCL+H	1.00
Comb 5-HV	Linear Add	Linear Static	DL	1.25
		Linear Static	LL	0.50
		FNA	EQ_KCL+HV	1.00
Comb 6-H	Linear Add	Linear Static	DL	1.25
		Linear Static	LL	0.50
		FNA	EQ_NSYL+H	1.00
Comb 6-HV	Linear Add	Linear Static	DL	1.25
		Linear Static	LL	0.50
		FNA	EQ_NSYL+HV	1.00

Table 4.2-3 Combination Definitions (continued)

Comb. Name	Comb Type	Analysis Case Type	Analysis Case Name	Scale Factor
Comb 7-H	Linear Add	Linear Static	DL	1.25
		Linear Static	LL	0.50
		FNA	EQ_ERZ+H	1.00
Comb 7-HV	Linear Add	Linear Static	DL	1.25
		Linear Static	LL	0.50
		FNA	EQ_ERZ+HV	1.00
Comb-SDC06	Linear Add	Linear Static	DL	1.5625
		Linear Static	LL	0.50

Table 4.2-3 shows totally 16 response combinations. Except one combination, all of them are generated per AASHTO strength requirements [20]. Comb-SDC06 is derived from the requirements stated in SDC 2006 [3]. In case of a vertical ground acceleration of less than 0.6g, this combination is suggested to be accounted for vertical EQ load. Since SDC 2006 requires application of additional 25% of the DL defined upward or downward, simultaneously with dead and live loads, Comb-SDC06 is considered to start from extreme event combination of AASHTO [20]. Then, the additional 25% of the DL is considered, instead of EQ load. As a result of multiplication of 1.25x1.25, a scale factor of 1.5625 is calculated. The combination of SDC 2006 [3] is defined to be able to make comparison between modal time history analysis and linear static analysis regarding vertical EQ effects.

4.3. *Results*

4.3.1. *Modal Analysis Outputs*

Initially, modal analysis outputs are given such as fundamental periods of each orthogonal direction for all mathematical models. Table 4.3-1 presents the fundamental periods of the models with predefined isolator and connection property. All modal outputs are calculated using Ritz-Vector analysis.

Table 4.3-1 Fundamental Periods in UX, UY and UZ Directions

	Fundamental Period (sec)		
Model	UX	UY	UZ
SCB1	1.046	0.937	0.285
SCB2	1.000	0.889	0.284
SCB3	0.911	0.794	0.276
SCB4	0.860	0.740	0.275
SCB5	0.829	0.708	0.275
SCB6	0.762	0.642	0.275
SCB7	0.715	0.597	0.274
SCB8	0.687	0.572	0.274
SCB9	0.651	0.541	0.274
SCB-Fix	0.080	0.210	0.253

4.3.2. EQ Response Spectra

Response spectra of seven EQs, each with three components are generated using the software Seismosignal [30]. Figures 4.3-1 through 4.3-7 shows the response spectra. Each figure involves three separate graphs. Graphs (a), (b) and (c) show the response spectra with respect to horizontal UX and UY directions and vertical UZ direction, respectively. Vertical axis shows pseudo acceleration and horizontal axis shows period. Pseudo acceleration is given in “g” and period is given in “seconds”. Additionally, each figure involves 10 different markers which correspond to fundamental periods of the given models with respect to the EQ components. These periods are taken from Table 4.3-1 and inserted to response spectra to observe if the fundamental period leads to critical pseudo acceleration or not.

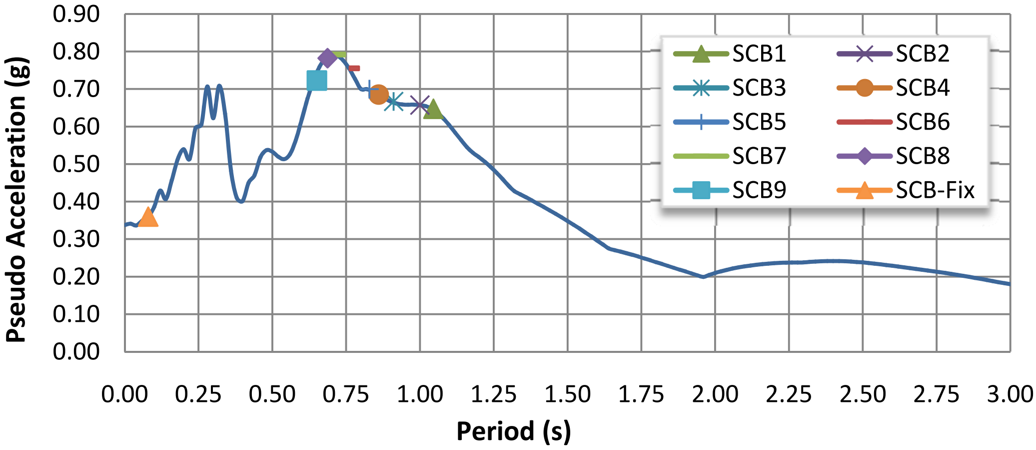

(a)

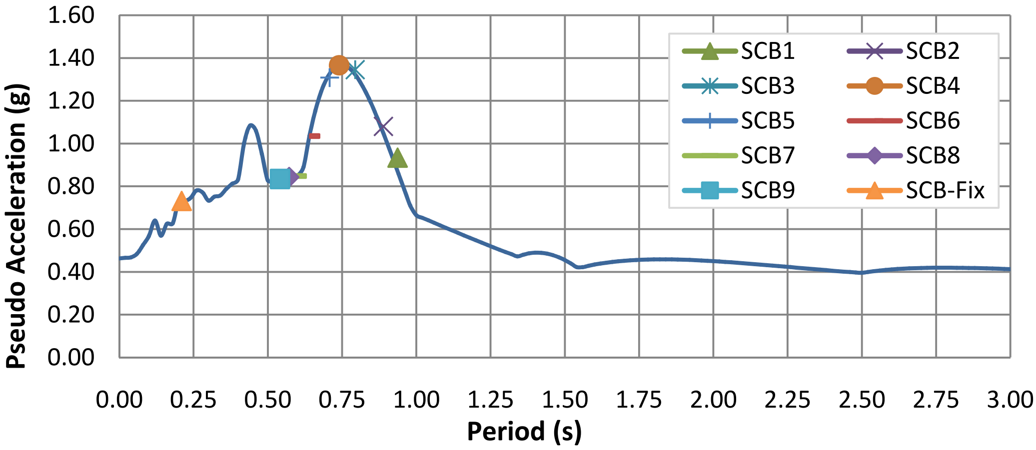

(b)

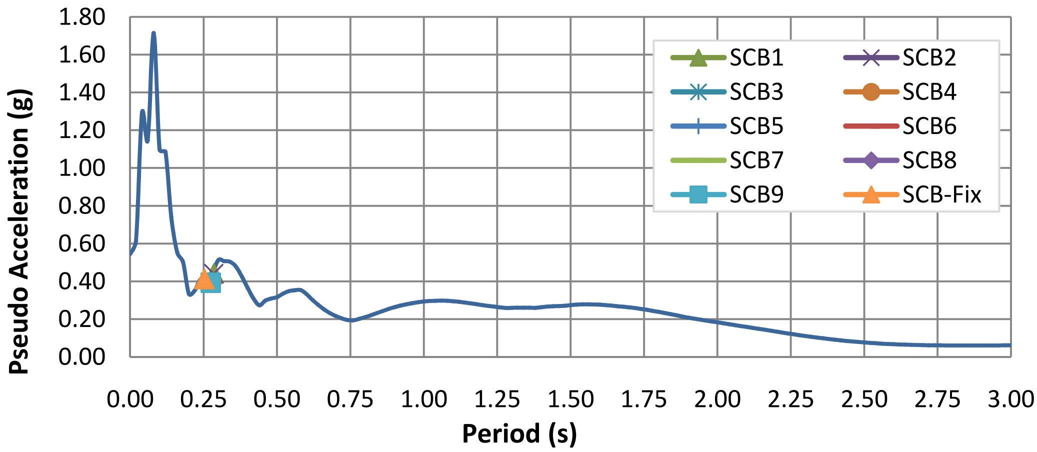

(c)

Figure 4.3-1 Response Spectrum of Imperial Valley EQ - Array #7, (a) UX (b) UY (c) UZ

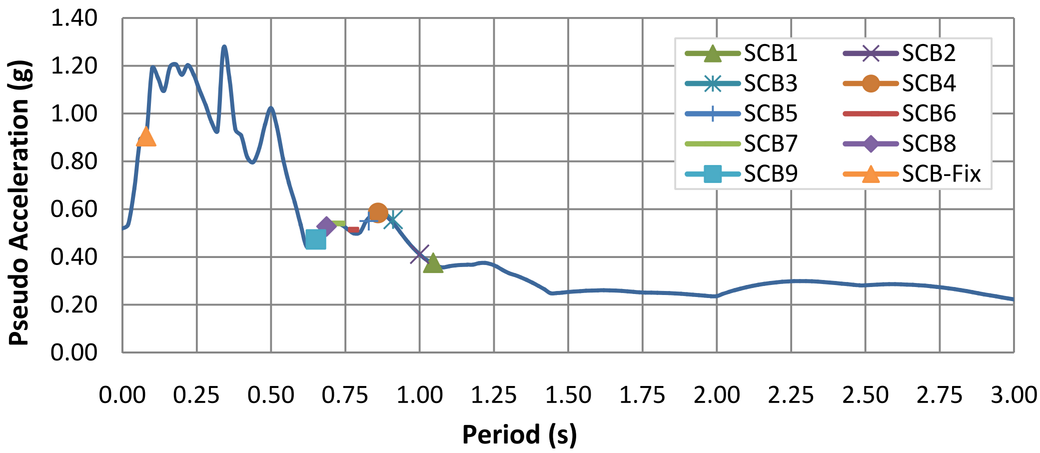

(a)

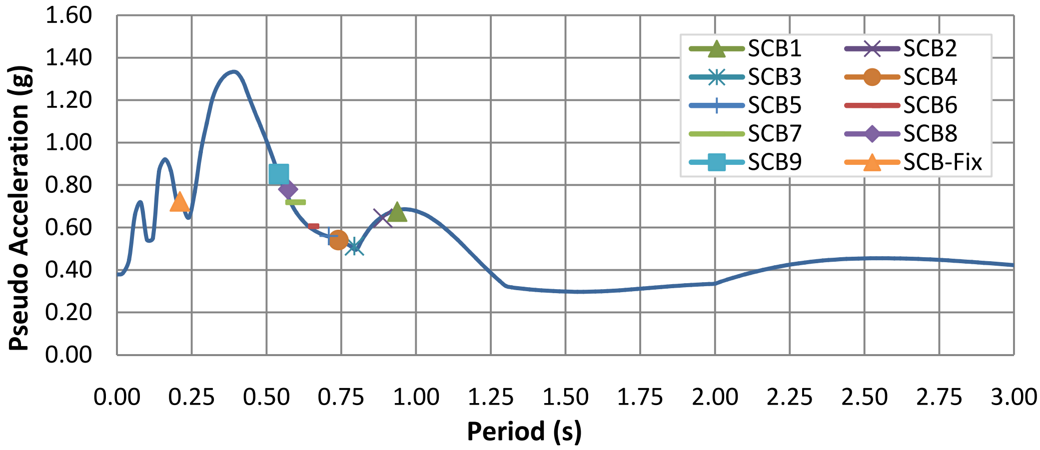

(b)

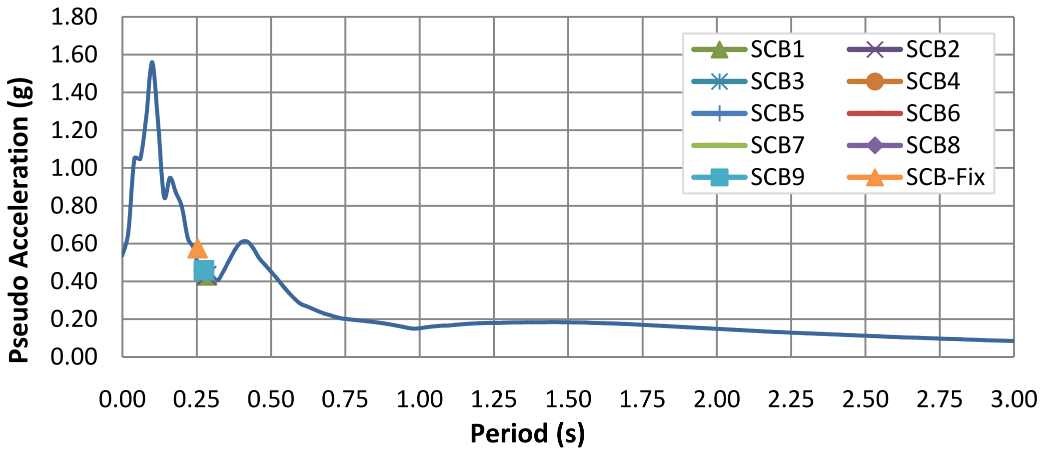

(c)

Figure 4.3-2 Response Spectrum of Imperial Valley EQ - Array #5,
(a) (UX) (b) (UY) (c) UZ

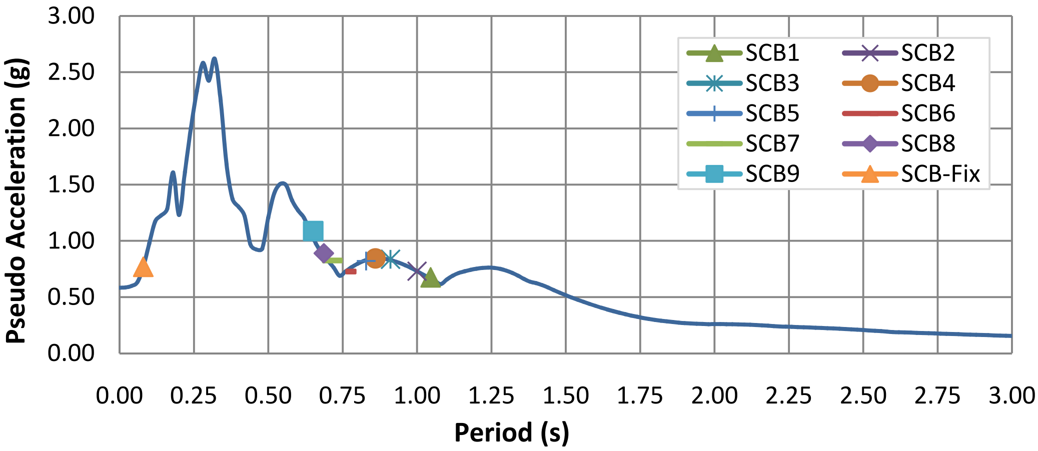

(a)

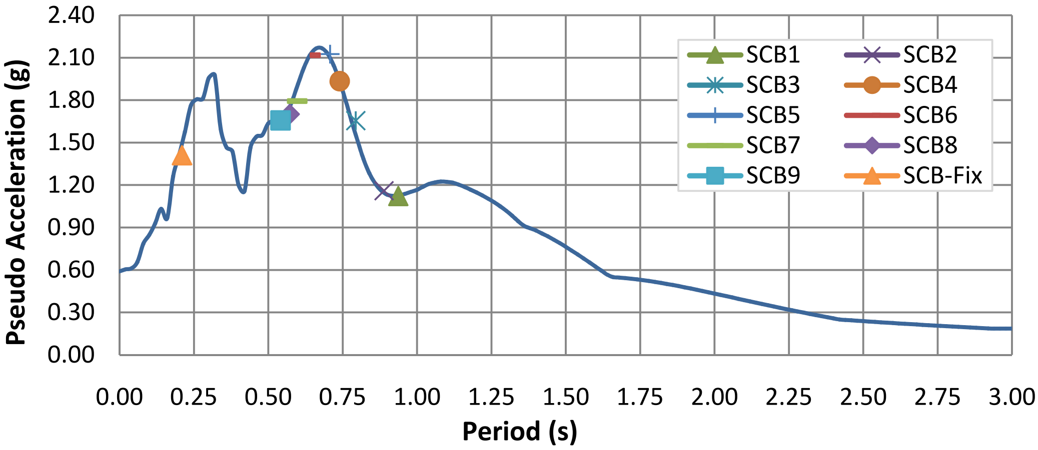

(b)

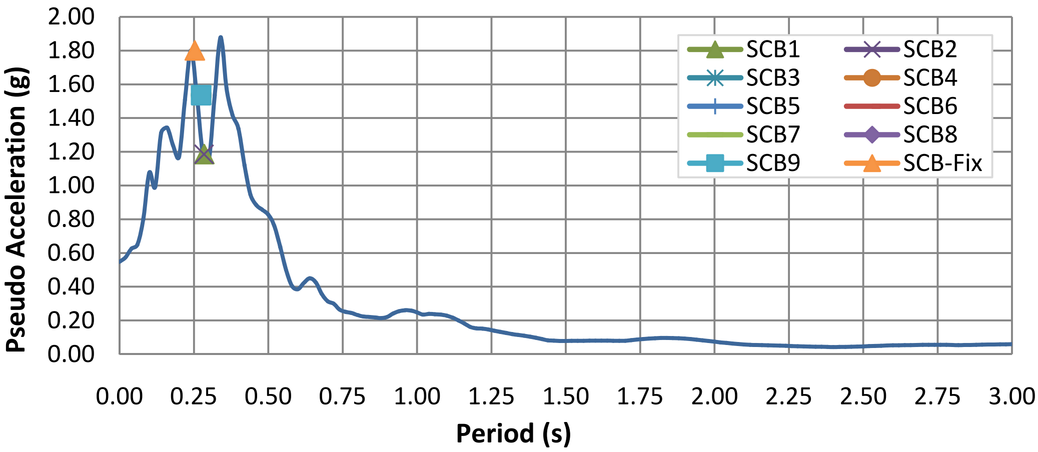

(c)

Figure 4.3-3 Response Spectrum of Northridge EQ - Newhall, (a) UX (b) UY (c) UZ

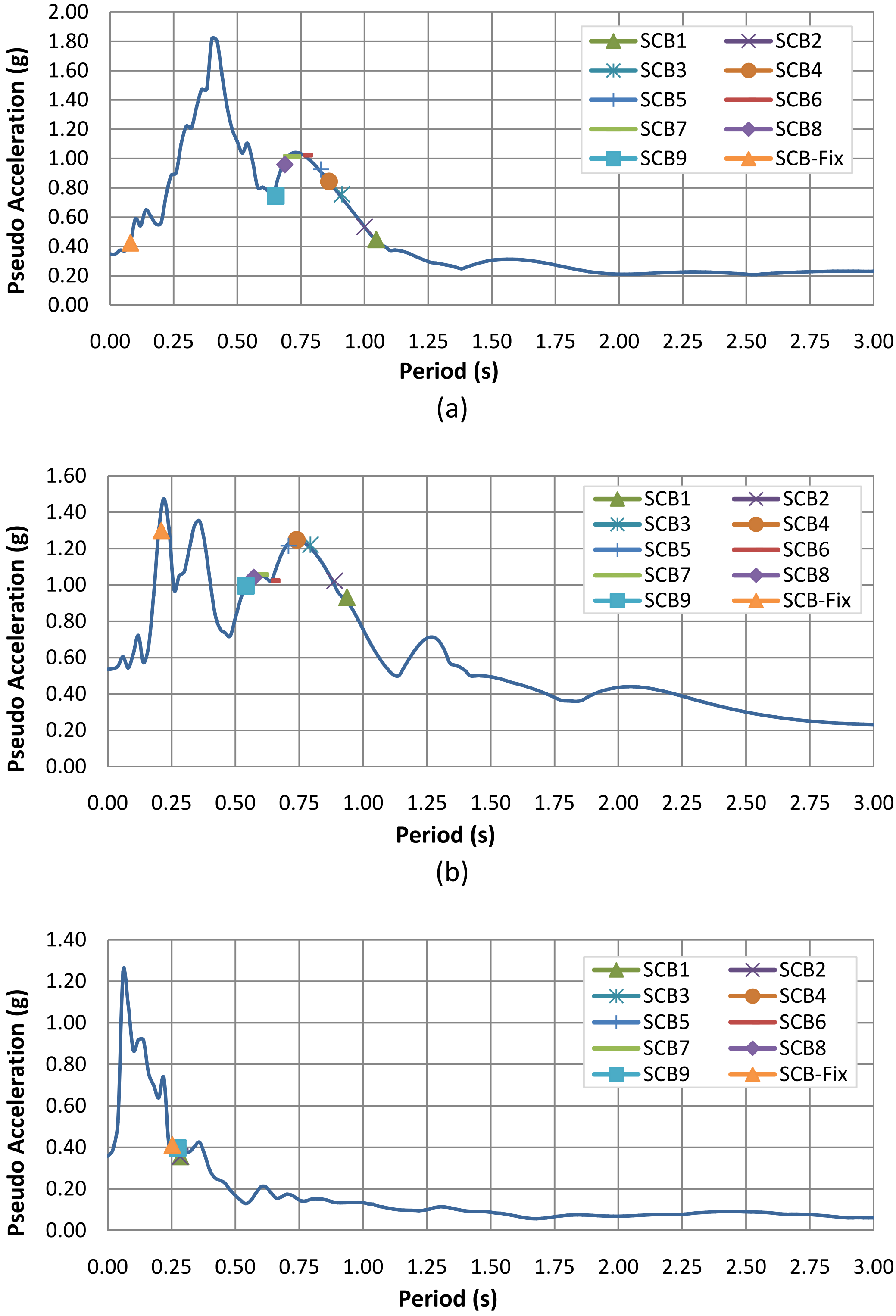

(a)

(b)

(c)

Figure 4.3-4 Response Spectrum of Düzce EQ - Düzce,
(a) UX (b) UY (c) UZ

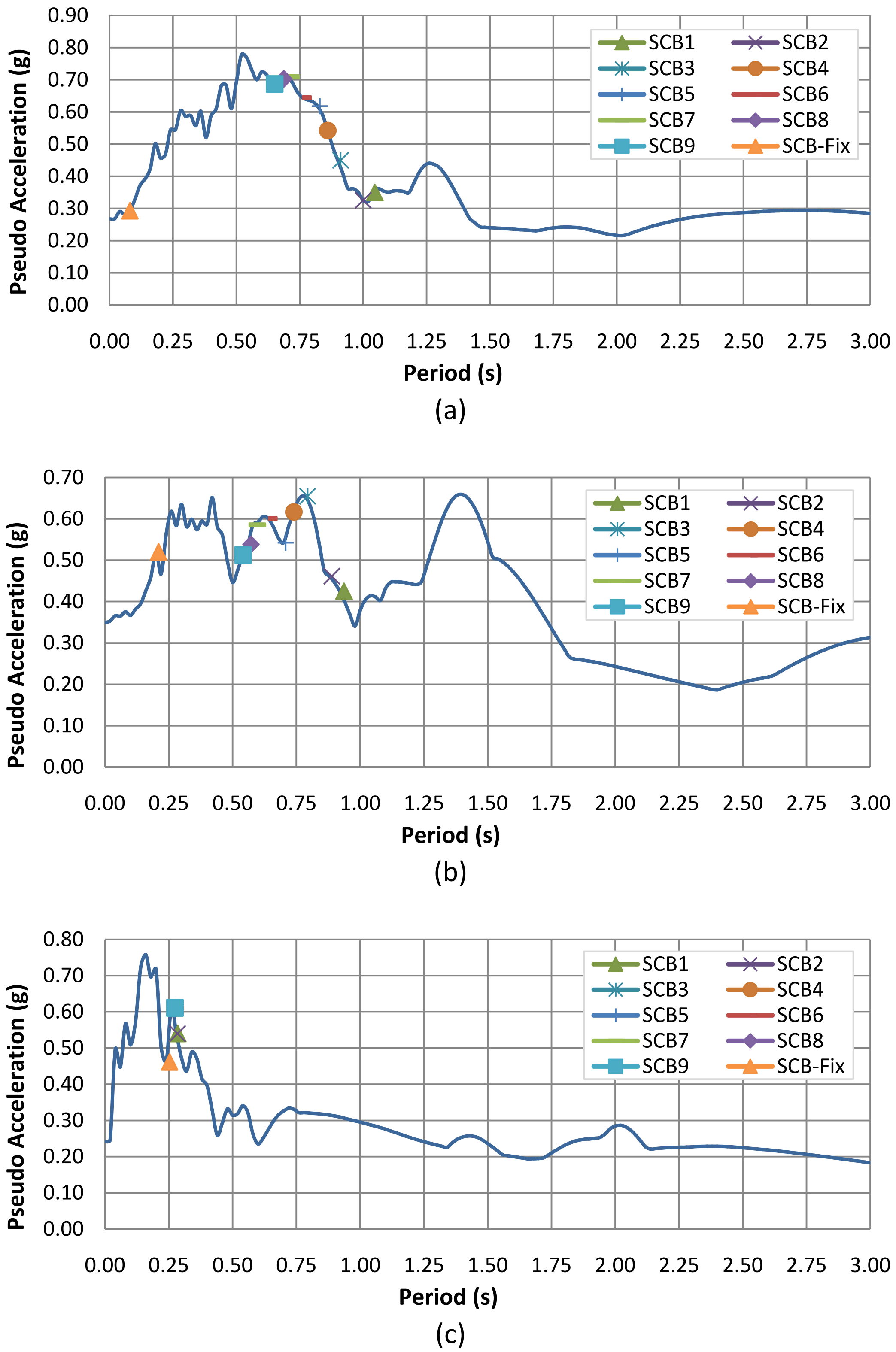

Figure 4.3-5 Response Spectrum of Kocaeli EQ - Yarımca,
(a) UX (b) UY (c) UZ

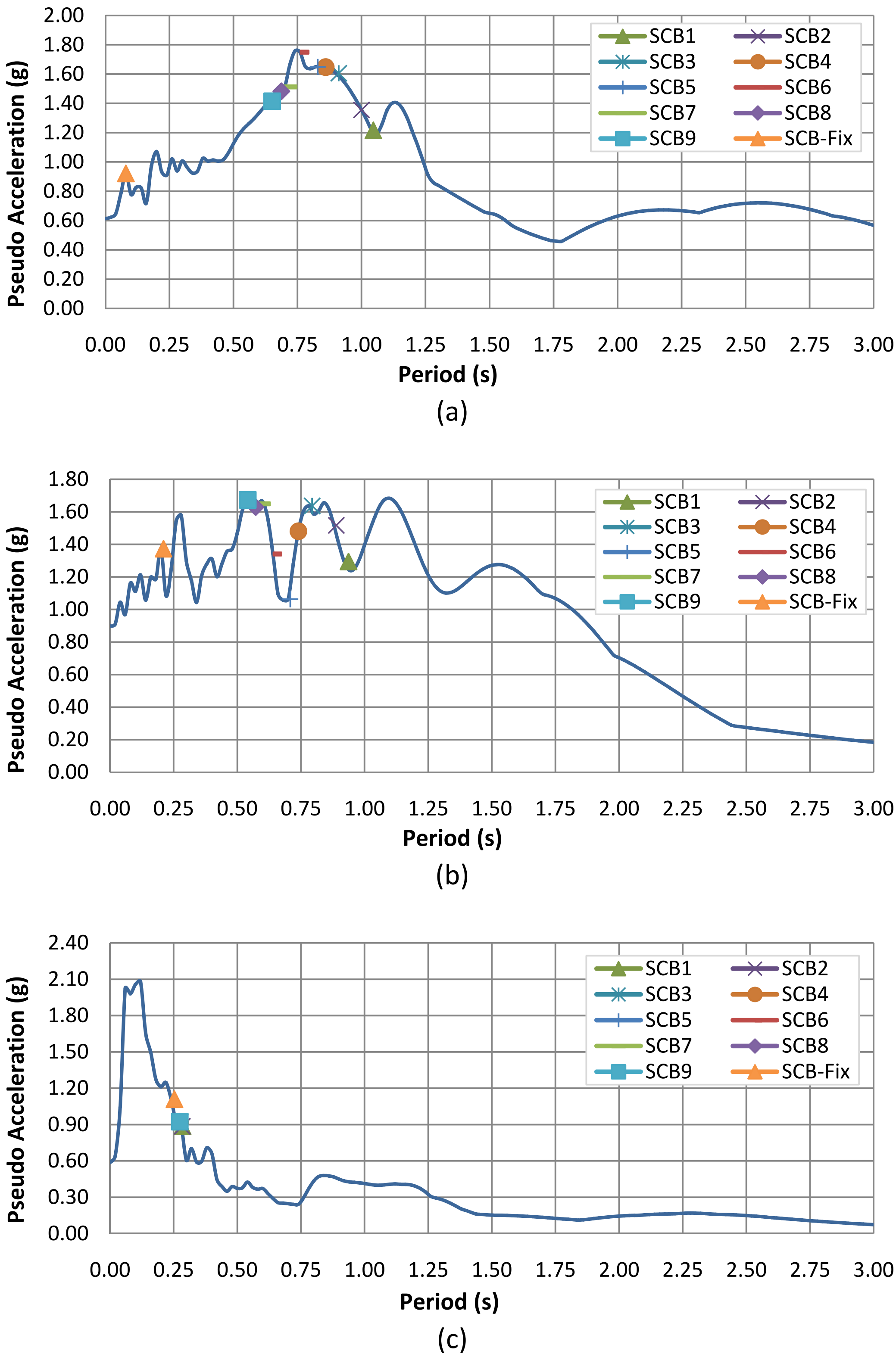

Figure 4.3-6 Response Spectrum of Northridge EQ - Sylmar, (a) UX (b) UY (c) UZ

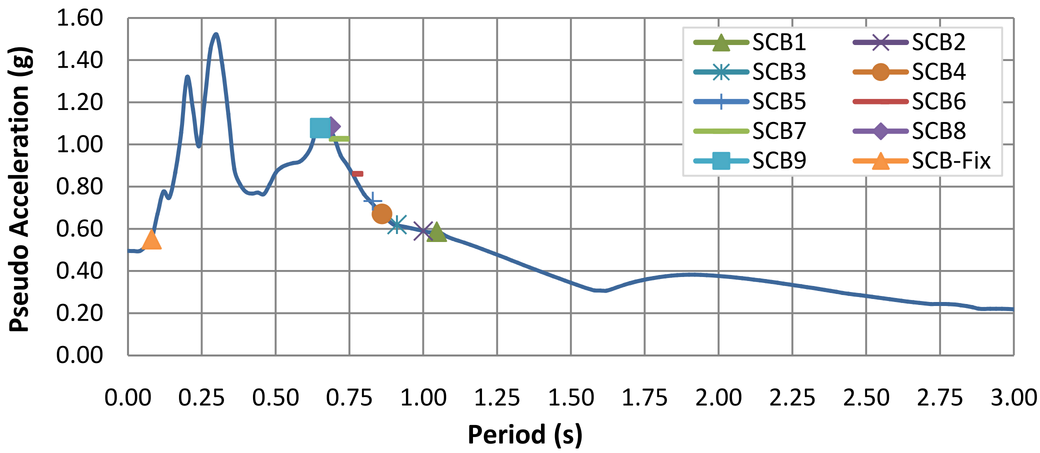

(a)

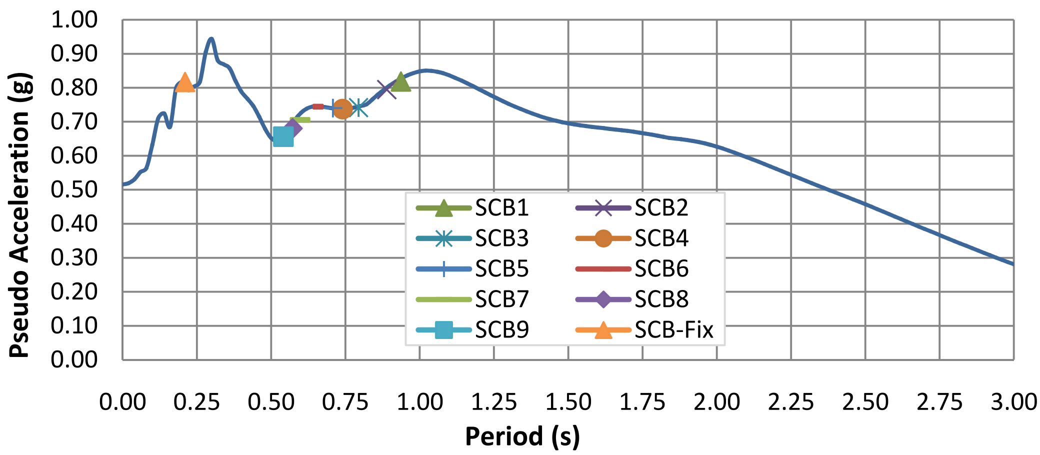

(b)

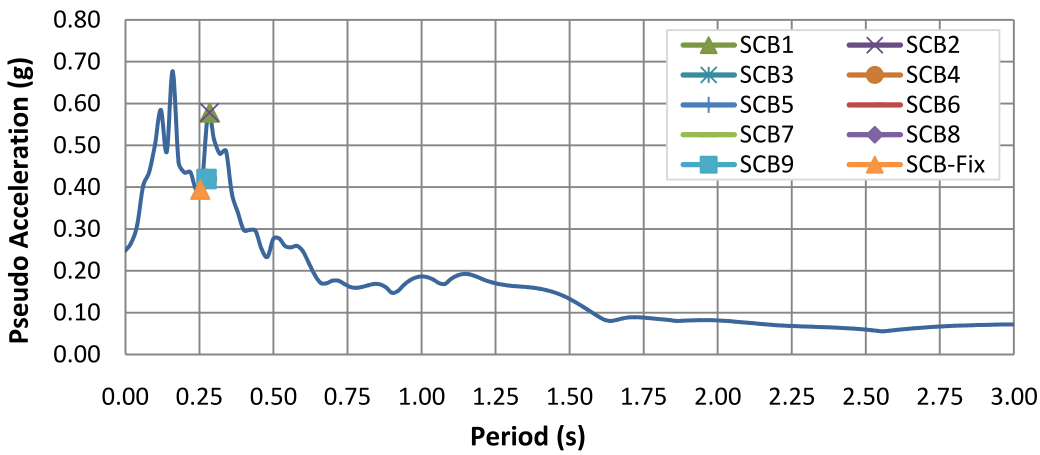

(c)

Figure 4.3-7 Response Spectrum of Erzincan EQ - Erzincan, (a) UX (b) UY (c) UZ

4.3.3. *Internal Force Outputs*

Eleven different internal force output tables are generated using ten bridges with different isolator properties and one bridge without isolation. Tables 4.3-2 through 4.3-11 show internal forces namely column axial force, isolator axial force, beam midspan axial force and beam midspan moment. Combinations from one to seven are sorted with respect to $A_{p,HOR}$ / $A_{p,VERT}$ ratios. Combination eight is defined according to SDC2006 [3] equivalent static load procedure. Combinations from one to seven have two components labeled as “H” and “HV”. H stands for load combinations which include only horizontal EQ components and HV stands for combinations which include horizontal and vertical EQ components. In addition to the internal forces, the table shows the isolator deformations in UX, UY and UZ directions with square root of sum of squares (SRSS) of horizontal components.

Table 4.3-2 Elements Internal Force Outputs for the Bridge with Isolator 01

ISOLATOR 01

Comb	Comp.	$A_{p.HOR}/V_{p.VERT}$	Column Axial(kN)	Isolator Deformation (m) UX	UY	SRSS	UZ	Isolator Axial(kN)	Beam Midspan Axial(kN)	Beam Midspan Moment(kNm)
1	H	1.054	-2369.475	0.052	0.116	0.127	-0.002	-267.301	1243.472	940.422
	HV		-3221.310	0.052	0.116	0.127	-0.002	-333.663	1567.863	1184.484
2	H	1.197	-2361.808	0.051	0.062	0.081	-0.003	-267.295	1243.397	940.418
	HV		-3035.584	0.051	0.062	0.080	-0.002	-334.235	1624.546	1227.530
3	H	1.514	-2425.343	0.127	0.038	0.132	-0.002	-291.388	1245.609	941.435
	HV		-3631.832	0.124	0.037	0.130	-0.001	-407.392	2226.955	1681.852
4	H	1.788	-2366.876	0.061	0.064	0.088	-0.002	-270.511	1243.540	940.955
	HV		-2812.115	0.060	0.064	0.088	-0.002	-312.887	1519.042	1148.482
5	H	1.818	-2350.519	0.022	0.037	0.043	-0.003	-265.882	1242.922	939.963
	HV		-2894.866	0.023	0.037	0.043	-0.002	-332.514	1643.752	1242.802
6	H	1.853	-2441.383	0.246	0.117	0.272	-0.002	-303.860	1247.095	942.665
	HV		-3106.024	0.247	0.117	0.273	-0.001	-351.625	1879.228	1419.734
7	H	2.883	-2372.368	0.039	0.015	0.041	-0.003	-278.233	1244.252	940.523
	HV		-3011.380	0.038	0.015	0.041	-0.002	-360.319	1749.384	1322.157
8	SDC06	-	-2827.574	-0.003	0.000	0.003	-0.003	-315.669	1496.561	1132.319

Table 4.3-3 Elements Internal Force Outputs for the Bridge with Isolator 02

ISOLATOR 02										
Comb	Comp.	$A_{p.HOR}/V_{p.VERT}$	Column Axial(kN)	Isolator Deformation (m) UX	UY	SRSS	UZ	Isolator Axial(kN)	Beam Midspan Axial(kN)	Beam Midspan Moment(kNm)
1	H	1.054	-2377.077	0.036	0.032	0.049	-0.003	-272.826	1246.040	941.964
	HV		-3220.262	0.036	0.032	0.048	-0.002	-335.526	1563.507	1181.656
2	H	1.197	-2359.901	0.033	0.054	0.064	-0.003	-271.025	1244.234	941.225
	HV		-3023.793	0.034	0.054	0.064	-0.002	-332.562	1627.295	1229.203
3	H	1.514	-2442.122	0.140	0.064	0.154	-0.002	-290.709	1248.571	943.093
	HV		-3633.149	0.138	0.064	0.152	-0.001	-421.474	2228.499	1683.155
4	H	1.788	-2390.542	0.056	0.041	0.070	-0.002	-273.690	1246.167	942.053
	HV		-2811.151	0.056	0.041	0.070	-0.002	-312.266	1517.506	1147.502
5	H	1.818	-2351.552	0.020	0.031	0.037	-0.003	-266.415	1243.022	940.362
	HV		-2893.038	0.020	0.031	0.037	-0.002	-332.059	1643.430	1242.520
6	H	1.853	-2442.567	0.092	0.073	0.118	-0.002	-288.480	1248.803	943.748
	HV		-3109.209	0.091	0.073	0.117	-0.001	-361.061	1876.719	1417.990
7	H	2.883	-2382.190	0.060	0.024	0.064	-0.002	-277.366	1245.848	942.032
	HV		-3015.222	0.059	0.024	0.064	-0.002	-358.394	1748.980	1322.226
8	SDC06	-	-2827.483	-0.003	0.000	0.003	-0.003	-315.660	1496.174	1132.163

Table 4.3-4 Elements Internal Force Outputs for the Bridge with Isolator 03

ISOLATOR 03										
Comb	Comp.	$A_{p.HOR}$ $/V_{p.VERT}$	Column Axial(kN)	Isolator Deformation (m) UX	UY	SRSS	UZ	Isolator Axial(kN)	Beam Midspan Axial(kN)	Beam Midspan Moment(kNm)
1	H	1.054	-2392.254	0.019	0.048	0.051	-0.001	-306.032	1244.633	941.283
	HV		-3073.651	0.019	0.048	0.051	0.000	-355.763	1540.978	1166.477
2	H	1.197	-2400.796	0.031	0.054	0.062	-0.001	-308.059	1246.160	942.536
	HV		-2934.814	0.031	0.054	0.062	0.000	-352.715	1603.596	1212.666
3	H	1.514	-2526.143	0.058	0.047	0.075	0.000	-336.897	1248.855	942.901
	HV		-3673.970	0.060	0.047	0.076	0.000	-479.848	2297.104	1733.843
4	H	1.788	-2397.055	0.041	0.026	0.048	-0.001	-309.913	1248.212	943.594
	HV		-2786.596	0.040	0.026	0.048	0.000	-344.747	1516.533	1146.176
5	H	1.818	-2367.261	0.014	0.025	0.029	-0.001	-293.204	1243.700	940.787
	HV		-2900.283	0.014	0.025	0.029	0.000	-357.281	1659.853	1254.234
6	H	1.853	-2475.548	0.066	0.034	0.074	0.000	-321.090	1248.665	943.435
	HV		-3211.652	0.066	0.034	0.074	0.000	-410.233	1961.511	1480.890
7	H	2.883	-2411.305	0.028	0.019	0.034	-0.001	-317.500	1247.034	942.753
	HV		-2990.287	0.028	0.019	0.034	0.000	-391.987	1685.739	1274.064
8	SDC06	-	-2836.456	-0.003	0.000	0.003	-0.001	-341.888	1497.851	1132.906

Table 4.3-5 Elements Internal Force Outputs for the Bridge with Isolator 04

ISOLATOR 04										
Comb	Comp.	$A_{p.HOR}/V_{p.VERT}$	Column Axial(kN)	Isolator Deformation (m) UX	UY	SRSS	UZ	Isolator Axial(kN)	Beam Midspan Axial(kN)	Beam Midspan Moment(kNm)
1	H	1.054	-2418.592	0.015	0.032	0.035	0.000	-314.747	1246.050	942.466
	HV		-3061.832	0.015	0.032	0.035	0.000	-370.086	1532.182	1160.109
2	H	1.197	-2426.554	0.025	0.051	0.057	0.000	-333.483	1247.162	943.297
	HV		-2915.966	0.025	0.051	0.057	0.000	-368.002	1598.633	1209.125
3	H	1.514	-2501.686	0.033	0.051	0.061	0.000	-345.770	1247.521	943.627
	HV		-3653.933	0.034	0.051	0.062	0.000	-481.985	2318.599	1749.577
4	H	1.788	-2432.918	0.030	0.029	0.042	0.000	-332.774	1248.148	944.169
	HV		-2779.301	0.030	0.029	0.042	0.000	-362.122	1516.425	1146.280
5	H	1.818	-2388.982	0.013	0.023	0.027	0.000	-310.641	1243.556	940.918
	HV		-2898.785	0.013	0.023	0.027	0.000	-372.438	1665.107	1258.225
6	H	1.853	-2452.829	0.045	0.032	0.055	0.000	-347.407	1249.005	944.666
	HV		-3247.646	0.044	0.032	0.054	0.000	-438.479	1962.804	1481.749
7	H	2.883	-2434.292	0.018	0.014	0.023	0.000	-327.991	1246.635	942.608
	HV		-2949.921	0.019	0.014	0.024	0.000	-394.404	1672.784	1264.192
8	SDC06	-	-2837.770	-0.003	0.000	0.003	0.000	-355.628	1497.433	1132.723

Table 4.3-6 Elements Internal Force Outputs for the Bridge with Isolator 05

ISOLATOR 05

Comb	Comp.	$A_{p.HOR}$ / $V_{p.VERT}$	Column Axial(kN)	Isolator Deformation (m) UX	UY	SRSS	UZ	Isolator Axial(kN)	Beam Midspan Axial(kN)	Beam Midspan Moment(kNm)
1	H	1.054	-2423.529	0.015	0.032	0.036	0.000	-321.289	1246.163	942.647
	HV		-3053.458	0.015	0.032	0.036	0.000	-376.065	1530.496	1157.900
2	H	1.197	-2436.482	0.027	0.051	0.057	0.000	-342.419	1247.757	943.745
	HV		-2914.083	0.027	0.051	0.057	0.000	-373.698	1596.640	1207.809
3	H	1.514	-2488.814	0.040	0.055	0.068	0.000	-355.295	1248.845	944.701
	HV		-3656.777	0.042	0.055	0.069	0.000	-493.814	2324.529	1754.170
4	H	1.788	-2440.481	0.031	0.030	0.043	0.000	-342.139	1249.116	944.941
	HV		-2777.773	0.031	0.030	0.044	0.000	-371.806	1516.225	1146.313
5	H	1.818	-2389.906	0.013	0.024	0.027	0.000	-316.349	1243.287	940.842
	HV		-2901.273	0.013	0.024	0.027	0.000	-379.099	1666.753	1259.711
6	H	1.853	-2470.222	0.045	0.032	0.055	0.000	-364.329	1251.394	946.425
	HV		-3261.554	0.044	0.032	0.055	0.000	-449.250	1965.690	1484.278
7	H	2.883	-2444.702	0.023	0.015	0.027	0.000	-332.730	1246.678	942.659
	HV		-2944.460	0.024	0.015	0.028	0.000	-398.559	1670.467	1262.619
8	SDC06	-	-2838.104	-0.003	0.000	0.003	0.000	-361.738	1496.952	1132.521

Table 4.3-7 Elements Internal Force Outputs for the Bridge with Isolator 06

ISOLATOR 06										
Comb	Comp.	$A_{p.HOR}$ $/V_{p.VERT}$	Column Axial(kN)	Isolator Deformation (m) UX	UY	SRSS	UZ	Isolator Axial(kN)	Beam Midspan Axial(kN)	Beam Midspan Moment(kNm)
1	H	1.054	-2423.300	0.007	0.019	0.020	0.000	-326.025	1244.798	942.017
	HV		-3041.253	0.007	0.019	0.021	0.000	-381.530	1522.503	1153.137
2	H	1.197	-2463.993	0.023	0.043	0.049	0.000	-341.125	1244.925	942.313
	HV		-2914.351	0.023	0.043	0.049	0.000	-379.089	1592.774	1205.336
3	H	1.514	-2549.504	0.034	0.044	0.056	0.000	-364.099	1248.679	945.015
	HV		-3620.184	0.036	0.044	0.057	0.000	-508.115	2332.456	1760.687
4	H	1.788	-2477.719	0.023	0.031	0.039	0.000	-349.305	1244.052	941.558
	HV		-2774.259	0.023	0.031	0.039	0.000	-365.611	1514.280	1145.479
5	H	1.818	-2399.968	0.016	0.019	0.025	0.000	-332.623	1242.697	940.581
	HV		-2911.972	0.017	0.019	0.025	0.000	-387.942	1670.132	1262.700
6	H	1.853	-2470.227	0.030	0.029	0.042	0.000	-362.404	1247.094	943.619
	HV		-3240.322	0.030	0.029	0.042	0.000	-447.914	1969.373	1487.861
7	H	2.883	-2436.005	0.017	0.013	0.022	0.000	-328.450	1243.744	940.925
	HV		-2944.635	0.017	0.013	0.021	0.000	-393.331	1659.474	1254.958
8	SDC06	-	-2838.190	-0.003	0.000	0.003	0.000	-368.158	1495.404	1131.886

Table 4.3-8 Elements Internal Force Outputs for the Bridge with Isolator 07

ISOLATOR 07										
Comb	Comp.	$A_{p.HOR}$ $/V_{p.VERT}$	Column Axial(kN)	Isolator Deformation (m) UX	UY	SRSS	UZ	Isolator Axial(kN)	Beam Midspan Axial(kN)	Beam Midspan Moment(kNm)
1	H	1.054	-2392.857	0.006	0.011	0.012	0.000	-323.798	1241.350	940.072
	HV		-3031.213	0.006	0.011	0.012	0.000	-387.727	1517.919	1150.547
2	H	1.197	-2471.784	0.018	0.030	0.035	0.000	-341.735	1241.722	940.006
	HV		-2917.962	0.018	0.030	0.035	0.000	-388.763	1592.035	1205.145
3	H	1.514	-2478.238	0.023	0.030	0.037	0.000	-355.918	1244.497	942.590
	HV		-3605.821	0.022	0.029	0.036	0.000	-505.836	2330.431	1759.831
4	H	1.788	-2537.458	0.029	0.026	0.039	0.000	-376.299	1244.185	941.717
	HV		-2773.728	0.030	0.026	0.040	0.000	-394.407	1520.856	1150.518
5	H	1.818	-2406.584	0.009	0.015	0.018	0.000	-333.838	1240.376	939.274
	HV		-2862.594	0.009	0.015	0.018	0.000	-396.181	1659.039	1255.046
6	H	1.853	-2475.297	0.017	0.023	0.029	0.000	-355.075	1244.299	942.149
	HV		-3247.995	0.018	0.023	0.029	0.000	-445.244	1949.078	1472.972
7	H	2.883	-2418.450	0.007	0.009	0.011	0.000	-326.059	1240.886	939.521
	HV		-2967.909	0.007	0.009	0.011	0.000	-398.911	1649.130	1247.994
8	SDC06	-	-2838.269	-0.003	0.000	0.003	0.000	-375.150	1493.894	1131.266

Table 4.3-9 Elements Internal Force Outputs for the Bridge with Isolator 08

ISOLATOR 08

Comb	Comp.	$A_{p.HOR}/V_{p.VERT}$	Column Axial(kN)	Isolator Deformation (m) UX	UY	SRSS	UZ	Isolator Axial(kN)	Beam Midspan Axial(kN)	Beam Midspan Moment(kNm)
1	H	1.054	-2394.971	0.004	0.008	0.009	0.000	-326.079	1239.968	939.607
	HV		-3026.426	0.004	0.008	0.009	0.000	-390.533	1515.265	1149.052
2	H	1.197	-2489.862	0.015	0.025	0.029	0.000	-346.903	1241.220	940.568
	HV		-2916.205	0.015	0.025	0.029	0.000	-393.168	1592.747	1205.907
3	H	1.514	-2507.603	0.023	0.026	0.035	0.000	-356.294	1241.782	940.752
	HV		-3645.457	0.022	0.026	0.034	0.000	-508.788	2332.228	1761.923
4	H	1.788	-2569.689	0.026	0.026	0.037	0.000	-378.383	1243.431	941.884
	HV		-2784.704	0.026	0.026	0.037	0.000	-398.250	1507.385	1141.355
5	H	1.818	-2391.079	0.004	0.012	0.013	0.000	-326.261	1239.609	938.988
	HV		-2893.653	0.004	0.012	0.013	0.000	-401.843	1649.056	1248.180
6	H	1.853	-2497.807	0.016	0.018	0.024	0.000	-361.756	1243.103	941.515
	HV		-3244.825	0.016	0.018	0.024	0.000	-442.618	1931.086	1460.165
7	H	2.883	-2436.216	0.005	0.010	0.012	0.000	-328.282	1240.100	939.263
	HV		-2968.316	0.005	0.010	0.011	0.000	-403.497	1642.314	1243.425
8	SDC06	-	-2838.212	-0.003	0.000	0.003	0.000	-378.106	1492.752	1130.799

Table 4.3-10 Elements Internal Force Outputs for the Bridge with Isolator 09

				ISOLATOR 09						
Comb	Comp.	$A_{p.HOR}/V_{p.VERT}$	Column Axial(kN)	Isolator Deformation (m) UX	UY	SRSS	UZ	Isolator Axial(kN)	Beam Midspan Axial(kN)	Beam Midspan Moment(kNm)
1	H	1.054	-2422.348	0.004	0.008	0.009	0.000	-327.625	1238.474	938.936
	HV		-3019.850	0.004	0.008	0.009	0.000	-391.883	1509.358	1145.426
2	H	1.197	-2533.960	0.012	0.020	0.024	0.000	-349.863	1239.739	939.655
	HV		-2909.638	0.012	0.020	0.024	0.000	-392.376	1585.797	1201.214
3	H	1.514	-2569.519	0.015	0.023	0.027	0.000	-356.110	1241.790	940.469
	HV		-3628.637	0.015	0.023	0.027	0.000	-520.860	2320.728	1754.626
4	H	1.788	-2565.214	0.018	0.024	0.029	0.000	-361.047	1241.392	940.815
	HV		-2768.370	0.017	0.024	0.029	0.000	-381.220	1505.770	1140.460
5	H	1.818	-2428.482	0.004	0.009	0.010	0.000	-329.400	1238.415	938.808
	HV		-2924.997	0.004	0.009	0.010	0.000	-407.094	1660.491	1257.085
6	H	1.853	-2496.972	0.012	0.015	0.019	0.000	-348.879	1240.410	940.381
	HV		-3344.191	0.012	0.015	0.019	0.000	-466.579	1936.797	1465.535
7	H	2.883	-2507.015	0.009	0.010	0.013	0.000	-336.950	1238.839	938.777
	HV		-3030.172	0.008	0.010	0.013	0.000	-413.283	1636.967	1239.969
8	SDC06	-	-2838.020	-0.003	0.000	0.003	0.000	-379.908	1490.981	1130.080

Table 4.3-11 Elements Internal Force Outputs for the Bridge without Isolator

W/O ISOLATOR										
Comb	Comp.	$A_{p.HOR}/V_{p.VERT}$	Column Axial(kN)	Isolator Deformation (m) UX	UY	SRSS	UZ	Isolator Axial(kN)	Beam Midspan Axial(kN)	Beam Midspan Moment(kNm)
1	H	1.054	-2288.988	-	-	-	-	-	731.916	822.712
	HV		-2706.304	-	-	-	-	-	930.772	1023.004
2	H	1.197	-2385.843	-	-	-	-	-	739.751	829.292
	HV		-2778.715	-	-	-	-	-	973.879	1083.276
3	H	1.514	-2435.048	-	-	-	-	-	736.977	829.124
	HV		-3740.038	-	-	-	-	-	1548.755	1687.790
4	H	1.788	-2346.694	-	-	-	-	-	731.154	823.166
	HV		-2707.079	-	-	-	-	-	972.254	1060.938
5	H	1.818	-2260.354	-	-	-	-	-	730.583	822.836
	HV		-2744.326	-	-	-	-	-	1029.643	1135.106
6	H	1.853	-2455.145	-	-	-	-	-	733.171	827.894
	HV		-3059.023	-	-	-	-	-	1264.330	1372.291
7	H	2.883	-2366.742	-	-	-	-	-	734.859	826.564
	HV		-2575.380	-	-	-	-	-	969.664	1081.037
8	SDC06	-	-2663.691	-	-	-	-	-	876.837	987.615

CHAPTER 5

COMPARISONS AND DISCUSSIONS

5.1. Fundamental Periods on Response Spectra

Figures 4.3-1 through 4.3-7 show the response spectra of the seven different earthquakes including the fundamental periods marked on the spectrum curves. The markers are specific to the bridge models. They are aimed to illustrate where the fundamental period of each bridge model takes place on the spectrum curve. There are three main discussions arisen from the figures. First, fundamental periods of seismically isolated bridge systems show an advantageous place on the response spectra for most of the cases regarding the vertical component of the EQs. On the other hand bridge systems without isolation yield greater pseudo acceleration. Second, existence of seismic isolation on the bridges doesn't have a remarkable contribution regarding dissipation of the EQ loads due to the horizontal components. Since response spectrum of horizontal components of the EQs have longer plateaus, both bridge systems with and without seismic isolation laid into it. Third, the vertical components of the EQs are not producing resonance in seismically isolated bridges. The influence of resonance is very critical for a bridge in all directions but particularly in vertical direction. Production of resonance causes more severe effects during an EQ.

5.2. *Artificially Generated Isolators*

Isolator 05 (ISO-05) is one of the isolators chosen from the commercially available isolation devices. Characteristic properties of all commercially available isolator that are used in this study were given in Chapter 2. However, the two important properties of which are effective stiffness and compression stiffness, vary simultaneously without any correlation between them. This causes a gap while comparing the isolators. In order to make a more dependable comparison between the isolators, 4 more isolators with artificial properties are generated. Basically, these are started with the properties of ISO-05 and both of the important properties are controlled against each other. First, two isolators with same effective stiffness and different compression stiffness and then, two isolators with same compression stiffness and different elastic stiffness are generated to control the dependency of the comparison. Each two new isolators set is controlled together with the ISO-05 as stated hereafter.

Table 5.2-1 shows the characteristic stiffness properties of these four generated isolators. Here, it should be noted that effective stiffness of an isolator depends on the; post yield stiffness, characteristic strength and design displacement which are given in the table for information. On the other hand, compression stiffness doesn’t have any influence on other properties of an isolator.

Table 5.2-1 Characteristic Stiffness Properties of the ISO-05, 05A, 05B, 05C and 05D

Isolators	Post Yield Stiffness (kN/mm)	Compression Stiffness (kN/mm)	Effective Stiffness (kN/mm)	Characteristic Strength (kN)	Design Displacement (mm)	K_{eff} / K_v -
ISO-05-A	0.70	**100**	**1.65**	355	373	0.0165
ISO-05	0.70	**1400**	**1.65**	355	373	0.0012
ISO-05-B	0.70	**6500**	**1.65**	355	373	0.0003
ISO-05-C	0.20	**1400**	**0.85**	65	100	0.0006
ISO-05	0.70	**1400**	**1.65**	355	373	0.0012
ISO-05-D	1.80	**1400**	**2.84**	630	607	0.0020

5.2.1. Effect of Compression Stiffness

To discuss the effect of compression stiffness on girder midspan moments, pier axial forces and isolator axial forces of ISO-05-A, 05 and 05-B are used.

Figure 5.2-1 shows the girder midspan moment ratios of H/HV for each EQ data and average of them with respect to K_{eff}/K_v ratio. It is clearly seen from the figure that there is not a significant change in H/HV ratio for different K_{eff}/K_v ratios. As a result it can be concluded that compression stiffness doesn't have a significant influence on the girder midspan moment.

Figure 5.2-2 shows the pier axial force ratios of H/HV for each EQ data and average of them with respect to K_{eff}/K_v ratio. It is clearly seen from the figure that there is not a significant change in H/HV ratio for different K_{eff}/K_v ratios. As a result it can be concluded that varying isolator property of compression stiffness with constant effective stiffness doesn't have a significant influence on the axial forces generated in the piers.

Figure 5.2-3 shows the isolator axial force ratio of H/HV for each EQ data and average of them with respect to K_{eff}/K_v ratio. Apart from girder bending moment and pier axial force ratios, isolator axial force ratios show a slight change for different K_{eff}/K_v ratios. However, the change in the isolator axial force ratio is around 4% and it can be neglected for most of the cases. Hence, one can say that there is not a significant change in H/HV ratio for different K_{eff}/K_v ratios.

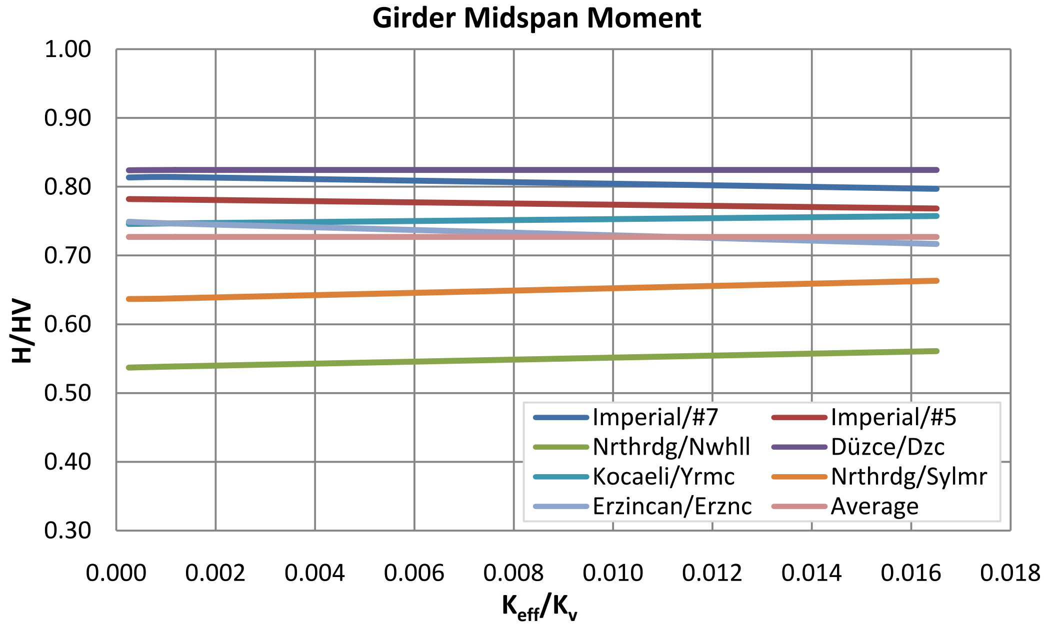

Figure 5.2-1 Girder Midspan Moment Ratios of the Bridges with ISO-05-A, ISO-05 and ISO-05-B wrt K_{eff}/K_v

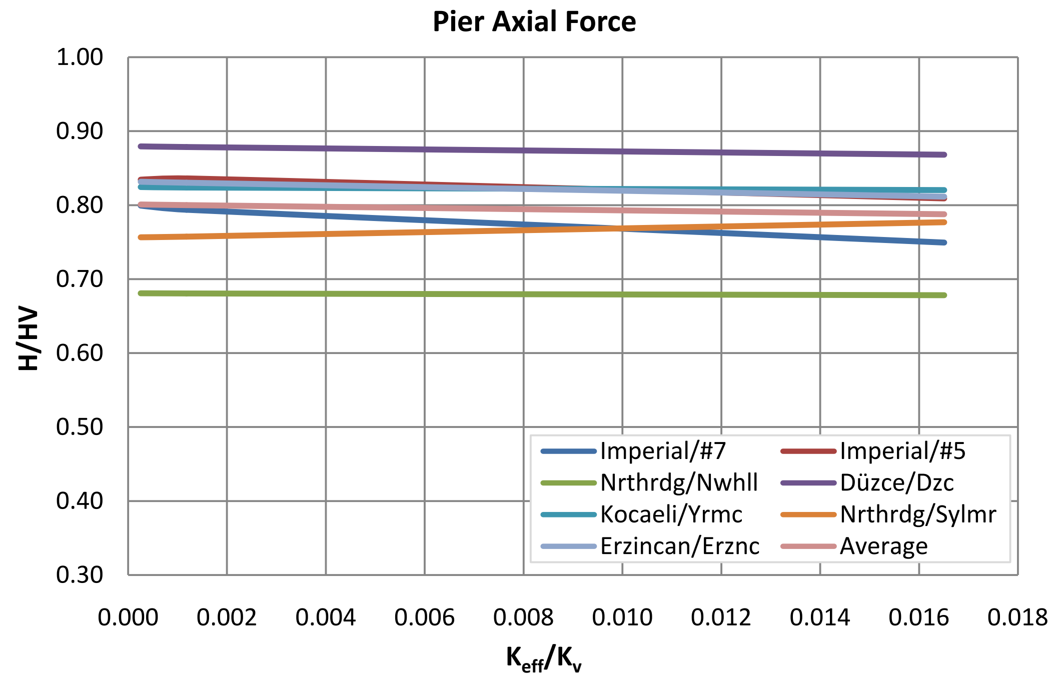

Figure 5.2-2 Pier Axial Force Ratios of the Bridges with ISO-05-A, ISO-05 and ISO-05-B wrt K_{eff}/K_v

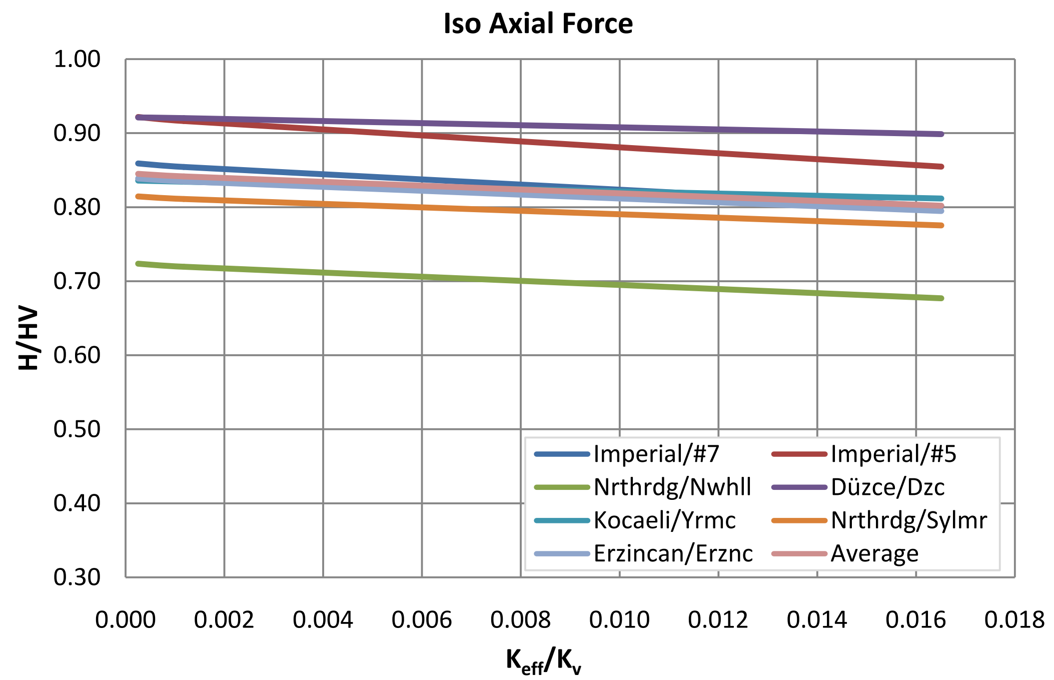

Figure 5.2-3 Isolator Axial Force Ratios of the Bridges with ISO-05-A, ISO-05 and ISO-05-B wrt K_{eff}/K_v

5.2.2. *Effect of Post Yield Stiffness*

To discuss the effect of post yield stiffness on the girder midspan momens, pier axial forces and isolator axial forces of ISO-05-C, ISO-05 and ISO-05-D are used.

Figure 5.2-4 shows the girder midspan moment ratios of H/HV for each EQ data and average of them with respect to K_{eff}/K_v ratio. It is clearly seen from the figure that there is not any change in H/HV ratio for different K_{eff}/K_v ratios. As a result it can be concluded that varying isolator property of effective stiffness with constant compression stiffness doesn't have a significant influence on the moments generated in the girder.

Figure 5.2-5 shows the pier axial force ratios of H/HV for each load combination and average of all load combinations with respect to K_{eff}/K_v ratio. Here, H/HV ratio increases as K_{eff}/K_v increases. However, this situation is a major issue since the increase in ratio is around 5% for all EQ data. As a result, it can be concluded that varying isolator property of effective stiffness with constant compression stiffness has a significant influence on the axial forces generated in the piers.

Figure 5.2-6 shows the isolator axial force ratio of H/HV for each EQ data and average of them with respect to K_{eff}/K_v ratio. Similar to girder midspan bending moment ratios, isolator axial force ratios don't change remarkably with respect to K_{eff}/K_v ratio. In the Figure 5.2-6, it is seen that ratios of Northridge / Newhall EQ and Northridge / Sylmar EQ tend to decrease significantly with respect to increasing K_{eff}/K_v ratios while, Imperial / El Centro Array #5 EQ shows a significant increase with increasing K_{eff}/K_v ratio. On the other hand if the average of the EQ data is used, it is seen that varying isolator property of effective stiffness with constant compression stiffness doesn't have a significant influence on the isolator axial forces generated in the isolation devices.

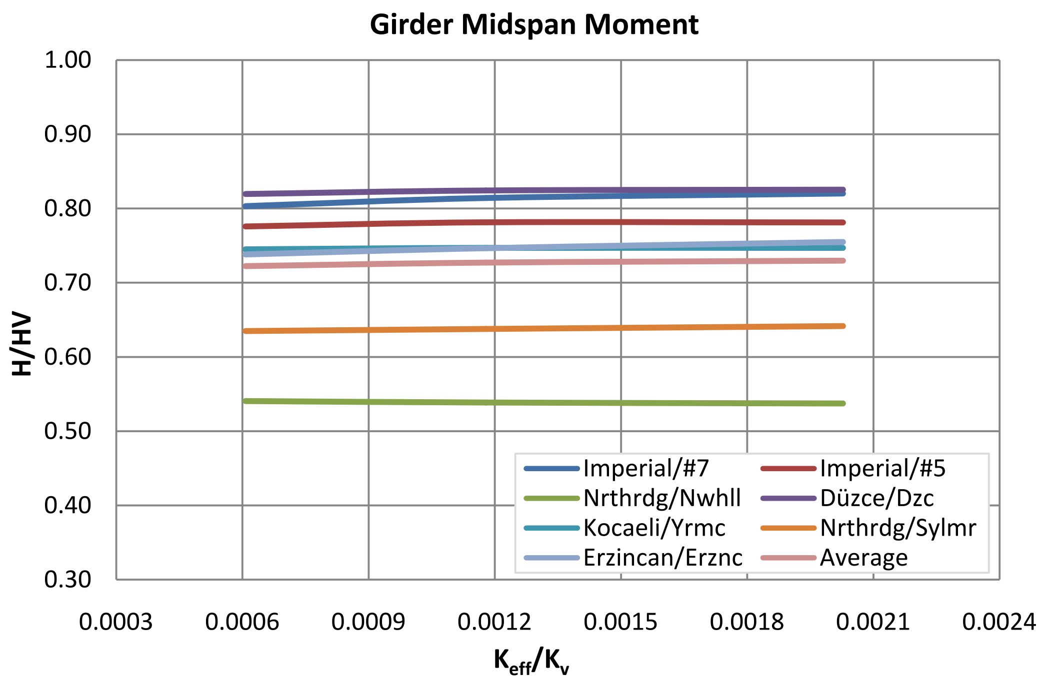

Figure 5.2-4 Girder Midspan Moment Ratios of the Bridges with ISO-05-C, ISO-05 and ISO-05-D wrt K_{eff}/K_v

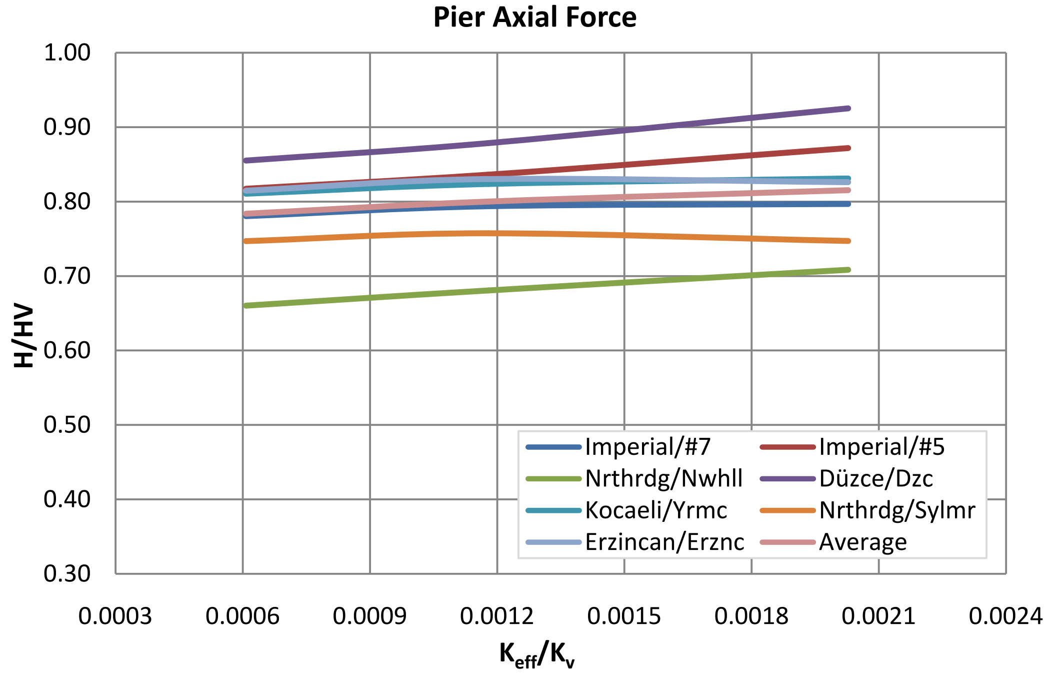

Figure 5.2-5 Pier Axial Force Ratios of the Bridges with ISO-05-C, ISO-05 and ISO-05-D wrt K_{eff}/K_v

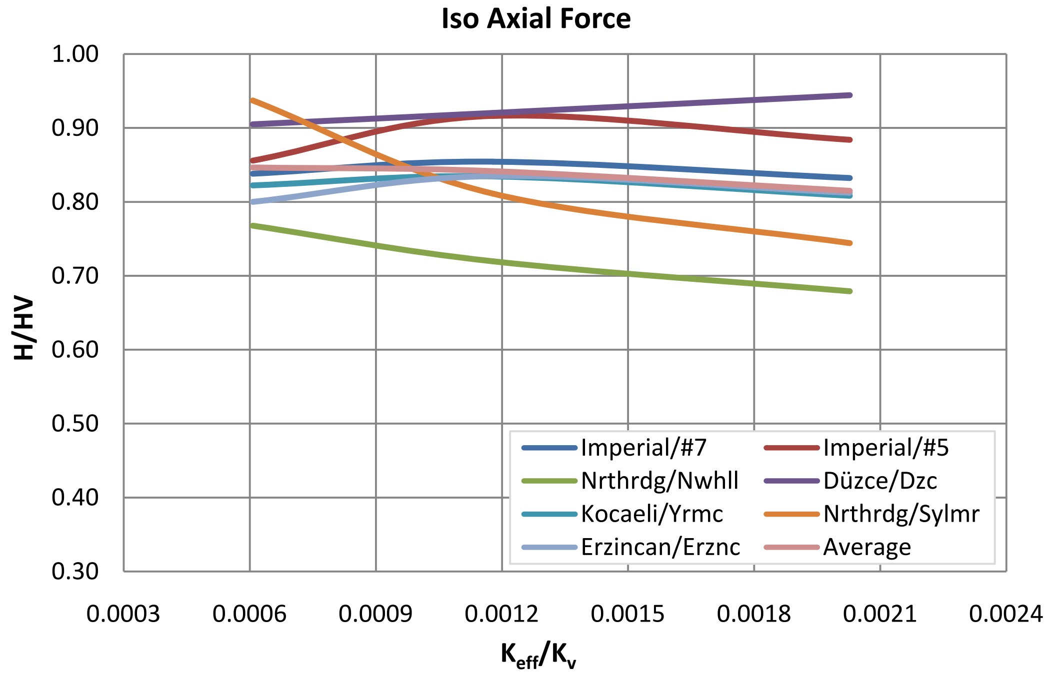

Figure 5.2-6 Isolator Axial Force Ratios of the Bridges with ISO-05-C, ISO-05 and ISO-05-D wrt K_{eff}/K_v

5.3. Member Forces

Nine steel girder bridge models are generated using nine different commercially available lead rubber bearings. Outputs from these models are normalized with each other to provide a complete investigation about influences of LRBs on member forces namely; girder midspan moment, pier axial force and isolator axial force. Moreover, the comparison between member forces from THA and member forces from SDC 2006 [3] static EQ load is introduced to investigate the adequacy of equivalent static load case against the dynamic load cases.

5.3.1. Girder Midspan Moment

Figure 5.3-1 illustrates the H/HV ratios of girder midspan moments with respect to K_{eff}/K_v for 7 different EQ data and average of them. Figure 5.3-1 shows that girder midspan moment of the bridge systems does not change with K_{eff}/K_v ratios for the same EQ data. If one uses the average result of the 7 EQ data for design purposes, the value of H/HV will be 0.72. This means including vertical ground motion in the analysis increases girder midspan moment by 40%.

Figure 5.3-2 illustrates the H/HV ratios of girder midspan moments with respect to $A_{p,HOR}/A_{p,VERT}$ for nine different rubber isolators. What is obvious in this figure is all isolators H/HV curves' fitting on each other which reveals isolator property doesn't have a significant effect on the girder midspan moments in steel girder bridges.

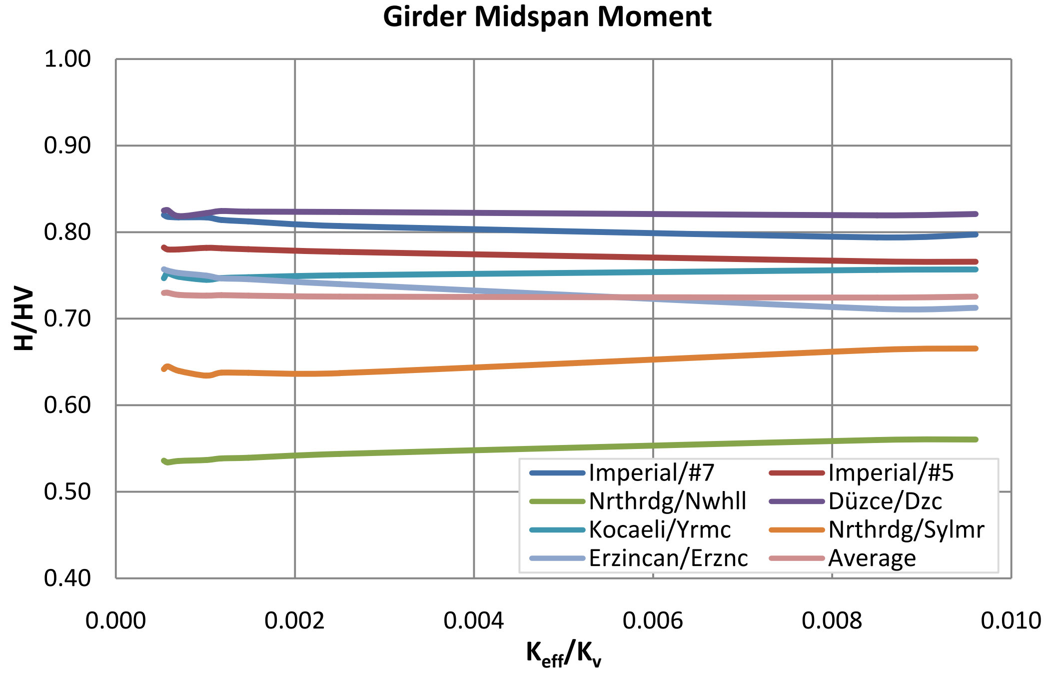

Figure 5.3-1 Girder Midspan Moment Ratios of the Bridges with ISO-01-02-03-04-05-06-07-08-09 wrt K_{eff}/K_v

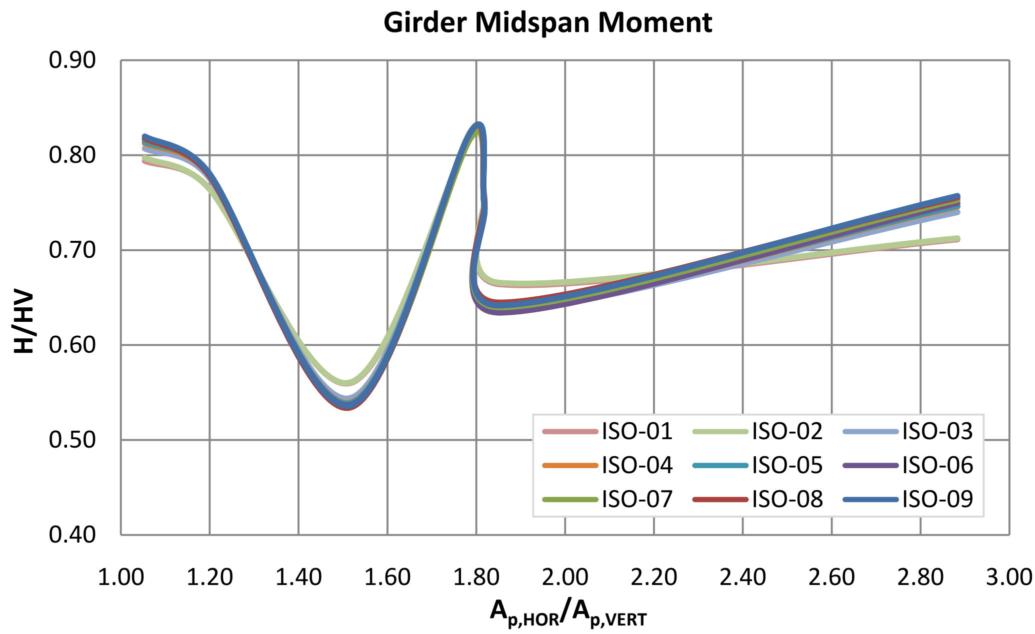

Figure 5.3-2 Girder Midspan Moment Ratios of the Bridges with ISO-01-02-03-04-05-06-07-08-09 wrt $A_{p,HOR}/A_{p,VERT}$

5.3.2. Pier Axial Force

Figure 5.3-3 illustrates the H/HV ratios of pier axial forces with respect to K_{eff}/K_v for 7 EQ data and average of them. It shows that effect of K_{eff}/K_v on pier axial force shows different behavior for different EQ data. Some of A/B ratio curves for different EQ data tend to follow almost a straight line while some others show a linearly decreasing behavior with the increase in K_{eff}/K_v. The H/HV ratio for the average of 7 EQ data is found as 0.79. This means including vertical ground motion in the analysis increases pier axial load by 27%.

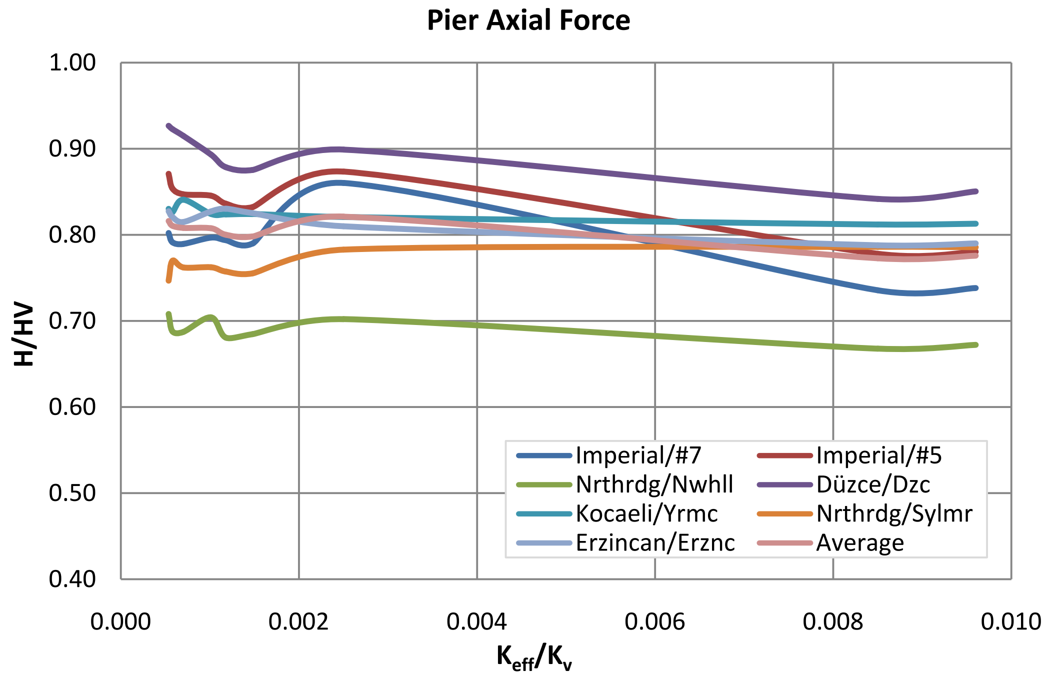

Figure 5.3-3 Pier Axial Force Ratios of the Bridges with ISO-01-02-03-04-05-06-07-08-09 wrt K_{eff}/K_v

5.3.3. *Isolator Axial Force*

Figure 5.3-4 illustrates the H/HV ratios of the isolator axial forces with respect to K_{eff}/K_v for 7 EQ data and average of them. It shows for very small values of K_{eff}/K_v ratio H/HV ratio varies significantly, while increasing K_{eff}/K_v ratio stabilize the H/HV ratio and leads to a constant value for it. The maximum change in H/HV ratio for the same EQ data is around 15% for very small values of K_{eff}/K_v ratio. On the other hand the H/HV ratio is 0.80 for the average of all EQ data. This leads to 25% increase in isolator axial force in case of inclusion of vertical ground motion.

Therefore, one can say that including the vertical ground motion data into the analysis results 25% increase on isolator axial force. It is known that, compression stiffness of LRBs are high and that much increase in axial force is not a problem. However, axial force level on isolator influences the shear modulus which also influences the vertical behavior of it.

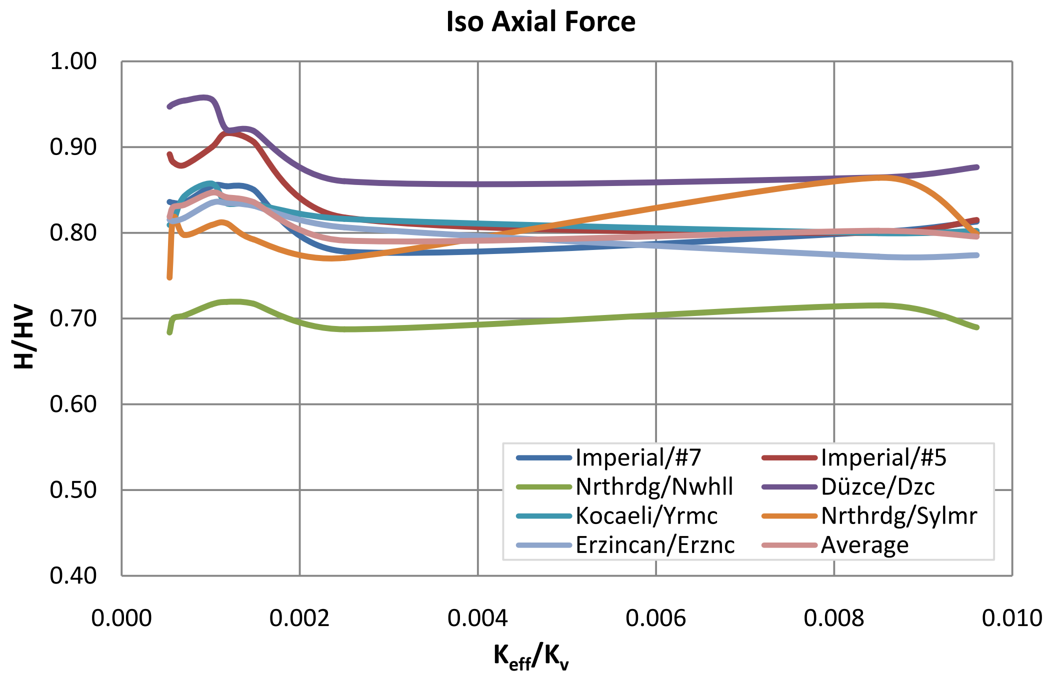

Figure 5.3-4 Girder Midspan Moment Ratios of the Bridges with ISO-01-02-03-04-05-06-07-08-09 wrt K_{eff}/K_v

5.3.4. *Member Forces Generated by SDC-2006 Loading*

Caltrans Seismic Design Criteria (SDC) [3] specifies the minimum seismic design requirements that are necessary to meet the performance goals established for Ordinary bridges in Memo to Designers (MTD) 20-1 [31]. There are some certain statements in SDC-2006 regarding the vertical ground motion effects on bridges. Briefly, the code calls for an equivalent static vertical load which shall be applied to the superstructure to estimate the effects of vertical acceleration for bridges where the site peak rock acceleration is 0.6g or greater. The equivalent static vertical load is defined as a uniformly applied vertical force equal to 25% of the dead load applied upward and downward. The code does not state anything for the ground acceleration smaller than 0.6g which means the vertical ground motion effects on the analysis is neglected.

In this chapter the adequacy of the SDC-2006 loading against dynamic load combinations is investigated. SDC-2006 loading is assigned to the bridge as per definition above and compared with the dynamic load combination outputs as follows.

Figure 5.3-5 shows the H/HV and H/SDC ratios of the girder midspan moments with respect to K_{eff}/K_v. On figure, H/HV stands for the mean ratio of girder span moment (average of the ratios from 7 EQ data) H/SDC stands for the ratio of the member forces due to the dynamic load of the horizontal EQ component to the member forces due to the equivalent static vertical load as per SDC-2006, i.e.

$$\frac{H}{HV} = \frac{Dynamic\ load\ comb.\ of\ two\ hor. EQ\ components}{Dynamic\ load\ comb.\ of\ two\ hor.+vert.\ EQ\ components}$$

$$\frac{H}{SDC} = \frac{Dynamic\ load\ comb.\ of\ two\ hor.\ EQ\ components}{Equivalent\ static\ vertical\ load\ comb.\ as\ per\ SDC - 2006}$$

It is seen that, the H/HV ratio is equal to 0.72 while H/SDC ratio is equal to 0.83. These values show that the girder midspan moment generated by dynamic load combination of vertical EQ component is greater than one generated by static vertical load combination as per SDC-2006 [3]. There is a significant difference which is around 13% between the ratios. Also, changes in the isolator properties don't have any influence on the girder midspan moment by the equivalent static vertical load combination just like the dynamic load combinations.

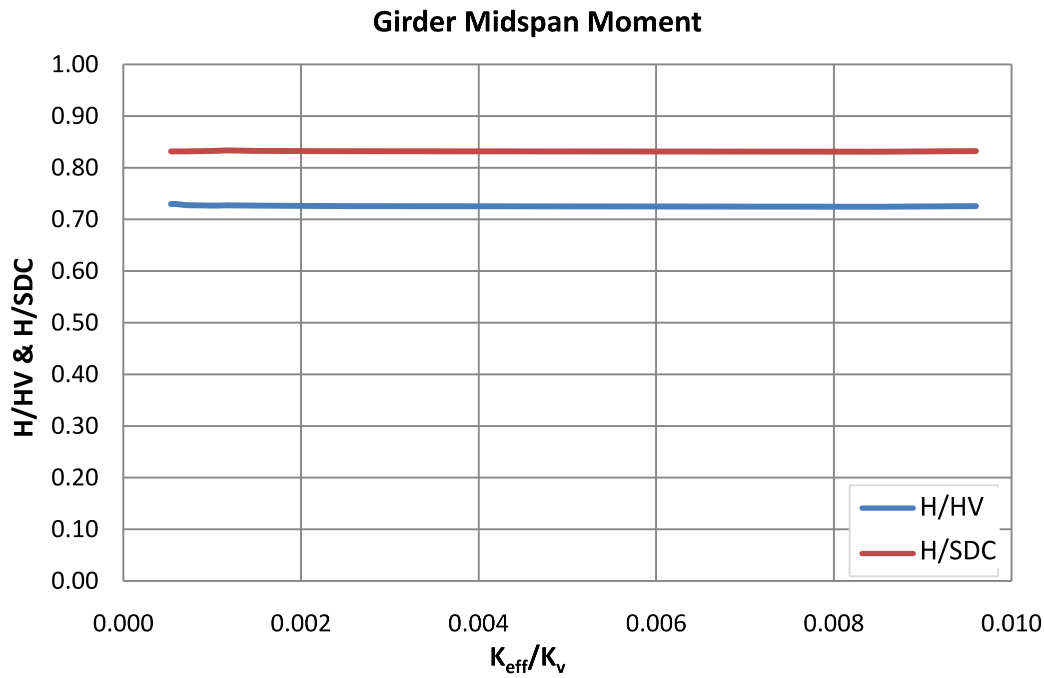

Figure 5.3-5 Girder Midspan Moment Ratios of the Bridges versus K_{eff}/K_v for Dynamic and SDC-2006 Load Cases

Figure 5.3-6 shows the H/HV and H/SDC ratios of the girder midspan moments with respect to $A_{p,HOR}/A_{p,VERT}$. This figure illustrates the importance of the dynamic analysis with real EQ data. As expected, dynamic analysis output shows variety depending on $A_{p,HOR}/A_{p,VERT}$ on the other hand for the equivalent static load analysis output doesn't have a dependency on $A_{p,HOR}/A_{p,VERT}$. This may lead to some issues while designing a bridge system because it is obvious that the topography can have direct effects on a bridge.

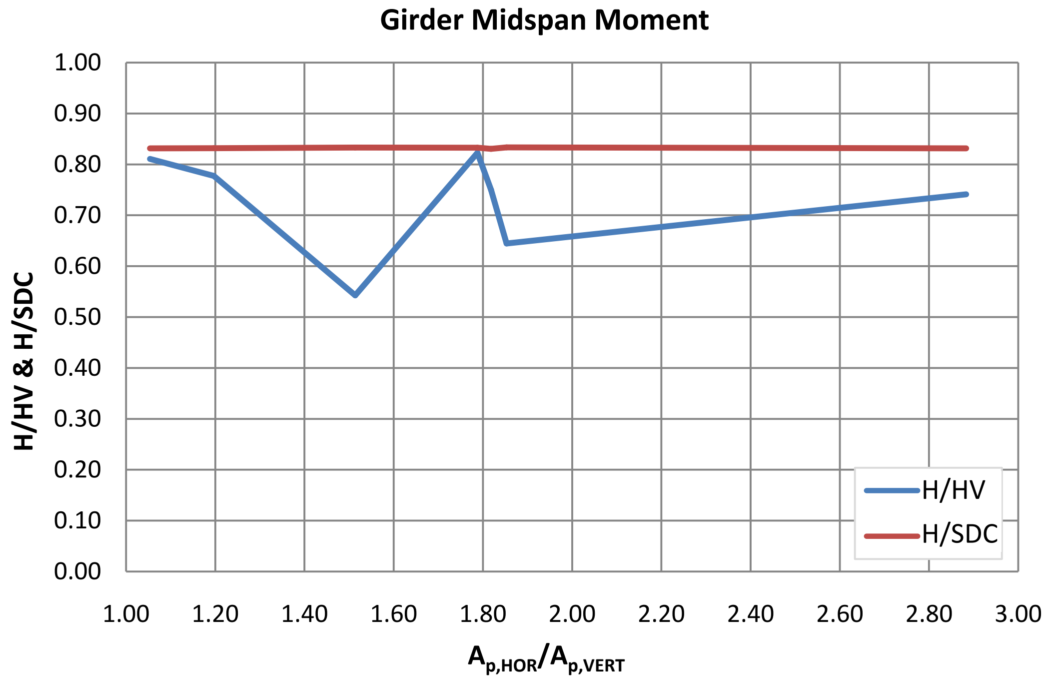

Figure 5.3-6 Girder Midspan Moment Ratios of the Bridges versus $A_{p,HOR}/A_{p,VERT}$ for Dynamic and SDC-2006 Load Cases

It is also seen that H/SDC ratio tends to be always greater than H/HV ratio, which means greater girder midspan moment generated with inclusion of vertical ground motion data. The H/SDC ratio is around 0.83 on the other hand the H/HV ratio values vary between 0.55 and 0.81. If the worst case scenario is considered for design, then the difference between the H/SDC and H/HV ratios is calculated as 34%. However, if the average of 7 EQ data is chosen as design case, then the average H/HV ratio is 0.72 and the difference between the H/SDC and H/HV ratios is calculated as 13%.

Whichever case is considered, there is a significant difference between the H/SDC and the H/HV ratios.

Figure 5.3-7 shows the H/HV and H/SDC ratios of the pier axial forces with respect to K_{eff}/K_v. As stated in the discussions on the girder midspan moment above, the pier axial forces generated by equivalent static load cases are also smaller than the forces generated with inclusion of vertical ground motion data. The difference of H/HV and H/SDC ratios of pier axial forces can be as high as 12%.

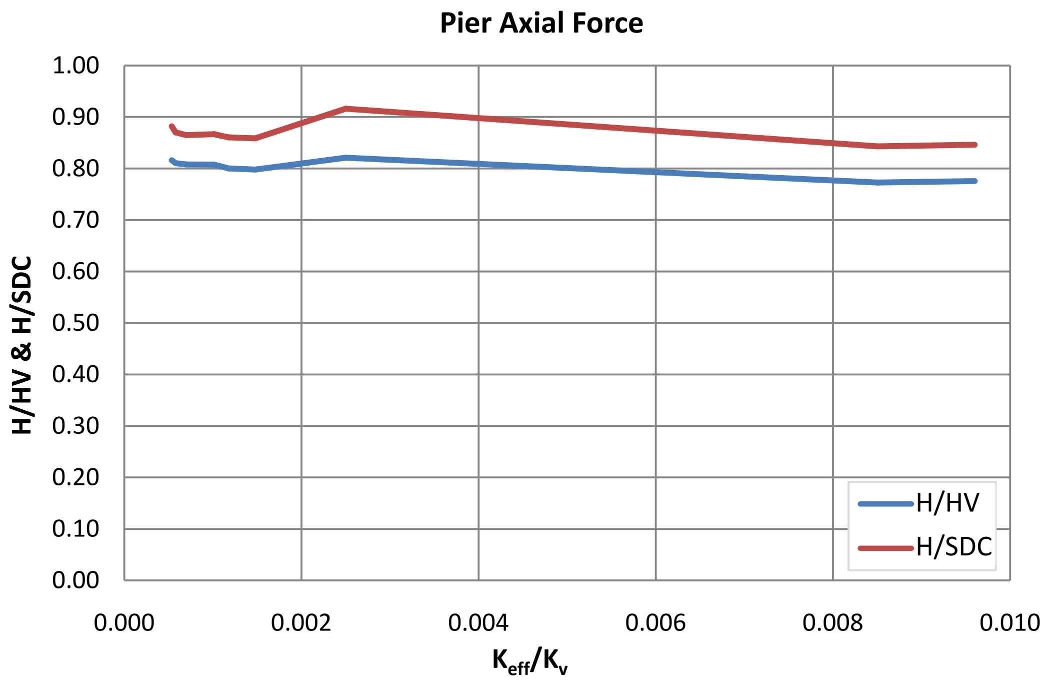

Figure 5.3-7 Pier Axial Force Ratios of the Bridges versus K_{eff}/K_v for Dynamic and SDC-2006 Load Cases

Figure 5.3-8 show the H/HV and H/SDC ratios of the isolator axial forces with respect to K_{eff}/K_v. Similar to the discussions on the girder midspan moment and the pier axial force, the isolator axial forces generated by equivalent static load cases are also smaller than the forces generated by dynamic load cases. The difference of H/HV and H/SDC ratios of isolator axial forces varies between 7% and 9%.

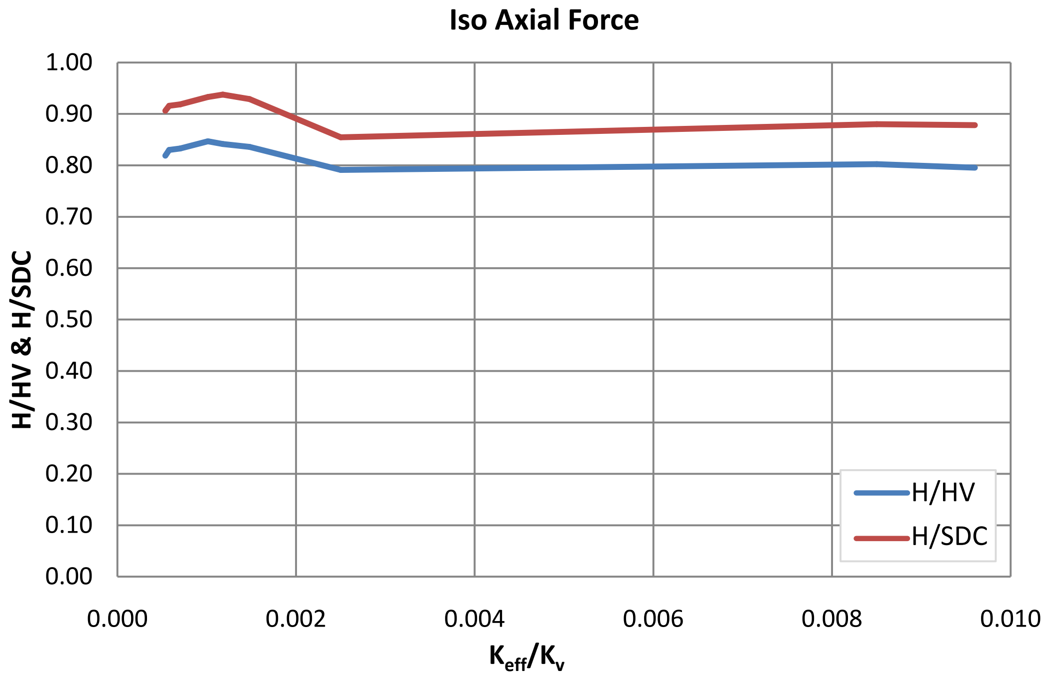

Figure 5.3-8 Isolator Axial Force Ratios of the Bridges versus K_{eff}/K_v for Dynamic and SDC-2006 Load Cases

5.4. Bridge Systems with and without Seismic Isolation

The model of the composite steel girder bridge with seismic isolation is reconstructed as a steel girder bridge without seismic isolation. Basically, the reconstruction includes replacement of the isolators at the connections of pier cap beams and steel girders with rigid links. On the issue of replacement, main objective is enabling axial force transfer from girders to piers or vice versa. Also, the both end of the girders are defined with moment releases to discard the moment transfer from connecting elements. As a result same sort of end conditions as in isolated bridge is achieved.

Table 5.4-1 shows the girder midspan moment and pier axial force of the bridges with and without isolation for all H and HV cases of EQs. In the table the percentage of increase in the moment and force value is also shown under the increase column. Also, H and HV cases for the bridge with seismic isolation show the mean member forces from the bridge models with nine different isolators. On the other hand H and HV cases for the bridge without seismic isolation show output from only one bridge. It is clearly seen from the table that, use of isolation in the studied bridge cause significant increase in girder midspan moment and pier axial force for both H and HV cases. The increase in girder midspan moment for H and HV cases can be as high as 14% and 17%, respectively. On the other hand, the increase in pier axial force for H and HV cases can be as high as 6% and 16%, respectively.

Table 5.4-1 Pier Axial Forces and Girder Midspan Moments of the Bridges with and without Seismic Isolation

Comb.	Comp.	Girder Moment (kNm) Without Isolation	Girder Moment (kNm) With Isolation	Increase %	Pier Axial Force (kN) Without Isolation	Pier Axial Force (kN) With Isolation	Increase %
1	H	822.71	941.05	14%	-2288.99	-2401.60	5%
	HV	1023.00	1160.98	13%	-2706.30	-3083.25	14%
2	H	829.29	941.53	14%	-2385.84	-2438.35	2%
	HV	1083.28	1211.55	12%	-2778.72	-2942.49	6%
3	H	829.12	942.73	14%	-2435.05	-2498.77	3%
	HV	1687.79	1737.74	3%	-3740.04	-3638.86	-3%
4	H	823.17	942.41	14%	-2346.69	-2464.22	5%
	HV	1060.94	1145.84	8%	-2707.08	-2785.33	3%
5	H	822.84	940.06	14%	-2260.35	-2386.04	6%
	HV	1135.11	1253.39	10%	-2744.33	-2897.94	6%
6	H	827.89	943.18	14%	-2455.15	-2469.21	1%
	HV	1372.29	1463.46	7%	-3059.02	-3223.71	5%
7	H	826.56	941.01	14%	-2366.74	-2426.95	3%
	HV	1081.04	1270.18	17%	-2575.38	-2980.26	16%

5.5. Design Loading Combination

In general, the design is governed by Strength-I loading combination. However, structural elements can generate more critical forces in case of use of vertical ground motion in analysis. This section compares the Strength-I combination with the EQ embedded combination H and HV.

Figure 5.5-1 and Figure 5.5-2 shows the member force ratios as St. I/H and St. I/HV with respect to the isolators. “St. I” stands for the AASHTO strength criteria Strength I and “H” and “HV” stands for the horizontal and vertical EQ embedded AASHTO extreme loading combinations, respectively.

Figure 5.5-1 presents the girder midspan moment ratio with respect to the isolators. One can clearly see the effect of the vertical ground motion in the figure. While, the St. I/H ratio is 1.43, the St. I/HV ratio is around 0.78. This means, inclusion of vertical ground motion in the analysis governs the design loading combination used for design of main girder.

Figure 5.5-2 presents the pier axial force ratio with respect to the isolators. Similarly, the influence of vertical ground motion can be seen clearly in the figure. While, the St. I/H ratio is 1.22, the St. I/HV ratio is around 0.84. This means, inclusion of vertical ground motion in the analysis governs the design loading combination used for design of piers.

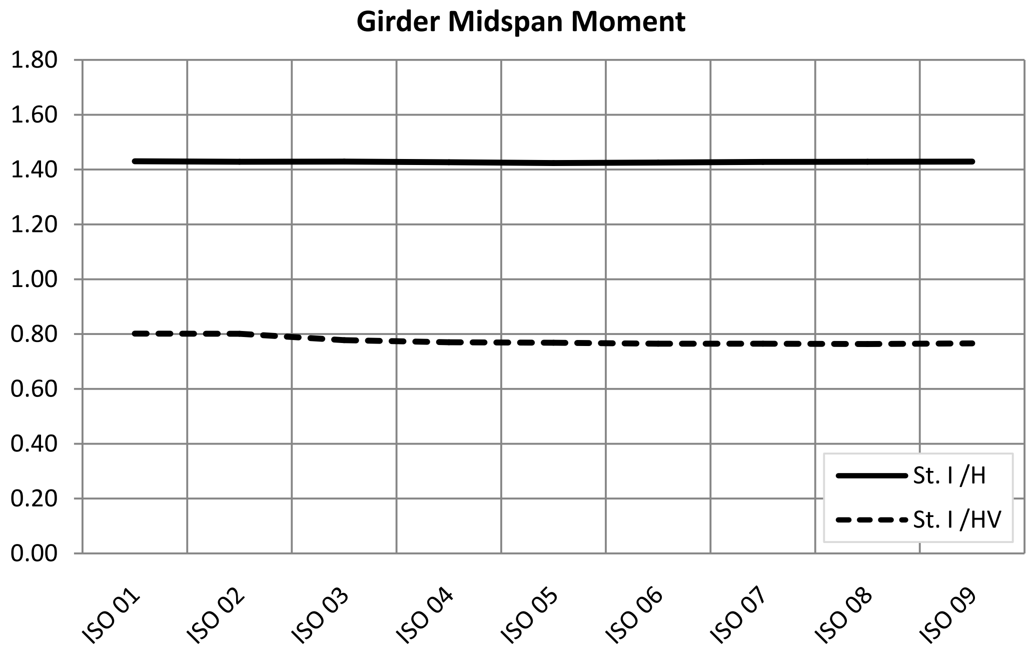

Figure 5.5-1 Girder Midspan Moment Ratios of the Isolators

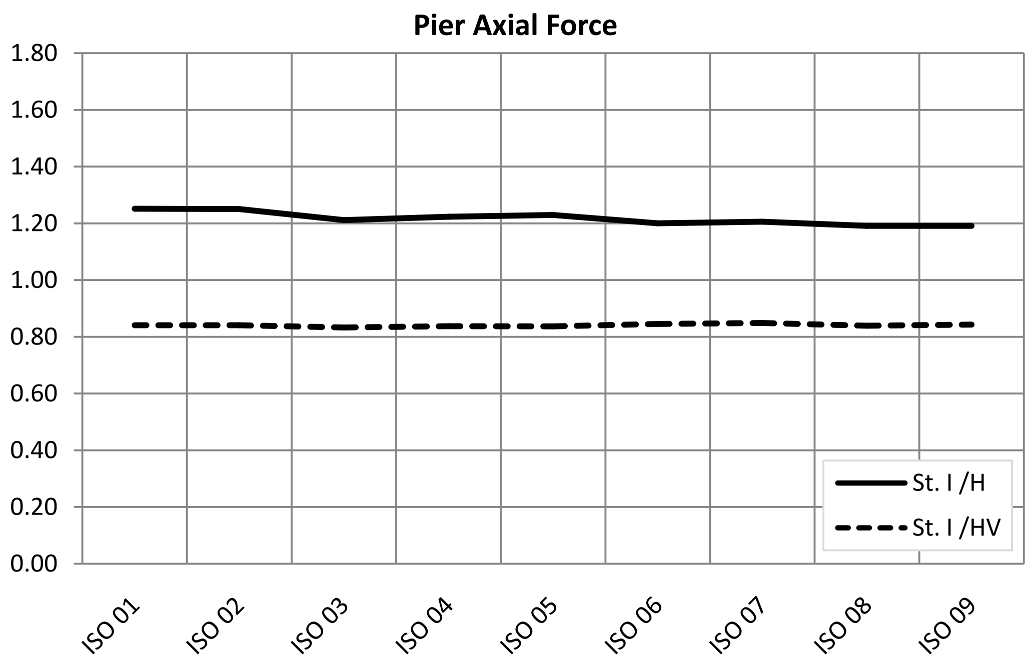

Figure 5.5-2 Pier Axial Force Ratios of the Isolators

CHAPTER 6

CONCLUSIONS

6.1. Conclusions

The main objective of this thesis was to investigate the influences of vertical ground motion on the bridges with and without seismic isolation. After a brief introduction on seismic isolation and devices, more specific information on seismic isolation on bridges was presented. Besides this, all required information on performing this numerical study was introduced one by one. The study was carried out using a steel girder composite bridge and 9 commercially produced LRBs with different characteristic properties. 9 mathematical bridge models with and without seismic isolation were built. Moreover, 7 different EQ data in same site class were selected. Two horizontal and one vertical components of the EQs were used in the analysis of bridges using some sort of nonlinear THA in the SAP2000 [14] software. In addition to THA, SDC-2006 [3] provisions were considered for incorporating vertical effects of EQs in bridges with seismic isolation even for the cases where PGA≤0.6g. Finally, numerical results were obtained and introduced. The member forces presented for comparison are girder midspan moment, pier axial force and isolator axial force.

This study reveals that;

- The vertical components of the EQs are not producing resonance in seismically isolated bridges for the ground motion data chosen in this study.

- Vertical ground motion affects the girder midspan moment, pier axial force and isolator axial force significantly.
- Disregarding the vertical ground motion from the analysis leads to an underestimation of 40% of girder midspan moment, 27% of pier axial force and 25% of isolator axial force.
- The bridge systems with different isolators have the same H/HV ratio of the girder midspan moment for same combination. Also, varying K_{eff}/K_v ratio doesn't have a significant effect on the girder midspan moments, pier axial force and isolator axial force. Hence, isolator property doesn't have a significant effect in steel girder bridge analyzed in this study.
- The girder midspan moment generated by dynamic load combination of vertical EQ component is greater than the one generated by static vertical load combination as per SDC-2006. There is a significant difference (13%) between the ratios.
- The difference of H/HV and H/SDC ratios of pier axial forces varies between 6% and 12%.
- The difference of H/HV and H/SDC ratios of isolator axial forces is approximately 8%.
- Use of isolation system in the studied bridge leads to significant increase in the girder midspan moment for both H and HV cases. The increase in the girder midspan moment for H and HV cases can be as high as 14% and 17%, respectively.
- Use of isolation system in the studied bridge leads to significant increase in the pier axial force for both H and HV cases. The increase in the pier axial force for H and HV cases can be as high as 6% and 16%, respectively.

- Inclusion of vertical ground motion in the analysis governs the loading combination used for design of main girder. While, the Strength I/H ratio is 1.43, the Strength I/HV ratio is around 0.78.
- Inclusion of vertical ground motion in the analysis governs the loading combination used for design of piers. While, the Strength I /H ratio is 1.22, the Strength I/HV ratio is around 0.84.

6.2. Recommendations for Future Studies

This study investigates one type of bridge with and without seismic isolation. It is a steel girder composite bridge with R/C piers and foundation. The main concern is to see the effects vertical ground motion using specific EQs. Eventually, several result specific to this type of a bridge is reached. Hence, for future studies, one may investigate the issues given below which are just some of the probable topics arisen from this study.

- Investigation of vertical ground motion effect on other types of seismically isolated bridges such as prestressed girder or cantilever cable stayed bridges.
- Investigation of vertical ground motion effect on steel girder composite bridges using EQs with a maximum ground acceleration of greater than 0.6g.
- Assessment of internal forces in structural members on seismically isolated bridges with finite soil-structure interaction models.
- Assessment of shear capacity of lead core rubber isolators exposed to near fault vertical ground motions.

REFERENCES

[1] Accessed on 05 December 2009, Structural Engineers Association of Northern California, Structural Engineers Celebrating Earthquake Safety, http://www.celebratingeqsafety.com/assets/images/_base_isolation_fig1.gif, 2005.

[2] Sashi K. Kunnath; Emrah Erduran; Y. H. Chai; and Mark Yashinsky, "Effect of Near-Fault Vertical Ground Motions on Seismic Response of Highway Overcrossings", Journal of Bridge Engineering, Vol. 13, No. 3, May, 2008.

[3] California Department of Transportation Technical Publications, Graphics and Outreach Services Branch, "Seismic Design Criteria", June 2006.

[4] Gordon P. Warn and Andrew S. Whittaker, M.ASCE, "Vertical Earthquake Loads on Seismic Isolation Systems in Bridges", Journal of Structural Engineering, Vol. 134, No. 11, November, 2008.

[5] Murat Dicleli and Srikanth Buddaram (September 2005), "Effect of isolator and ground motion characteristics on the performance of seismic-isolated bridges", Earthquake Engng Struct. Dyn. 2006; 35:233–250.

[6] American Association of State Highway and Transportation Officials, "AASHTO LRFD Bridge Design Specifications", 4th Edition, 2007.

[7] Nicos Makris and Cameron J. Black, “Evaluation of Peak Ground Velocity as a ‘‘Good’’ Intensity Measure for Near-Source Ground Motions”, Journal of Engineering Mechanics, Vol. 130, No. 9, September, 2004.

[8] Bolt, B. A. (1971) ‘‘The San Fernando Valley, California earthquake of February 9, 1971: Data on seismic hazards.’’ Bull. Seismol. Soc. Am., 61, 501–510.
Bolt, B. A. (1975) ‘‘San Fernando earthquake 1971. Magnitude, aftershocks and fault dynamics.’’ Chapter 21, Bulletin 196, California Division of Mines and Geology.

[9] Bertero, V. V., Mahin, S. A., and Herrera, R. A. (1978) ‘‘A seismic design implications of near-fault San Fernando earthquake records.’’ Earthquake Eng. Struct. Dyn., 6(1), 31–42.

[10] G.A. McRae and H. Tagawa, “Methods to Estimate Displacements of PG&E Structures”, A Final Report on Research Conducted Under PG&E/PEER Research Program, PG&E/PEER Task No: 505, August, 2002.

[11] Prepared by the American Society of Civil Engineers for the Federal Emergency Management Agency (FEMA), “Prestandard and Commentary for the Seismic Rehabilitation of Buildings (FEMA 356)”, 2001.
Prepared by the American Society of Civil Engineers for the Federal Emergency Management Agency (FEMA), “Prestandard and Commentary for the Seismic Rehabilitation of Buildings (FEMA 273)”, 1997.

[12] Applied Technology Council, "Seismic Evaluation and Retrofit of Concrete Buildings Volume 1 (ATC 40)", Report No. SSC 96-01, November, 1996.

[13] Accessed on 10 December 2009, U.S. Geological Survey (USGS) Earthquake Hazard Program, "What is Directivity?", http://earthquake.usgs.gov/ regional/nca/rupture/directivity/ , February, 2009.

[14] Computers and Structures, Inc, Integrated Software for Structural Analysis & Design, SAP2000 Nonlinear Version: 11, 2007.

[15] Accessed on 17 December 2009, Rubber Seismic Isolation Technology, Rubber Seismic Isolators, http://www.seismic-isolators.com/en/products/ images/ rsit-02.jpg, 2008.

[16] Accessed on 17 December 2009, Direct Industry, The Virtual Industrial Exhibition, http://img.directindustry.com/images_di/ photo-g/bridge-bearing-299168.jpg, 2009.

[17] Accessed on 17 December 2009, Ile Bridge, http://www.whitings-writings. com/images/ile_bridge.jpg, 2009.

[18] Accessed on 17 December 2009, Wikipedia, Bridge structural and evolutionary taxonomy, http://en.wikivisual.com/images/b/ bf/BridgeTaxonomy_BW.png, 1998.

[19] Murat Eröz, Reginald DesRoches,(2007), "Bridge seismic response as a function of the Friction Pendulum System (FPS) modeling assumptions", Engineering Structures, doi:10.1016/j.engstruct. 2008.04. 032, April, 2008.

[20] American Association of State Highway and Transportation Officials, "AASHTO LRFD Bridge Design Specifications" "Section 3.4.1- Load Factors and Load Combinations", 4th Edition, 2007.

[21] Murat Eröz, Reginald DesRoches,(2007), "Bridge seismic response as a function of the Friction Pendulum System (FPS) modeling assumptions"-Figure 6 Multi-span continuous (MSC) steel girder bridge general elevation and modeling details & Figure 7 Pier configuration and bent and column discretization, Engineering Structures, doi:10.1016/ j.engstruct. 2008.04. 032, April, 2008.

[22] Turkish Standards Institution, "Requirements for Design and Construction of Reinforced Concrete Structures", (TS 500), February, 2000.

[23] Turkish Standards Institution, "Building Code for Steel Structures" (TS 648), December 1980.

[24] Joseph E. Bowles, "Foundation Analysis and Design", McGraw-Hill, Inc., 1988.

[25] National Earthquake Hazards Reduction Program (NEHRP), NEHRP Provisions, 1994

[26] International Code Council, Inc, “2006 International Building Code” (IBC 2006), 2006.

[27] Accessed on 10 January 2009, Pacific Earthquake Engineering Research Center (PEER), The Regents of the University of California, PEER Strong Ground Motion Database, http://peer.berkeley.edu/smcat/search. html, 2000.

[28] Computers and Structures, Inc., “CSI Analysis Reference Manual For SAP2000®, ETABS®, and SAFE™”, 1995.

[29] A. Ibrahimbegovic and E. L. Wilson, “Simple Numerical Algorithms for the Mode Superposition Analysis of Linear Structural Systems with Non-proportional Damping”, Computers and Structures, Vol. 33, No. 2, pp. 523–531, 1989.

E. L. Wilson, “An Efficient Computational Method for the Base Isolation and Energy Dissipation Analysis of Structural Systems”, ATC17-1, Proceedings of the Seminar on Seismic Isolation, Passive Energy Dissipation, and Active Control, Applied Technology Council, Redwood City, California, 1993.

[30] SeismoSoft Ltd. Earthquake Engineering Software Solutions, Software to Process Strong-Motion Data, SeismoSignal Version 3.3.0, 2009

[31] California Department of Transportation Technical Publications, Graphics and Outreach Services Branch, “Memo to Designer20-1 Seismic Design Methodology”, January 1999.

[32] M. W. Yuan, J. M. Dickens and E. L. Wilson, “Dynamic Analysis by Direct Superposition of Ritz Vectors,” Earthquake Engineering and Structural Dynamics, Vol. 10, pp. 813–823, 1982.